Modelling Hysteresis in the Bending of Fabrics

by

Timothy John Lahey

A thesis

presented to the University of Waterloo

in fulfilment of the

thesis requirement for the degree of

Master of Applied Science

in

Systems Design Engineering

Waterloo, Ontario, Canada, 2002

I hereby declare that I am the sole author of this thesis. This is a true copy of the thesis, including any required final revisions, as accepted by my examiners.

I understand that my thesis may be made electronically available to the public.

Abstract

This thesis presents a model of fabric bending hysteresis. The hysteresis model is designed to reproduce the fabric bending measurements taken by the Kawabata Evaluation System (KES) and the model parameters can be derived directly from these property measurements. The advantage to using this technique is that it provides the ability to simulate a continuum of property curves. Results of the model and its components are compared and constrasted with experimental results for fabrics composed of different weaves and yarn types.

An attempt to incorporate the bending model as part of a fabric drape simulation is also made.

Acknowledgements

Over the duration of this thesis I have received a great deal of advice, assistance, and encouragement. I would first like to thank Shekar for his encouragement in pursuing a graduate degree. Without him, I would not have considered it. My sincere thanks go to to Rebecca Kaufman without whose support I would have not have completed this thesis.

The critiques offered by members of CGL, the ConStruct group, and members of the Systems Modelling and Simulation lab helped me refine the concepts and my understanding. I would especially like to thank Ajay, Ivan, and Hank for their help, encouragement, and distractions during this thesis. My thanks go to Dr. Jeffrey Eischen for providing me with a copy of Shigan Deng's thesis which contained the necessary data for this thesis work.

I received a great deal of help from my former supervisor Richard Bartels even if it was only asking the right question. Lastly, I would like to thank my supervisor, Glenn Heppler for his patience, help, and encouragement.

Contents

List of Tables

List of Figures

Chapter 1

Introduction

Do not seek to follow in the footsteps of the men of old; seek what they sought.
– Basho

Textiles have become more prominent in engineering applications in recent years, with uses such as airbags and domes. Since the 1930s, there has been research reported in the textile engineering literature regarding the mechanical properties of fabric, its behaviour and, recently, on how to model its behaviour in computer graphics applications.

The initial goal of this thesis was to develop a model of fabric mechanics from property curves to be employed as part of a computer simulation of fabric drape. Efforts to model the shear and tensile behaviour were abandoned in favour of focusing on the bending model. The decision to focus on accurately modelling the bending behaviour, including hysteresis, was taken because bending rigidity and hysteresis were found to be important in determining fabric drape [HC98, JP98].

1.1 Previous Work

Work on models of fabric behaviour has been done in two fields, computer graphics and textile engineering with little overlap. The work done in computer graphics is focused upon a good visual approximation while the work in textile engineering focuses on a model that is physically justified.

1.1.1 Research in Computer Graphics

The first paper on modelling fabric drape in the computer graphics field was done by Weil [Wei86] at SIGGRAPH '86. This model was purely geometric and as a result, only provided a static representation. In that same year Nisselson gave a talk [Nis86] on the relationship of computer graphics and fashion. This lead to a panel discussion [NWGC87] on the same topic at SIGGRAPH '87.

Over the years a large number of lumped parameter models (called particle models in the literature) have been presented in the computer graphics literature for the dynamic simulation of fabric behaviour. Considerable work was done by N. Magnenat Thalmann, D. Thalmann and their research groups using a linear elastic model for clothing on virtual actors [CYMTT92, MT98, VCMT95, VMT94, VMT95, VMTJT96, VT98]. The work of Dias *et al.* in the textile engineering literature appears very similar [DGR00]. Also of note is the work of Breen *et al.* [BHG92, BHW94, HB98] whose model is a grid of particles where energy potential functions (based upon results from the Kawabata Evaluation System (KES) [Kaw80]) dictate the particle interactions. However, there is no physical justification given for the energy potential equations and only the loading portion of the KES data is used (see Chapters 2 and 4 for information on the KES). A similar approach is taken by Eberhardt *et al.* [EW97, EW99, EWS96, SE98] who also used energy potentials but include both the loading and unloading KES data. The difficulty with their approach is that polynomial fits to the loading and unloading

curves are used and there no is discussion on how the transition from loading to un-loading is handled. The work of Baraff and Witkin [BW98a, BW98b] is the basis for the model in the Alias-Wavefront Maya Cloth software and for likely the basis for Pixar's cloth model used in Monsters Inc. [Rob01]. Their particle model gives no physical justification for the energy functions between neighbouring particles. In addition to the particle models mentioned above, there are a number of other particle models in the literature [Eis98a, LDG96, LKC96, LPC95, NGA95, Pro95, Pro96, VOVL92].

In addition to the work done in the computer graphics literature, work on computer-aided design (CAD) with textiles has also been done. Work on garment design was done by Hinds and McCartney [HM90, HM91], and Okabe *et al.* [OITN92] but their work is strictly geometric. That is, their model does not account for differences due to fabric properties. Aono *et al.* presented a useful framework [ABW93] which was fleshed out with techniques for mapping fabric onto curved surfaces [ABW94] and handling darts in fabric [ADBW96]. These papers do not present a mechanical model of fabric.

1.1.2 Research in Textile Engineering

There have been a number of fabric simulation models developed in the textile engineering literature. The majority of the models are based upon standard engineering approximation methods such as finite elements or finite volumes. A notable exception is Postle and Postle's model [PP99] which used techniques from non-linear dynamics to analytically solve their equations. Note that this model does not include internal friction as part of the fabric model. Another exception is the model of Chen *et al.* [CSWY99] which uses a multigrid approach to solve the energy minimisation. This model neglects bending rigidity but adds a term they call "wrinkling energy" to compensate.

One early model was that of Moskowitz *et al.* [MDS66] which considered uniform lateral loads acting on two sets of plane, parallel elements superimposed at $90°$ to each

other. This was done to represent the weave of the fabric. A finite difference approximation was used to solve the equations derived through the theory of minimum potential energy. Later, Shanahan *et al.* [SLH78] presented a discussion of how the theory of plates and shells could be applied to fabrics.

The majority of the models [CG95, GLS95, HC00a] found in the literature use an orthotropic, linear elastic assumption for material behaviour. Where these models differ is in their element choice. Gan *et al.* [GLS95] use a non-linear shell model as do Chen and Govindaraj [CG95] while Hu and Chen [HC00a] use a finite volume method.

There have been some models that include non-linear effects. Bias-Singh *et al.* [BSBG98] developed a non-linear finite element model for non-woven fabrics that includes a bi-linear tension model. Shigan Deng [Den94, EDC96, Eis98b] developed a non-linear, orthotropic shell model that includes a polynomial fit to the KES bending data. However, this model does not include bending hysteresis.

1.2 Layout of this document

The remaining portion of this thesis is divided into three main parts. The first part (Chapters 2 and 3) details the background research done in developing the model. This research includes background on fabric structure, fabric properties, and models of hysteresis. The second part presents the bending model (Chapter 4) and an effort to incorporate it into a fabric drape simulation (Chapter 5). The final chapter summarizes the thesis. In addition, due to the number of unfamiliar terms used in this thesis a glossary is provided in Appendix A.

Chapter 2

Fabric Mechanical Properties

Fabrics vary in type, fibre, geometric structure and their basic mechanical properties. Using the classification system given by Hearle *et al.* [HGB69], fabrics and laminae can be composed of material from five different classes. This system is described in Table 2.1.

Class	Title	Description
A	Interlaced Yarns	The traditional textiles. Once fibres with particular properties are selected for the yarn, the arrangement of fibres within the yarn and the arrangement of interlaced yarns determine the properties of the fabric. This class includes textiles such as: woven cloth, knitted cloth, lace, and crochet.
B	Non-interlaced Yarns	This class is composed of bonded yarn sheets. A yarn sheet is laid down without interlacing and a bonding material is applied to the yarns, providing a coarse network structure. This class includes a wide variety of composite material (e.g., laminated composites).

Class	Title	Description
C	Fibre Assemblies	These are materials where individual fibres are laid down in a web. This class includes textiles such as felt, bonded fibre fabric, and spun-bonded filament fabric.
D	Fibrous Sheets	This class of materials has fibres but they are not easily identifiable as separate entities, instead the whole material is fibrous in form. Examples of this class of materials are leather and paper.
E	Non-fibrous Sheets	This class of materials has no discernible fibres, and includes materials such as plastic film, rubber sheets, metal foil, and foamed plastic.

Table 2.1: Classes of Fabric

A fabric or laminae can be made of material from a single class or they can be also composed of material from a combination of classes. For example, fur is composed of materials from classes C and D while synthetic leather is made of materials from classes C and E. While the results of this thesis can likely be applied to all classes of fabrics, due to the use of property curves instead of a micromechanical model, only fabrics from class A are considered herein.

2.1 Woven Fabric Structure

The geometric structure of woven fabric plays a significant role in determining the mechanical properties of the fabric and therefore some discussion of the structure of fabric is necessary. Initially, a purely geometrical model was done by Pierce (described in Hearle *et al.* [HGB69]) which is illustrated in Figure 2.1 which shows the geometrical

model in cross-section. The main components in Pierce's model are, crimp height h,
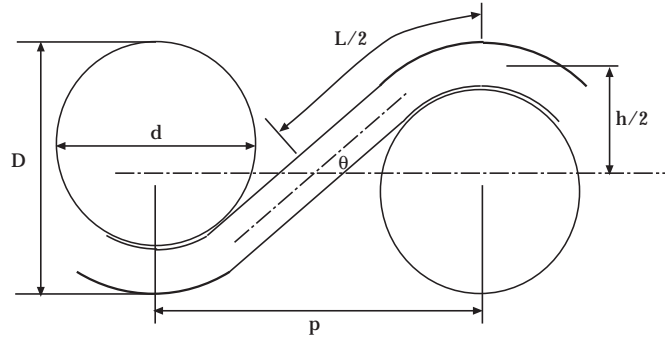
Figure 2.1: Pierce's Geometrical Model [HGB69]

yarn length l, yarn spacing p, yarn diameter d, crimp angle θ, and the sum of the two yarn diameters, D. With the exception of D, each of the model components can have different values in each of the weft (1) and warp (2) directions. The basic equations for the weave are:

$$p = (l - D\theta)\cos\theta + D\sin\theta \tag{2.1}$$

$$h = (l - D\theta)\sin\theta + D(l - \cos\theta) \tag{2.2}$$

$$D = h_1 + h_2 \tag{2.3}$$

The basic model parameters are: h_1, h_2, l_1, l_2, p_1, p_2, and D (crimp angles are considered to be dependent variables). If we have four of the parameters, the other three can be calculated (and optionally the crimp angles).

Pierce's model relies upon the assumptions that the bending resistance of the yarns is negligible and that the yarns are circular in cross-section. These assumptions are mutually consistent because if the yarn bending resistance is not negligible, then the yarn cross-section will deform, producing a flatter cross-section. Alternative yarn

cross-sections have been proposed to solve this problem (see Hearle *et al.* pp 325-326 [HGB69]). The most popular alternative is a race-track cross-section as shown in Figure 2.2 which was proposed by Kemp in 1958. This cross-section is used in the calculation of the "jamming" condition of fabrics.
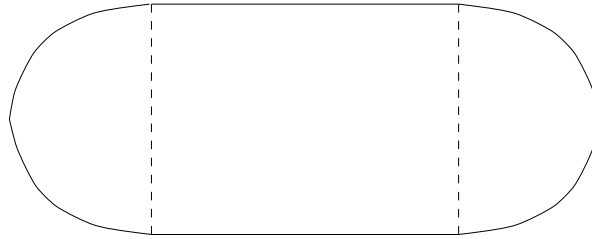
Figure 2.2: Race-Track Cross-section [HGB69]

Both of these models suffer from the problem that they ignore the internal forces in the fabric and the deformation of the cross-section that results. To compensate for this, Olofsson developed a model that calculates the yarn geometry from the point loads acting at the intersections (see Hearle *et al.* pp. 326-330 [HGB69]). This approach gives a better approximation to observed yarn geometry than Pierce's model. If V is the point load at the cross-section (see Figure 2.3) then the bending moment at any point is given by:

$$M_x = -Vx \tag{2.4}$$

and the radius of curvature of the bent yarn (ρ) is given by:

$$\rho = -\frac{m}{Vx} \tag{2.5}$$

where m is the bending modulus of the yarn. We also have that:

$$\rho d\psi = ds \tag{2.6}$$

$$dx = \cos\psi ds \tag{2.7}$$

where ds is the infinitesimal arc length along a yarn. Therefore, the relationship between the x coordinate and the yarn angle is:

$$m\cos\psi d\psi = -Vxdx \tag{2.8}$$

Due to symmetry considerations it is assumed that the boundary condition at $x = 0$ is $\rho = 0$. Therefore, integrating equation (2.8) we get:

$$V = \frac{2m}{x^2}(\sin\theta - \sin\psi) \tag{2.9}$$

which gives a relationship between the force and the yarn geometry. At the yarn intersection, $x = p/2$, and $\psi = 0$, therefore:

$$V = \frac{8m\sin\theta}{p^2} \tag{2.10}$$

To obtain the shape of the elastica, we also need the relationship between y and x:

$$dy = \tan\psi dx \tag{2.11}$$

The shape is determined by V, m, and θ. Equations for x, y, and s still need to be derived. An equation for x can be obtained by rearranging equation (2.9):

$$x = \sqrt{\frac{2m}{V}}\sqrt{\sin\theta - \sin\psi} \tag{2.12}$$

Equations for y and s (arclength) are derived in Appendix B.1. The final results are:

$$y = \sqrt{\frac{m}{V}}(F(\frac{\pi}{2}) - 2E(\frac{\pi}{2}) - F(\phi_0) + 2E(\phi_0)) \tag{2.13}$$

$$s = \sqrt{\frac{m}{V}}(F(\frac{\pi}{2}) - F(\phi_0)) \tag{2.14}$$

where

$$E(v) = \int_0^v \sqrt{1 - k^2 \sin^2 \phi} d\phi \tag{2.15}$$

$$F(v) = \int_0^v \frac{1}{\sqrt{1 - k^2 \sin^2 \phi}} d\phi \tag{2.16}$$

$$k = \sin(\frac{\theta}{2} + \frac{\pi}{4}) \tag{2.17}$$

$$\sin \phi = \frac{\sin(\frac{\psi}{2} + \frac{\pi}{4})}{k} \tag{2.18}$$

with $\phi = \phi_0$ when $\psi = 0$ so that $\sin \phi_0 = \frac{1}{\sqrt{2}k}$

Note that this model was extended by Leaf and Anandjiwala [LA85] to include a bi-linear bending model for the yarn.
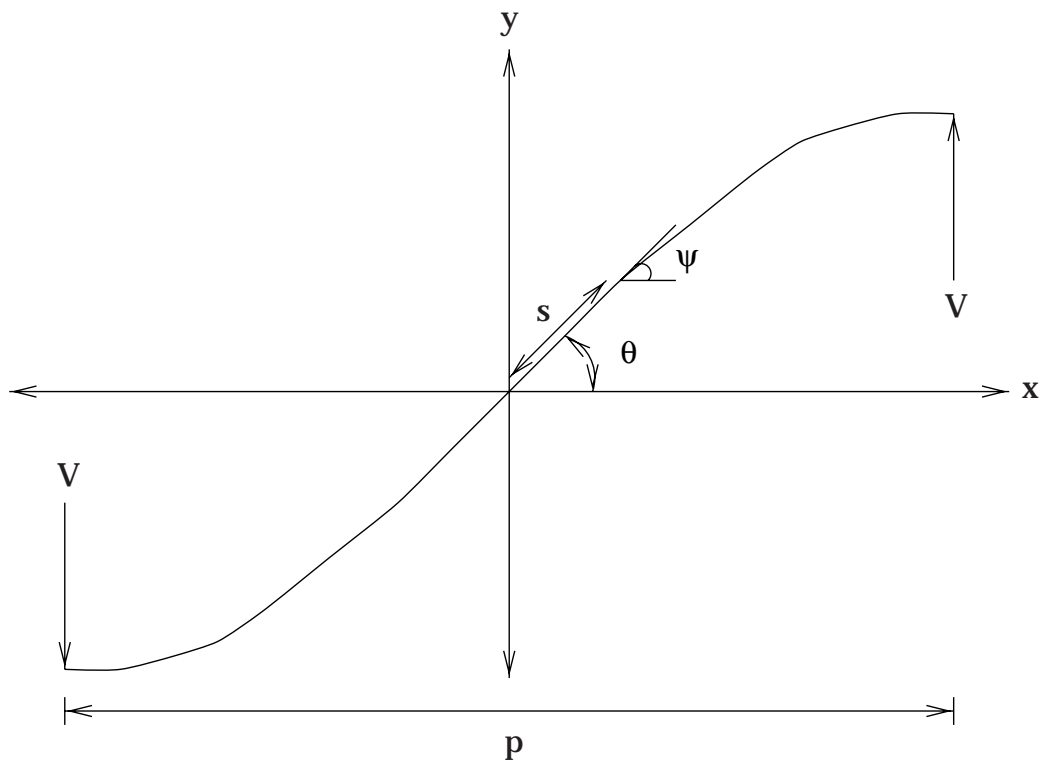
Figure 2.3: Forces on Olofsson's elastica [HGB69]

2.2 Tension

Consideration of the tensile properties of woven fabrics involves a number of different problems because the cloth is orthotropic and its modulus varies considerably with strain. Not only does the modulus vary in the two principal directions (warp and weft) but extension in the 45 degree direction (the bias) involves a different mechanism than extension in the principal directions. In addition, extension along the bias is usually of a higher order of magnitude. The mechanism for extension in the bias direction is determined by the shear behaviour.

The main mechanisms for extension in the principal directions [HGB69] are: crimp redistribution (for the initial extension), fiber extension and yarn compression (after decrimping). Generally, there are three stages to the extension mechanism (see Figure 2.4). First, a high initial modulus is observed until the frictional resistance to the yarn bending is overcome. Next, a low modulus occurs while the yarns unbend. As the crimp is decreased, the force needed to cause fibre extension increases. In the final stage, the load extension behaviour of the fabric is governed by the extension properties of the yarns.

One of the earliest models for fabric tension was done by Grosberg [Gro66a] who developed a micromechanical model similar to Olofsson's [HGB69]. Grosberg included a tensile force U in addition to the crossing yarn force V (see Figure 2.5) and calculated the change in yarn spacing for a given extension.

Another micromechanical model is that of Realff *et al.* [RBB97] which uses a simple unit cell and derives its model from the constitutive yarn properties. Sun *et al.* [SSG97] also developed a micromechanical model but their unit cell geometry allows for more complex weaves than that of Realff *et al.*, but uses a simpler model of the yarn mechanics.

An alternative approach for the modelling of fabric tension was taken by Sinoimeri
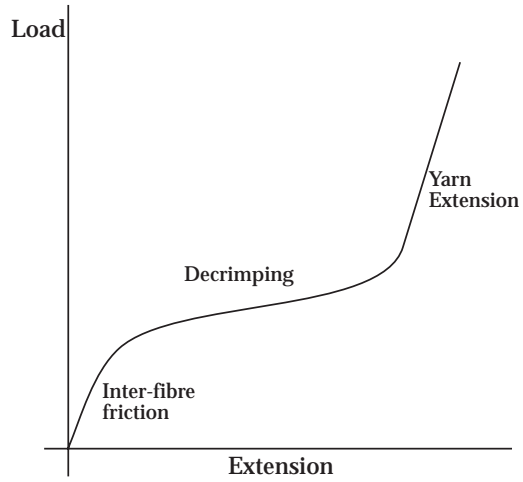
Figure 2.4: Generalised Tensile Load-Extension Curve [HGB69]
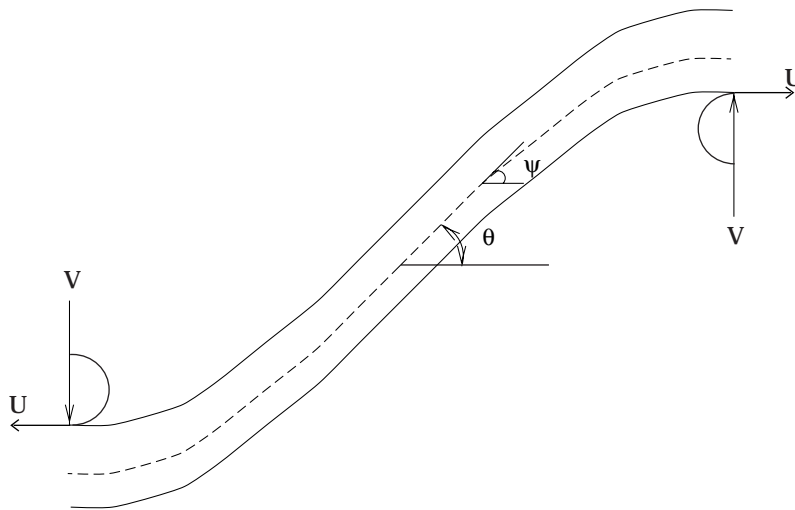
Figure 2.5: Grosberg's micromechanical model [Gro66a]

and Dréan [SD97] using the energy methods of de Jong and Postle [DJP78] where constrained minimisation of the strain energy of the fabric structure is performed using optimal control theory.

None of the the research discussed previously in this section has tried to include the recovery process or examine how their models behave during the recovery process. In addition, the micromechanical models are limited in their application to general fabric mechanical behaviour (e.g., drape) since they do not consider interactions between fabric properties. Energy methods are difficult to apply to complex deformations because of they require new derivations for each loading condition.

2.3 Shear

Modes of deformation involve several forms depending on the degree of shear imposed upon the fabric. These modes are (from Grosberg and Park [GP66]): Deformation due to rigid intersections, when the shear cannot overcome the friction. Once the friction is overcome, the yarns begin to slip at the intersection. Next, an elastic deformation of the yarns occurs. Finally, jamming occurs in the fabric structure.

The mechanics of shear are highly dependent upon the geometric construction of the fabric. For example, tightly woven fabric close to the jammed condition and will behave elastically, while loosely woven fabric behaviour is more dependent on the frictional resistance between the yarns (see Lindberg *et al.* [LBD61])

It is generally assumed that the hysteresis produced during shear is the result of the frictional forces at the yarn intersections [GP66, LBD61, Ske76]. All of the models in these papers assume a frictional resistance to the deformation proportional to the normal force acting on the intersection.

2.4 Bending

It has been difficult to characterise the mechanisms of fabric bending. Abbott [Abb51] compares five different labratory tests for bending stiffness. These are: cantilever test, heart loop test, Schiefer Flexometer, Planoflex, and the M.I.T. Drapemeter to subjective measurements of stiffness. The cantilever test was preferred over the other methods due to the simplicity of the test and the high correlation to the subjective measurements. Grosberg and Abbott [GA66a] discuss the apparatus of Livesey and Owen that bends the fabric in almost constant curvature. They also discuss [GA66b] the importance of friction during the bending process and note that large errors are present if a linear bending approximation is used.

One of the initial models of fabric bending was done by Grosberg and Swani [Gro66b, GS66] which modelled bending with an initial frictional restraint M_o that must be first overcome then a linear moment-curvature relationship. The M_o represents frictional resistance to bending at the yarn intersections. Once this frictional resistance is overcome, the yarns can be bent, hence the linear relationship once the initial resistance is overcome.

One of the more developed models of fabric bending was done by Zhou and Ghosh [ZG99] which represented the bending behaviour with a piecewise linear model that includes hysteresis (see Figure 2.6). This allowed the authors to include cyclic bending behaviour in their measurement system.

The work of Shi *et al.* [SHY00] used a rheological model of fabric bending that includes a spring and frictional elements that are strictly functions of the curvature (see Figure 2.7).

Other investigations of bending include the work of Hu and Chung [HC00b] which examined the effect of vertical seams on bending stiffness (using a linear bending model) and the work of Hu *et al.* [HLL00] which examined the bending hysteresis
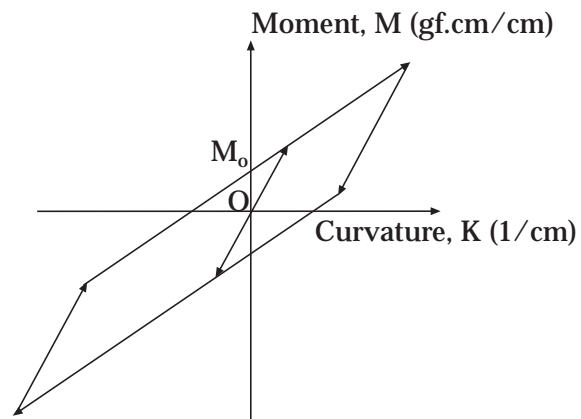
Figure 2.6: Zhou and Ghosh Bending Model [ZG99]
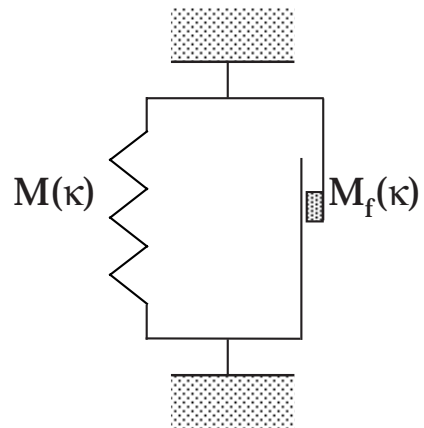
Figure 2.7: Shi *et al.* Bending Model [SHY00]

in various directions.

2.5 Kawabata Evaluation System

The Kawabata Evaluation System (KES) [Kaw80] is a widely used system of fabric mechanical tests that are designed to provide an objective measurement of fabric hand. Unfortunately, the characterisation of hand does not yield data which is easily exploited for an engineering characterisation of the material. However, since this system is used for quality control of fabrics the KES is common. The various KES properties and the associated testing procedures are described in the following sections.

2.5.1 Tension

The tensile force is applied to a 5 cm by 20 cm fabric specimen as shown in Figure 2.8. The standard [Kaw80] states that the test is conducted to a maximum loading level of 500 gf/cm . It also states that the test is conducted at a constant strain rate of 4.0×10^{-3}/sec.
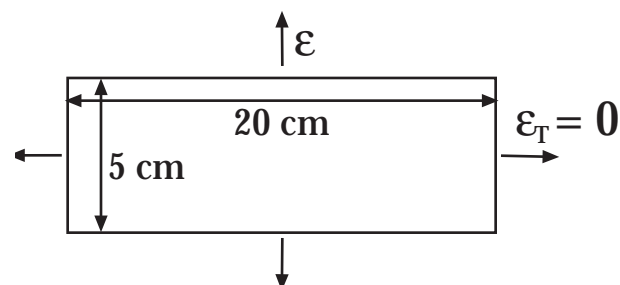
Figure 2.8: KES: Application of Tension Force [Kaw80]

The system measures both the loading and unloading responses. Three values are used to characterise the tension response. Linearity (LT), Tensile Energy per unit area

(WT) (see Figure 2.9), and Resilience (RT) where they are defined as:

$$WT = \int_0^{\epsilon_m} F d\epsilon \tag{2.19}$$

$$LT = 2WT/(F_m \epsilon_m) \tag{2.20}$$

$$RT = WT'/WT \tag{2.21}$$

where WT' is the WT value integrated over the unloading response as shown in Figure 2.9.
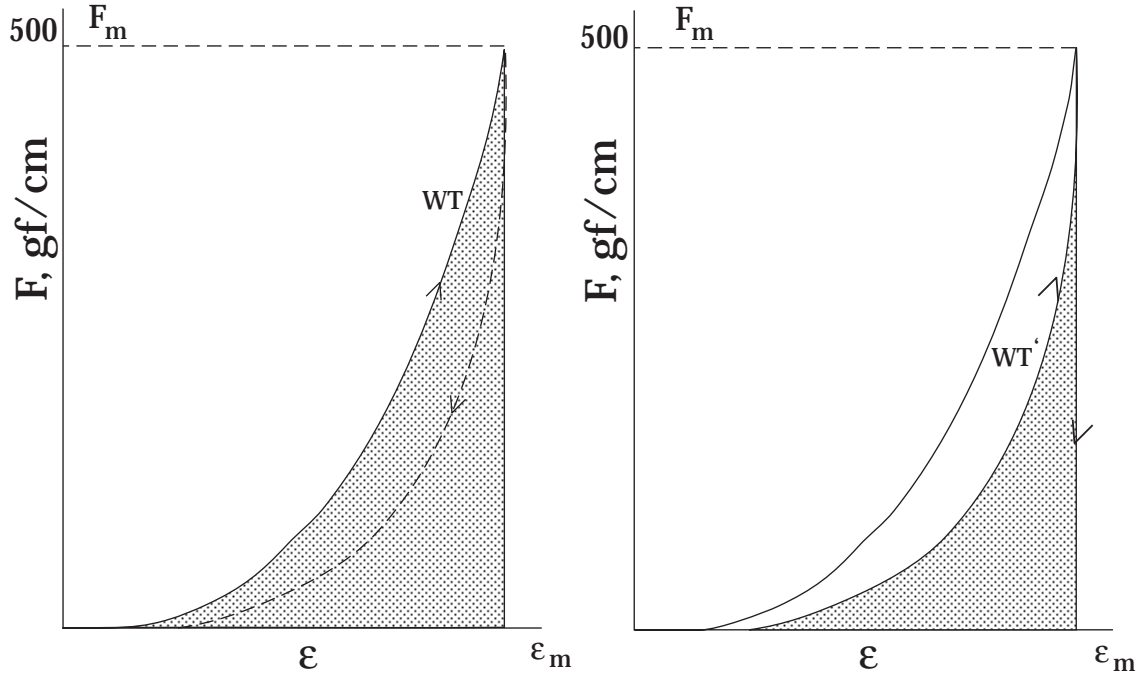
Figure 2.9: KES: Tension Measurements

2.5.2 Shear

Shear tests are conducted with a constant tension W applied in the direction orthogonal to the test (see Figure 2.10). The test is conducted at a velocity of $0.417\ mm/s$ which gives a rate of shear strain of approximately $8.34 \times 10^{-3}\ s^{-1}$. In addition, the characteristic values of G (shear stiffness), $2HG$ (hysteresis at $\phi = 0.5°$), and $2HG5$ (hysteresis at $\phi = 5°$) are calculated. See Figure 2.11 for the relationship between the recorded curve and the characteristic values. G is defined as:

$$G = \frac{F_s}{\phi} \tag{2.22}$$

which is the slope of the recorded curve. This is measured in the region from $0.5°$ to $5°$. The standard also states that in the event that the curve is not linear, the mean slope should be used. Note that this definition is not the same as shear modulus, and as a result, Hu and Zhang [HZ97] performed finite element analysis of the process and determined a conversion from the G given by the KES to a shear modulus.
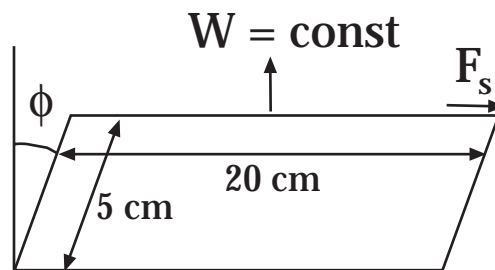
Figure 2.10: KES: Shear Process [Kaw80]
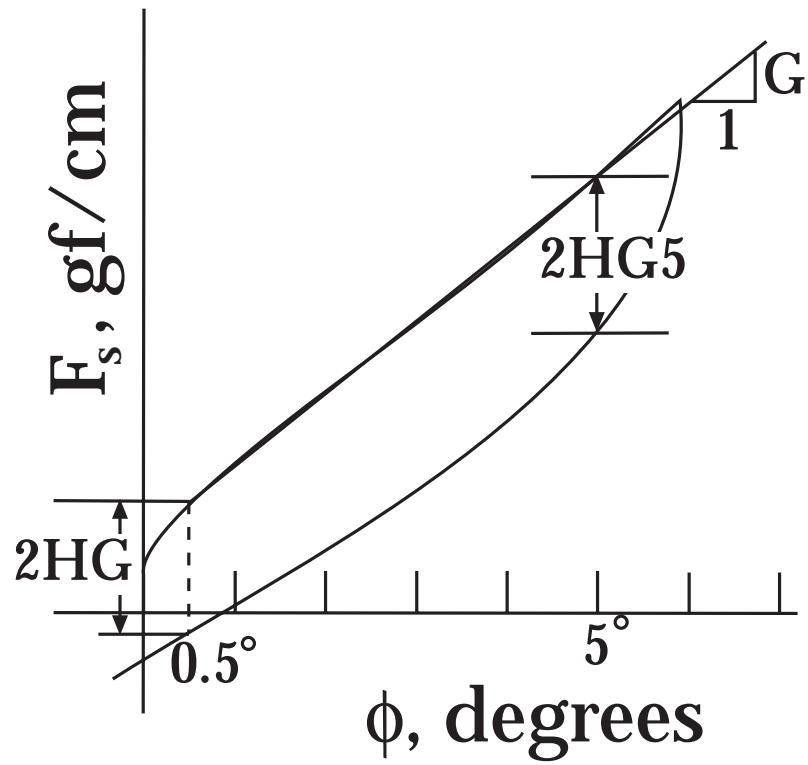
Figure 2.11: KES: Shear Measurements [Kaw80]

2.5.3 Bending

The bending moment is measured as a sample of fabric is bent through a range of curvatures between 2.5 and $-2.5\ cm^{-1}$. Kawabata [Kaw80] states that the KES bending test is conducted at a constant rate of $0.5\ cm^{-1}/s$. However, acceleration transition regions are necessary to achieve that speed from rest and back. No discussion of these transition regions is made in Kawabata [Kaw80]. The test sample is mounted vertically to prevent the effect of gravity influencing the experiment. The system measures forward and backwards bending as shown in Figure 2.12. The characteristic values recorded by the system are: B, the bending rigidity per unit length, and $2HB$, the moment of hysteresis per unit length. Note that in addition to measuring these values for the weft and warp directions, they are also measured in the forward and backward directions as shown in Figure 2.12.
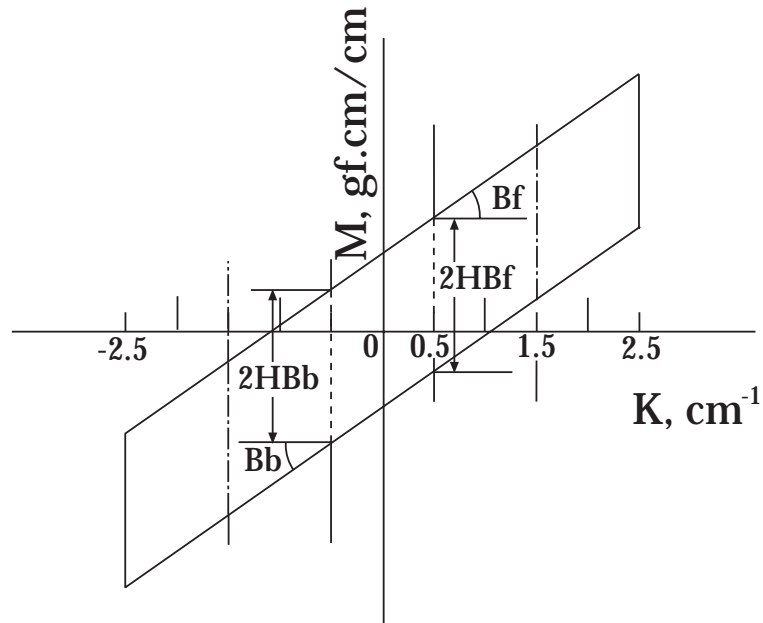
Figure 2.12: KES: Bending Measurements [Kaw80]

Chapter 3

Previous Work on Hysteresis

In order to represent the hysteresis exhibited during fabric mechanical tests, it is first necessary to understand hysteresis and how to model it. To that end, this chapter discusses a number of different models of hysteresis, some specific to mechanical systems, others more general. Finally, one model of friction is discussed in-depth in Section 3.3.

3.1 Early Mechanical Material Hysteresis Models

Some of the earliest work in this area was done by Ramberg and Osgood [RO43], who developed a three parameter model of stress-strain behaviour. The results are similar to those of Dahl [Dah76] (who modelled dynamic friction) and Martin *et al.* [MTS71] (whose model is used in fatigue research).

Martin, Topper, and Sinclair's paper [MTS71] describes a hysteresis model used in fatigue research. This paper details a simple, extensible model involving only springs and frictional elements (Figure 3.1) which can provide a good approximation to the experimental stress-strain curve (see Figure 3.2). Each of the slider elements are set with a yield value of $\sigma_{i+1} > \sigma_i$ such that the corresponding springs are added in sequence.

Upon unloading each of the frictional elements lock up, and retain a residual stress. However, in order for the residual stress to be retained, σ_{max} (the maximum stress experienced during the loading) must be less than twice the stress value at which the slider is activated. While this is true in the case of metals where the model is typically used, this is not true of fabrics.
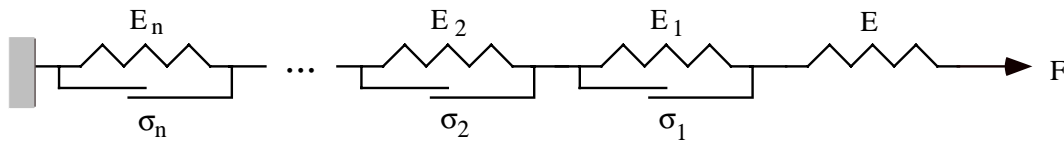
Figure 3.1: Fatigue Mechanical Model [MTS71]
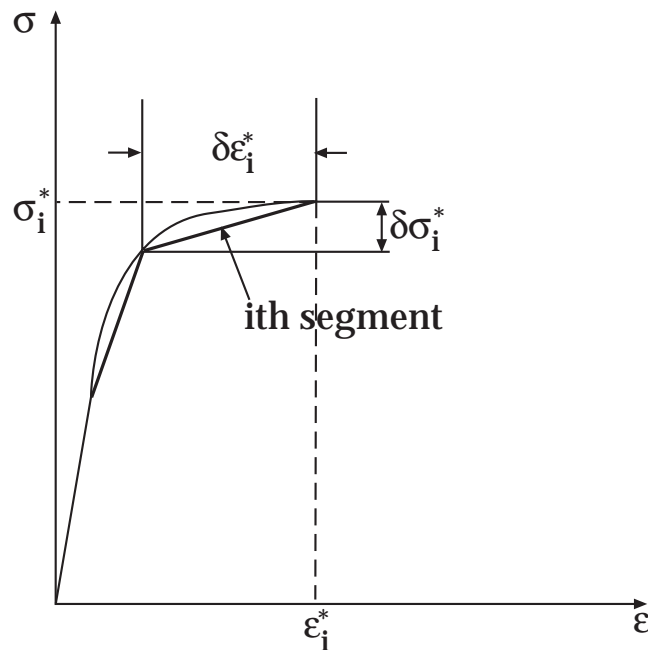
Figure 3.2: Piecewise Linear Approximation to Stress-Strain Curve [MTS71]

3.2   General Hysteresis Models

A general mathematical framework for modelling hysteresis was presented by Krasnosel'skii and Pokrovskii [KP89]. They also describe lumped parameter models for systems composed of plays (Figure 3.3), stops (Figure 3.4), and relays (Note that M_o in Figures 3.3 and 3.4 indicates the initial condition of each system respectively). The combination of these elements can represent a wide variety of hysteretic systems. In addition, in the English translation [KP89] a section detailing graph-theoretic representations of the lumped parameter models is presented.
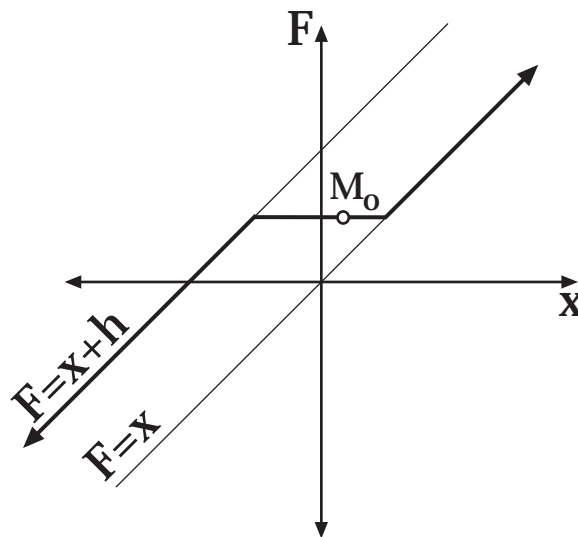
Figure 3.3: Ordinary Play [KP89]

Another type of hysteresis model is the differential automata model proposed by Tavernini [Tav93]. This type of model discretises the continuous problem into a set of continuous subproblems with possibly discontinuous transitions. The transitions
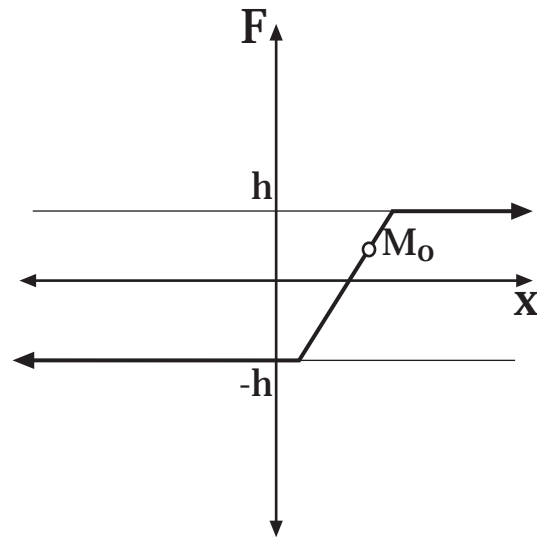
Figure 3.4: Ordinary Stop [KP89]

between the subproblems are described as a finite state machine where each of the subproblems is represented by a state.

3.3 A Differential Model of Frictional Hysteresis

Bliman and Sorine [BS93a, BS93b, BS95] detailed a differential equation model for hysteresis arising from friction. Their model is capable of producing a subset of Dahl's friction models [Dah76] but is also able to model other types of friction as well. Note that this model is built upon the hysteresis framework of Krasnosel'skii and Pokrovskii [KP89].

The general form of their model is given in Equation (3.1) where x is a state vector and u is the displacement from rest.

$$\dot{x} = |\dot{u}|Ax + B\dot{u}, \quad x(0) = 0 \tag{3.1}$$

$$F(u)(t) = Cx(t) \tag{3.2}$$

For a form that reproduces a subset of Dahl's model they use the following substitutions [BS95] for A, B, and C. Note: This corrects an omission in their earlier paper [BS93a] and is different than the parameter values used in [BS93b].

$$A = -\frac{1}{\epsilon_f}, \quad B = \frac{f_1}{\epsilon_f}, \quad C = 1 \tag{3.3}$$

However, this model does not include static friction. To include both static and dynamic friction we need a second order model. For this model we perform the substitutions given in Equation (3.4). Note: These substitutions also come from [BS95] and are also different than those given in [BS93b].

$$A = -\frac{1}{\epsilon_f}\begin{bmatrix} \frac{1}{\eta} & 0 \\ 0 & 1 \end{bmatrix}, \quad B = \frac{1}{\epsilon_f}\begin{bmatrix} \frac{f_1}{\eta} \\ -f_2 \end{bmatrix}, \quad C = \begin{bmatrix} 1 & 1 \end{bmatrix} \tag{3.4}$$

If we make the change of variables $ds = |\dot{u}|dt$ in Equation (3.1) we get the Linear Space Invariant (LSI) system:

$$\frac{dx_s}{ds} = Ax_s + Bu_s, \quad x(0) = 0 \tag{3.5}$$

$$y_s = Cx_s \tag{3.6}$$

From this point on we will only concern ourselves with the combined dynamic and static friction model.

3.3.1 Physical Parameters and Their Model Equivalent

For the above model, Bliman and Sorine [BS95] defined the following relationships between physical parameters and the model (see Figure 3.5). The dynamic friction f_k is defined as the friction asymptote when $\dot{u} > 0$:

$$f_k = \lim_{\dot{u}>0, u(t)} F(u)(t) \qquad (3.7)$$

and s_p is the displacement above which $F(u)(t)$ is within 5% of f_k. For the systems of concern, the static friction is given as:

$$f_s = \sup_{u,t>0} F(u)(t) \qquad (3.8)$$

and s_e is the displacement value where this value of f_s is reached. The minimal and maximal slopes of the F versus u curves are given as:

$$k_F{}^{\pm} = \sup_{u,t>0} \pm\frac{F(u)(t)}{\dot{u}(t)} \qquad (3.9)$$

These parameters, as well as the other parameters in Figure 3.5, are given in terms of the model parameters in [BS95]. However, in re-deriving these results (see Appendix

B.2) some errors were discovered in the original paper. The new results are:

$$f_k = f_1 - f_2 \tag{3.10}$$

$$f_s = f_k + f_2 \left(\frac{\eta f_2}{f_1}\right)^{\frac{\eta}{1-\eta}} (1 - \eta) \tag{3.11}$$

$$s_e = \frac{\epsilon_f \eta}{1 - \eta} \log\left(\frac{f_1}{\eta f_2}\right) \tag{3.12}$$

$$s_p = 3\epsilon_f \tag{3.13}$$

$$k_F{}^- = \frac{f_2}{\epsilon_f} \left(\frac{\eta^2 f_2}{f_1}\right)^{\frac{\eta}{1-\eta}} (1 - \eta) \tag{3.14}$$

$$k_F{}^+ = \frac{f_1 - f_2 \eta}{\eta \epsilon_f} \tag{3.15}$$

Note: The $k_F{}^+$ result given in the original paper (with the factor of 2 removed from the appropriate equations) corresponds to the difference between the actual $k_F{}^+$ and $k_F{}^-$ given here. Also of note is that the $k_F{}^+$ given here occurs at $t = 0$.
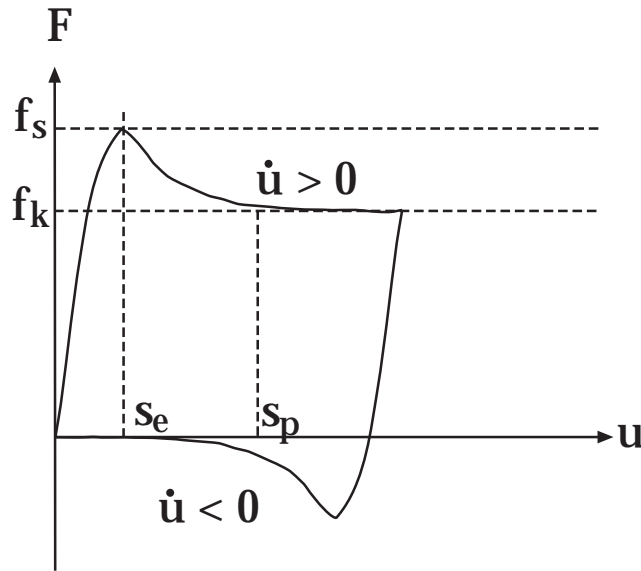
Figure 3.5: Bliman and Sorine 2nd order model

3.3.2 Other Results

Bliman and Sorine [BS95] also give a few other results (also derived in Appendix B.2). If u and $\dot{u}$ are integrable, $F(u)$ is given by:

$$F(u)(t) = \int_0^t C e^{A \int_{t'}^t |\dot{u}(\tau)| d\tau} B\dot{u}(t')dt' \tag{3.16}$$

If $s(0) = 0$, making the substitutions for A, B, and C we can reduce the above to (see Appendix B.2:

$$F(u)(t) = \text{sign}(\dot{u}(t))(f_1 - f_2) + \text{sign}(\dot{u}(0))\left(e^{-\frac{s(t)}{\epsilon_f}}f_2 - e^{-\frac{s(t)}{\epsilon_f \eta}}f_1\right) \tag{3.17}$$

So, the only necessary components are the total distance covered $s(t)$, the sign of the displacement rate at the current time and at the start of the interval.

Finally, in order to ensure that the system is dissipative Bliman and Sorine [BS95] give the following conditions:

$$f_1 > \quad f_2 \quad \geq 0 \tag{3.18}$$

$$\epsilon_f > 0 \quad \text{and} \quad 0 < \eta < 1 \tag{3.19}$$

Chapter 4

A Model for Fabric Hysteresis

From the discussion of fabric bending in Chapter 2, it is clear that there are a number of mechanisms that influence the bending behaviour. From Kawabata [Kaw80] hysteresis is exhibited in the results from the KES. So, any model that purports to accurately reproduce the bending behaviour should contain elements that can model hysteretic effects. There has been little work in modelling the hysteresis shown in fabric mechanics. As a result, the current techniques used in fabric simulations are unable to capture all (or even most) of the characteristics of the mechanical property curves. To remedy this it is necessary to borrow modelling techniques from other fields.

This chapter focuses on a modification to the friction modelling technique by Bliman and Sorine [BS93a, BS93b, BS95] to model the bending behaviour of fabrics. The specifics of the model as well as investigations in fitting parameters to experiments are detailed in this chapter.
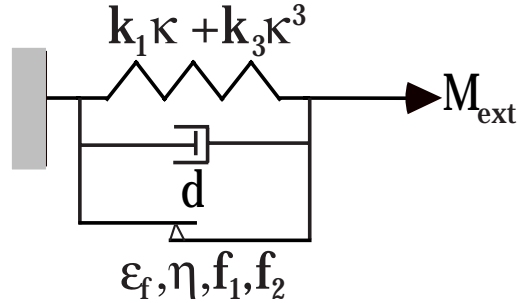
Figure 4.1: Model of Fabric Bending

4.1 The Model

A simple model of linear elastic bending is a spring element. In order to capture rate-dependent effects, a damper element is also necessary. Lindberg *et al.*[LBD61] introduced both friction and damper elements in their load-deformation model of fabric. The shape of the initial bending curve indicates that there is likely more than a linear viscoelastic behaviour so we will also include a non-linear cubic spring element in the model. Finally, we include a frictional element to model the hysteresis exhibited in the experiment. This model is depicted in Figure 4.1. The equation for the model is given in Equation (4.1) below. In Section 4.3, we investigate the effect of the different model components.

$$m\ddot{\kappa} = k_1\kappa + d\dot{\kappa} + k_3\kappa^3 + M_f(\kappa) + M_{ext} \tag{4.1}$$

To model the frictional hysteresis produced during bending we use the second order model of Bliman and Sorine [BS95] described in Section 3.3. We have two forms of the frictional model that we can use. First, we have the differential equation form as represented in Equation (3.1). Second, we have the integral form as shown in Equation

(3.16). The first form is useful if the displacement history is to be calculated, the second is useful if the displacement history is known. If we assume (or know) that there is no initial displacement from rest, we can use Equation (3.17) to model the frictional bending restraint. This form is useful for our purposes because the displacement is controlled during the KES-FB test. Converting the notation into the moment-curvature form we get:

$$M_f(\kappa)(t) = (f_1 - f_2)\text{sign}(\dot{\kappa}(t)) + \text{sign}(\dot{\kappa}(0))\left(e^{-\frac{s(t)}{\epsilon_f}}f_2 - e^{-\frac{s(t)}{\epsilon_f\eta}}f_1\right) \qquad (4.2)$$

where $s(t)$ is the total curvature that the fabric has experienced at time t as given in Equation (4.3):

$$s(t) = \int_0^t |\dot{\kappa}| dt \qquad (4.3)$$

4.2 Determining Model Parameters from Experiments

Now that the model has been determined, it is necessary to fit the model to experimental results. If we are trying reproduce the KES bending test we know the curvature and its corresponding derivatives at each point in time and we are trying to calculate the correlated external moment. Therefore, looking at a different problem to that in Equation (4.1), and we can write the new problem as:

$$M_{ext} = m\ddot{\kappa} - k_1\kappa - d\dot{\kappa} - k_3\kappa^3 - M_f(\kappa) \qquad (4.4)$$

where $M_f(\kappa)$ is determined by Equation (4.2). As was mentioned in Chapter 2, acceleration transition regions are needed between the points of rest and the constant rate of 0.5 cm^{-1}/s mentioned in Kawabata [Kaw80]. However, since they are not discussed in Kawabata, they will have to be estimated. Given that the above model is dependent upon the acceleration, velocity, and position these transition regions will be important.

4.2.1 Modelling the KES Bending Test Position, Velocity, and Acceleration Profiles

The KES Bending Test consists of three phases:

1. Bending to a maximum positive curvature K_+;

2. Bending to a maximum negative curvature K_-; and

3. Bending back to zero curvature.

Each of these phases consists of an initial acceleration to constant velocity, a period of constant velocity, and deceleration to rest. Thus, we must define the position, velocity and acceleration profiles for these nine regions. These are shown in Figure 4.2.

Nomenclature

In addition to the nine regions in Figure 4.2, we can also divide the curves into other categories:

1. **Initial Loading Path**. Consists of the first three regions.

2. **Unloading Path**. Consists of region 4 and the portion of region 5 until the moment axis.

3. **Reverse Loading Path**. Consists of the remaining portion of region 5 and all of region 6.

4. **Reverse Unloading Path**. Consists of the final three regions.

In the following subsections, displacement is used to mean curvature, velocity to mean curvature rate, and acceleration to mean the second derivative of curvature with respect to time.
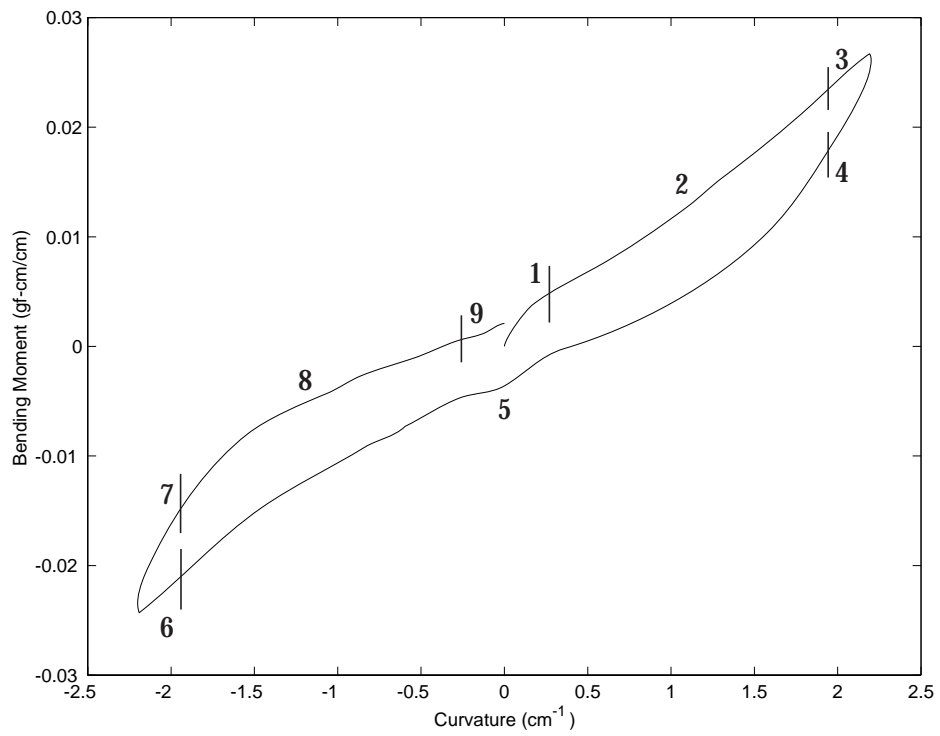
Figure 4.2: KES Bending Test Regions

The Initial Acceleration Region (1)

In order to achieve a constant velocity, it is necessary to accelerate up to some maximum value and then reduce the acceleration back to zero with the integral over that time frame equal to the desired constant velocity value. However, there are a wide range of acceleration profiles that acheive that task. The basic constraints are given below:

$$v(0) = 0 \tag{4.5}$$

$$v(T) = 0.5 \, cm^{-1}/s \tag{4.6}$$

$$a(0) = 0 \tag{4.7}$$

$$a(T) = 0 \tag{4.8}$$

where T is the total time taken to reach constant velocity. The simplest equation that can meet these constraints is a quadatric polynomial. The chosen polynomial is given in Equation (4.9). A plot of the acceleration profile with a time period of one second is given in Figure 4.3. Note that this does not give zero jerk at zero or at the transition time T. While it may be possible to acheive the above constraints with zero jerk at the transition points with a spline curve, polynomials of higher degree than quadratic must have some negative acceleration region in order to meet the zero jerk requirement.

$$a_1(t) = -3\frac{t(t-T)}{T^3} \tag{4.9}$$

The resulting velocity profile that arises is given in Equation (4.10). A plot of this profile with a time period of one second is given in Figure 4.4.

$$v_1(t) = -\frac{1}{2}\frac{t^2(2t-3T)}{T^3} \tag{4.10}$$
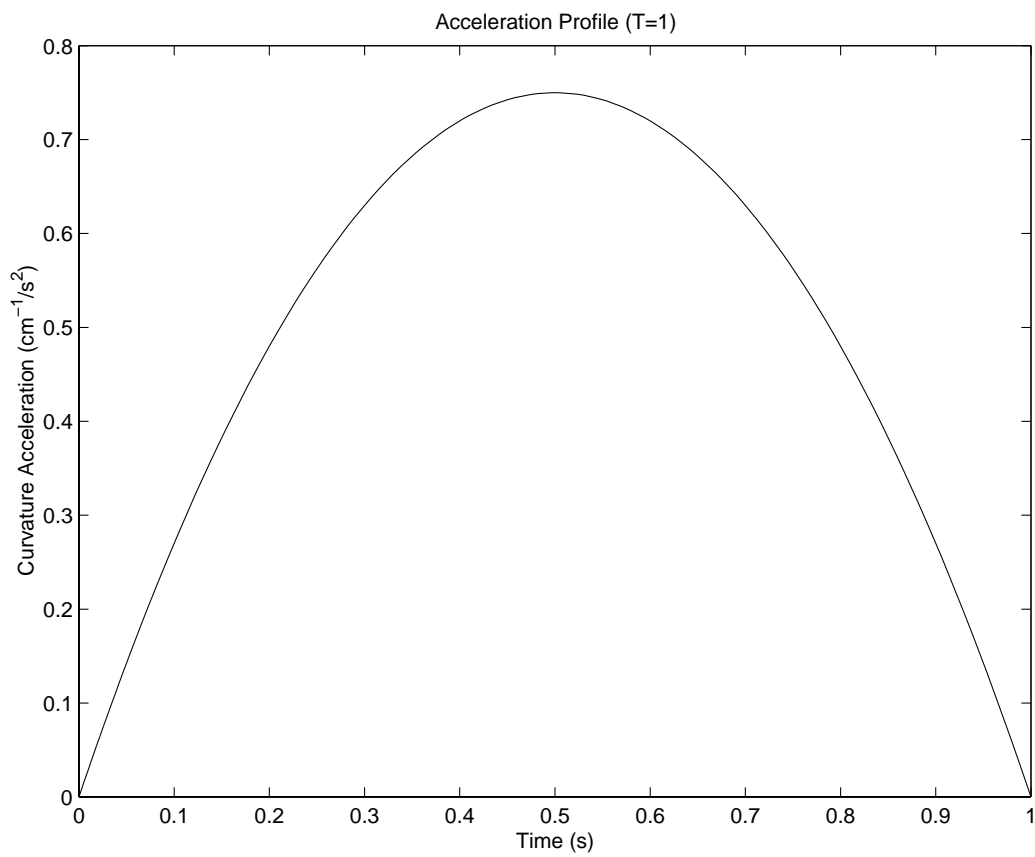
Figure 4.3: Acceleration Profile (T=1)
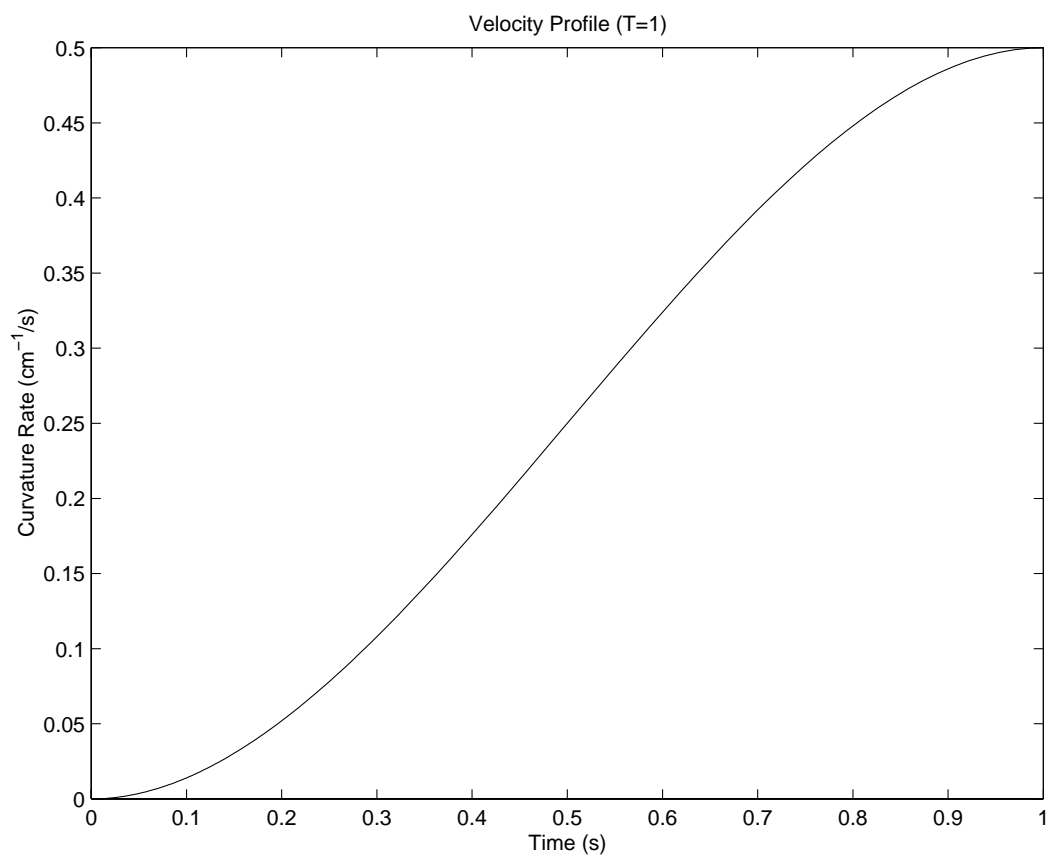
Figure 4.4: Velocity Profile (T=1)

The displacement in this region is given by the integral of the velocity profile. The displacement equation is shown in Equation (4.11).

$$d_1(t) = -\frac{1}{4}\frac{t^3(t-2T)}{T^3} \tag{4.11}$$

The total displacement in this region is $\frac{T}{4}$.

The Constant Velocity Region (2)

In this region, we know that the acceleration is zero and that the velocity is $0.5\ cm^{-1}/s$. The displacement equation for this region (including the displacement from the previous region) is:

$$d_2(t) = \frac{t}{2} - \frac{T}{4} \tag{4.12}$$

The Deceleration Region (3)

The acceleration profile used in this region is the negative of that given in Equation (4.9) with the substitution of $t = t - t_2$ where t_2 is the time where deceleration begins. This results in Equation (4.13).

$$a_3(t) = 3\frac{(t-t_2)(t-t_2-T)}{T^3} \tag{4.13}$$

Since we know the final displacement in this region from experiment, we can determine the total time for the loading path T_{fl}. Knowing that the deceleration starts at time $T_{fl} - T$ we can make this substitution for t_2 in Equation (4.13) and get:

$$a_3(t) = 3\frac{(t-T_{fl}+T)(t-T_{fl})}{T^3} \tag{4.14}$$

We know that the initial velocity is V_d and that the change in velocity is given by:

$$v_c(t) = -v_1(t - t_2) \qquad (4.15)$$

where $v_1(t)$ is the velocity profile in the acceleration region. Therefore, the velocity profile in the deceleration region is:

$$v_3(t) = \frac{1}{2} + \frac{(t - T_{fl} + T)^2(2t - 2T_{fl} - T)}{2T^3} \qquad (4.16)$$

Using the same approach, the acceleration, velocity, and displacement equations can be derived for the remaining sections of the test curve. For complete details see Appendix B.3.

4.2.2 Fitting the Model Parameters to Experiments

Optimisation techiques are used in order to determine the values of the model parameters that best approximate the experimental results. To facilitate the optimisation, the position, velocity, and acceleration for the experiment were pre-calculated. Thus, one can vectorise the solution for M_{ext} in Equation (4.4). The design variables are f_1, f_2, ϵ_f, η, k_1, d, and k_3. It is assumed that T (the acceleration time) is a constant for the test equipment and will be set *a priori*.

Since the equipment to perform the experimental tests is not available at this university, Deng's experimental data [Den94] was used. Model fits were attempted for two types of fabric with varying weaves and yarn types. The types of fabric are given in Table 4.1. The basic fabric properties are given in Table 4.2.

Quantifying the Fit

In order to quantify the quality of the fit, a least squares criterion was used. The objective function to minimise is given in Equation (4.17). However, since M_{exp} is not

Fabric No.	Colour	Weave	Description
Fabric 1	White	Satin	100% Polyester. Bleached, dyed, and pre-shrunk in a resin finish.
Fabric 2	White	Twill	100% Cotton. Bleached, dyed, and pre-shrunk in a pure finish.

Table 4.1: Details of Fabrics Tested [Den94]

Fabric No.	Thickness (cm)	Weight Density (gmf/cm^2)
Fabric 1	0.0254	0.01715
Fabric 2	0.0489	0.02665

Table 4.2: Fabric Properties [Den94]

defined as a continuous function, fourth order polynomials were fit to the loading, un-load/reverse loading, and re-loading paths. These were substituted for M_{exp} for each of the paths. While the total number of points varied depending upon the experimental results, the model and polynomial fits to experiment were sampled at intervals of one millisecond.

$$R(\kappa) = \sum (M_{model}(\kappa) - M_{exp}(\kappa))^2 \tag{4.17}$$

A portion of the objective surface for the weft direction of Fabric 1 is shown in Figure 4.5. We can see that this hyperplane has a line of optimal solutions. While this portion of the surface could be optimised through SQP methods, there may be difficulties with other parts of the objective surface.

Optimisation Techniques

Initially, the optimisation was attempted using a genetic algorithm implemented in MATLAB by Ajay Seth [Set00]. A genetic algorithm was used because it is a global search technique that has the possibility of finding the global optimum. Using this
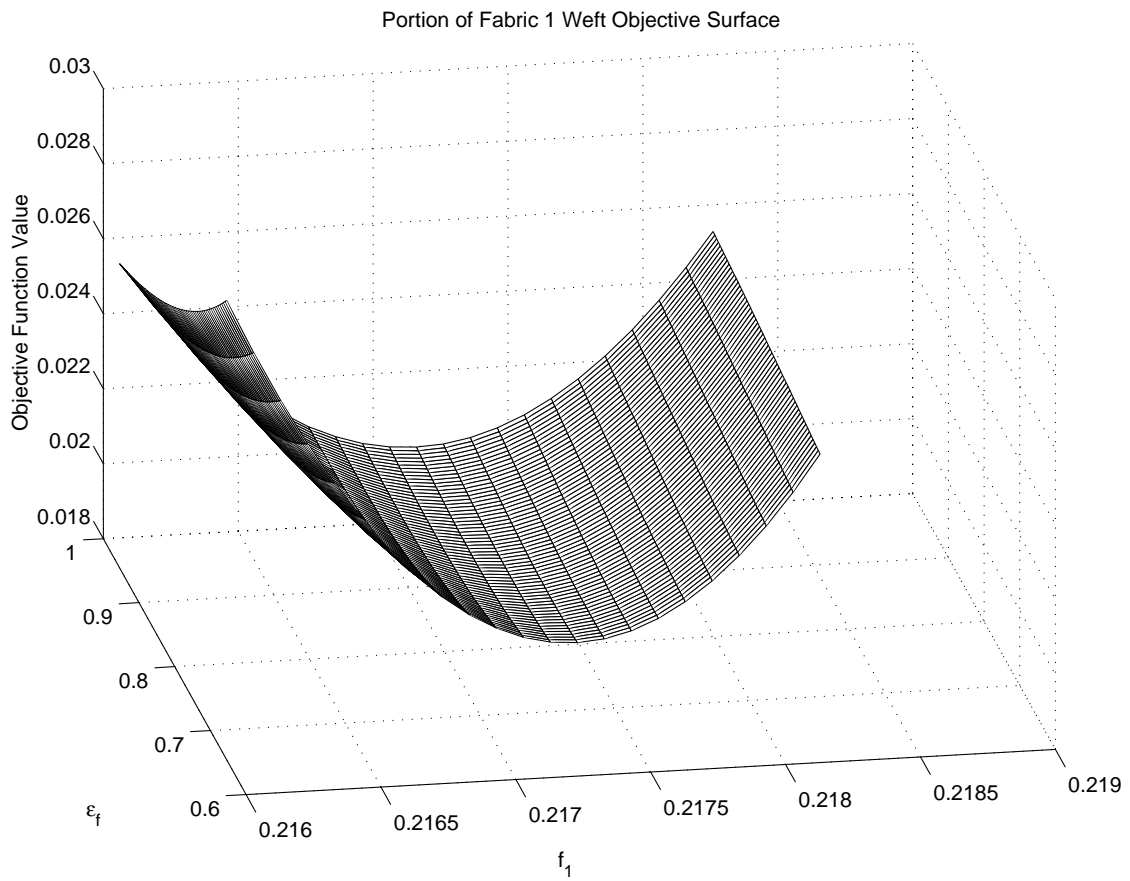
Figure 4.5: Portion of Fabric 1 Weft Direction Objective Surface

implementation, some difficulties were found. There was considerable difficulty in describing what constitutes a converged solution. As a result, the genetic algorithm never converged to the same solution.

Because of the above difficulties, MATLAB's non-linear least squares solver, LSQCURVEFIT (part of the Optimization toolbox) was used to find the optimal solution. Because this algorithm requires an initial guess, the best solution from the genetic algorithm tests were used as a seed to the solver. In all cases, the results from the genetic algorithm were improved.

Because of the difficulties in converging to a globally optimal solution with the earlier methods, a MATLAB interface [Sak00] to publically available simulated annealling code [Ing00] (described in [Ing89],[Ing92],[Ing93], [Ing96]) was also tried. This approach produced better results than with either the genetic algorithm or GA/LSQCURVEFIT combination. As such, the optimisation results in the following section were produced with this technique.

4.3 Simulation Results

To understand some of the difficulties in capturing the behaviour of these fabrics we present the $+\kappa$ and $-\kappa$ slopes and their differences for each fabric and direction. They are shown in Table 4.3. In all cases, the slope of the moment-curvature graph shows large differences between the bending directions. In addition, one direction showed a increase in slope rather than a decrease.

The following cases were considered for each of the fabric types and directions.

1. Complete model including friction and a cubic spring;

2. As above, assuming no slowing to rest at the end of test;

3. Complete model but excluding friction;

Fabric No. and Direction	$+\kappa$ slope	$-\kappa$ slope	% Difference
Fabric 1 - Warp	0.322	0.264	18.0 %
Fabric 1 - Weft	0.199	0.125	37.2 %
Fabric 2 - Warp	0.598	0.477	20.2 %
Fabric 2 - Weft	0.145	0.196	-26.0 %

Table 4.3: Directional Slope Comparsion

4. Complete model but excluding the cubic spring;

5. A linear model that excludes both friction and the cubic spring.

4.3.1 Fabric 1 Results
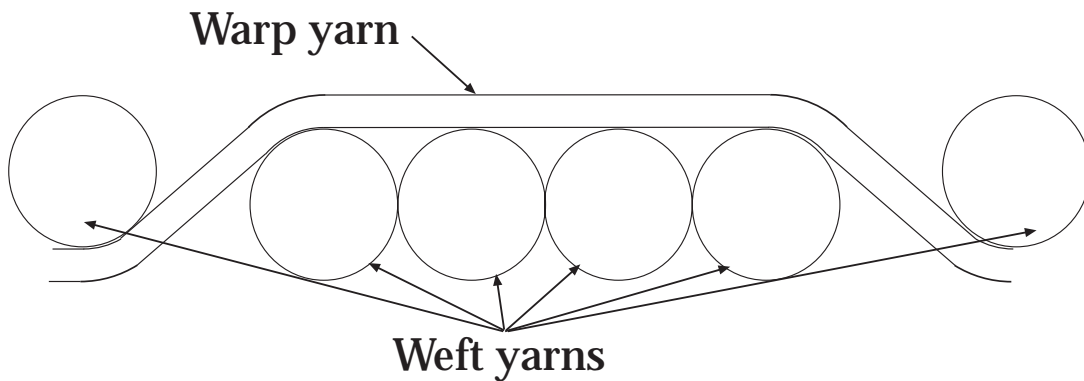
Figure 4.6: Warp-float Satin (4x1) Weave Cross-section

Figure 4.6 shows a cross-section of a 4x1 warp-float satin weave while Figure 4.7 shows the pattern. The warp is represented in black while the weft is represented in white.
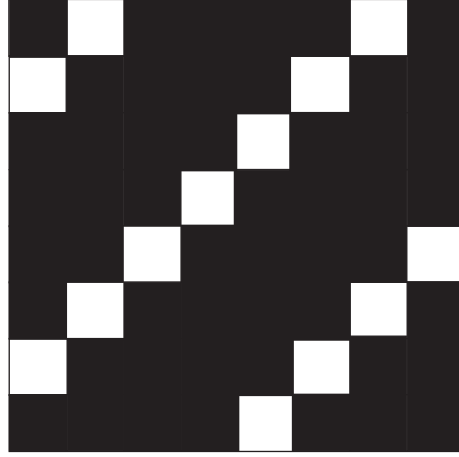
Figure 4.7: Warp-float Satin (4x1) Weave Pattern

Parameter	Value
f_1	$6.184 \times 10^{-1} \ gmf - cm$
f_2	$6.164 \times 10^{-1} \ gmf - cm$
η	9.998×10^{-1}
ϵ_f	$7.302 \times 10^{-1} \ gmf - cm/cm$
d	$5.793 \times 10^{-3} \ gmf - cm/s$
k_1	$6.380 \times 10^{-3} \ gmf - cm$
k_3	$8.656 \times 10^{-4} \ gmf - cm^3$

Table 4.4: Fabric 1 - Warp Direction: Model Parameters

Parameter	Value
s_e	$10.92 \ cm^{-1}$
s_p	$2.19 \ cm^{-1}$
f_k	$0.198 \times 10^{-2} \ gmf - cm$
f_s	$0.198 \times 10^{-2} \ gmf - cm$

Table 4.5: Fabric 1 - Warp Direction: Supplementary Friction Results

Warp Direction

The final parameters determined through the optimisation procedure are given in Table 4.4. Examining Table 4.5 we see some interesting results. First, the curvature value s_e required for reaching the maximum static friction value f_s is greater than the value s_p required to reach the dynamic friction threshold f_k. Second, there is no difference between the static and dynamic friction values. These two observations combined, indicate that only dynamic friction is present.

In Table 4.6 we can quickly compare the quality of the model fit for each of the different test cases. The complete model provides the best fit, as measured by the residual, out of all the test cases and we can see that the cubic term is very important to the model as the quality of the fit decreases significantly in the cases where it is not included.

Most figures in the remainder of this chapter show comparisons of three different curves. The dash-dotted line is the digitised version of experimental results from Deng's thesis [Den94]. The dotted line is constructed from three separate fourth order polynomial fits to the digitised data. One polynomial is fit to the loading path, another to the unloading/reverse loading path, and the third to the reverse unloading path. The solid line shows the model simulation results.

Examining Figure 4.8, we can see that the model provides an excellent fit throughout most of the experiment. In the initial loading stage, the model provides a better fit than the fourth order polynomial. The greatest disagreement in the model appears in the final reloading path. The model result curves inwards due to the slowing of the curvature rate.

Figure 4.9 shows the result if we assume that there is no final deceleration region. While the final inward curvature from Figure 4.8 is not presenet, the path continues to diverge from the experimental results, but nearly completes a cycle. This implies that this model does not exhibit any hardening or softening behaviour. This behaviour is

also shown with the weft direction and in both directions for the other fabric. As a result, the plots of those results are not shown.

If we remove the friction term from the model and then try to fit the model to the experimental data as is shown in Figure 4.10, it is not possible to acheive the final M_{ext} value. Instead, the model returns to zero external moment. In addition, the model is unable to fit parts of the initial loading and final reloading paths as closely as in the full model.

If we remove the cubic term from the model the best result is shown in Figure 4.11. Without this term, the path followed is generally straight with the curves resulting from the transition to and from a constant curvature rate.

Lastly, if we consider a linear viscoelastic model, that is a model without the cubic or the friction term, we get the results shown in Figure 4.12 which is a very poor fit, with a residual nearly 9x that of the full model.

Test Case	Residual
Full Model	1.104×10^{-2}
No Deceleration at End	1.545×10^{-2}
No Friction Term	2.523×10^{-2}
No Cubic Term	5.792×10^{-2}
No Friction or Cubic Term	8.977×10^{-2}

Table 4.6: Fabric 1 - Warp Direction: Model Comparision

To understand the relative contribution of the frictional component of the model in Figure 4.8 we will separate the friction component from the other components of the model resulting in Figures 4.13 and 4.14. From Figure 4.13 we can see that the model exhibits first-order behaviour. That is, no static friction is observed, only dynamic friction. Also of note is the fact that the maximum frictional moment is two orders of magnitude
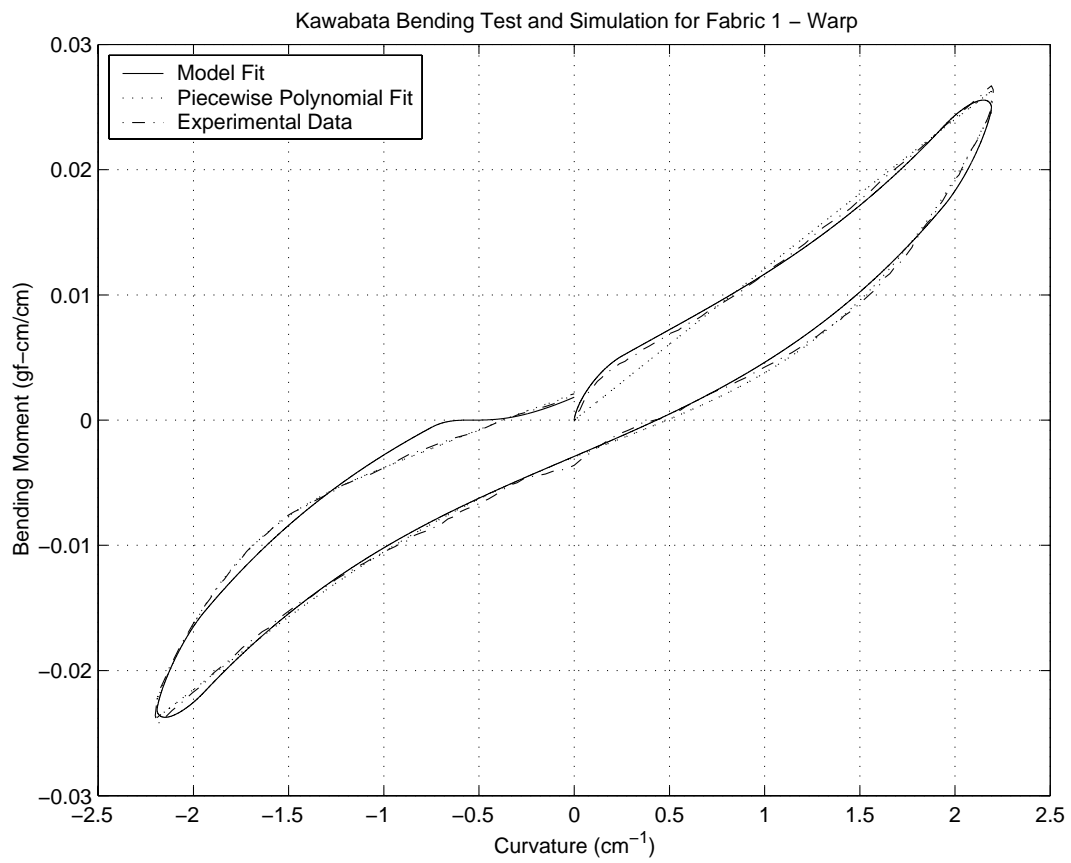
Figure 4.8: Fabric 1 - Warp Direction Full Model
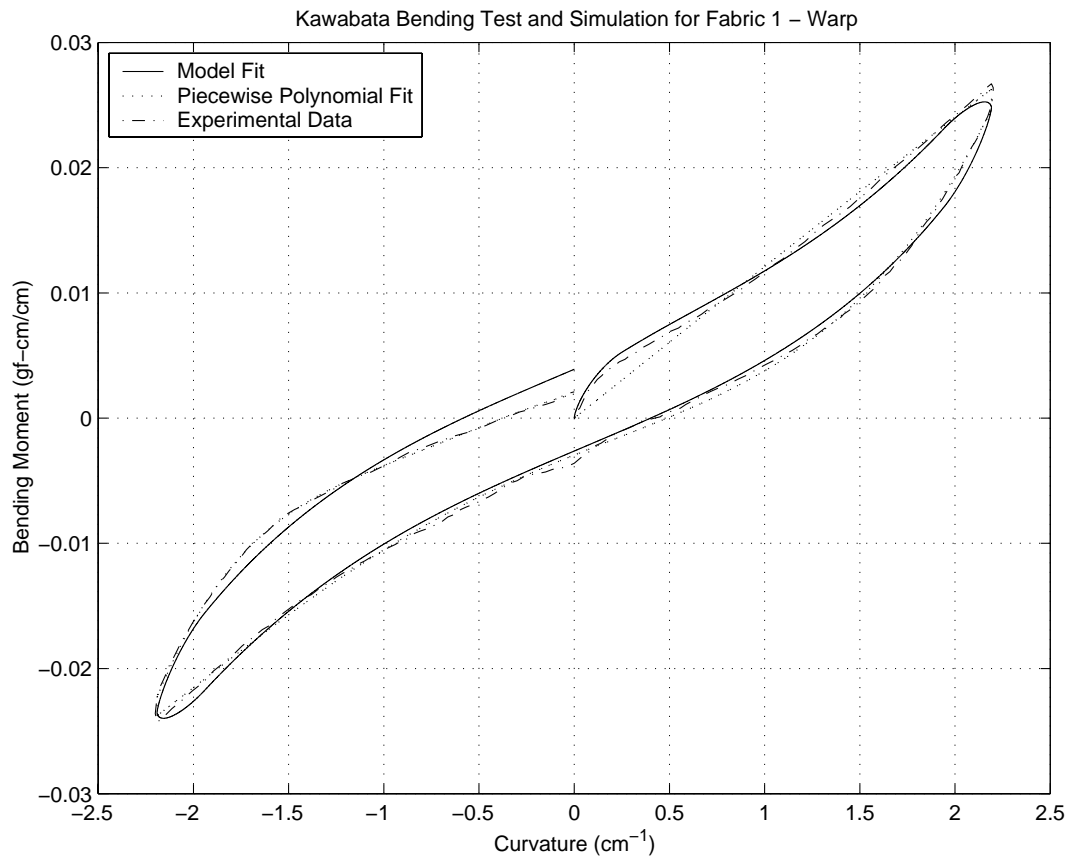
Figure 4.9: Fabric 1 - Warp Direction (No Slowing at End)
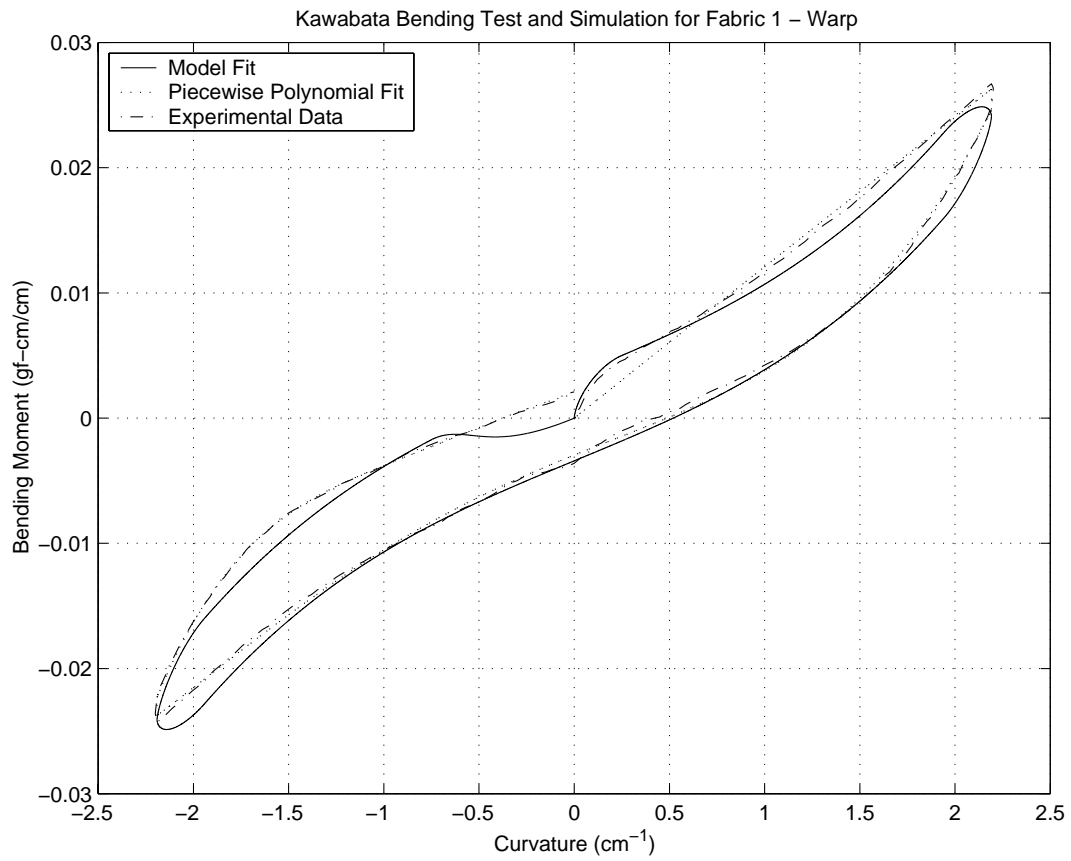
Figure 4.10: Fabric 1 - Warp Direction (No Friction Term)
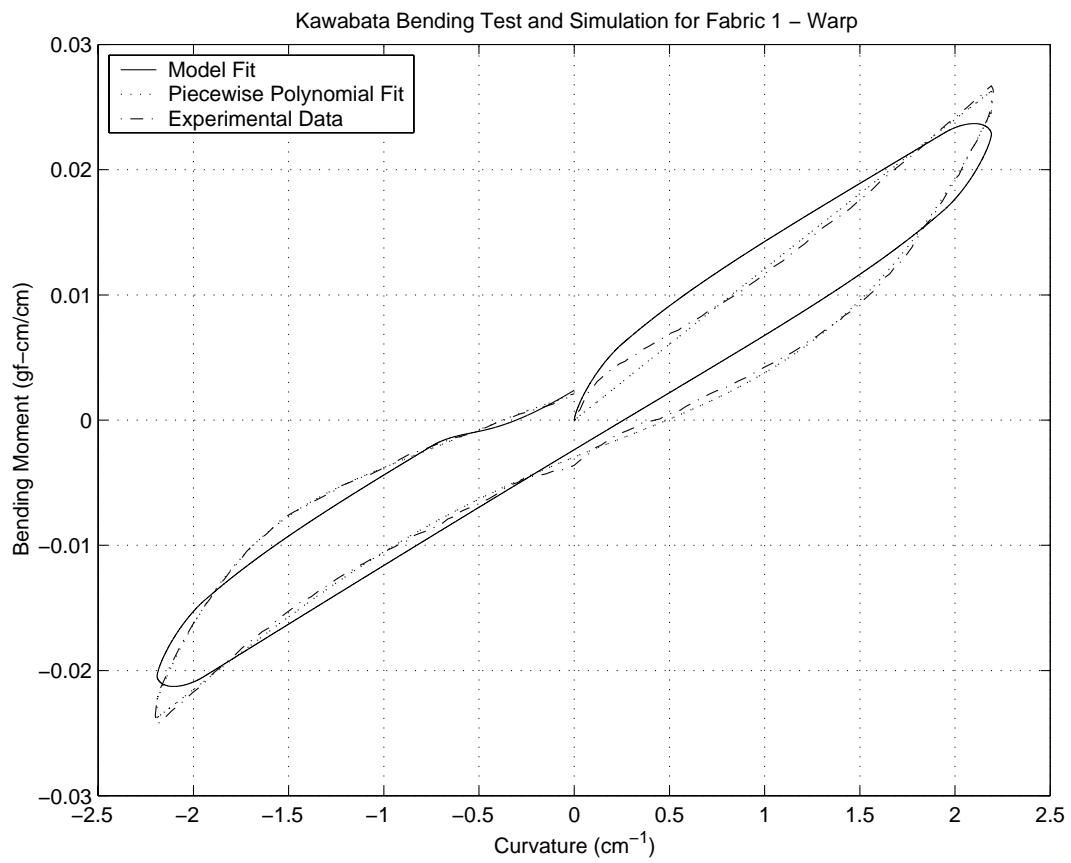
Figure 4.11: Fabric 1 - Warp Direction (No Cubic Term)
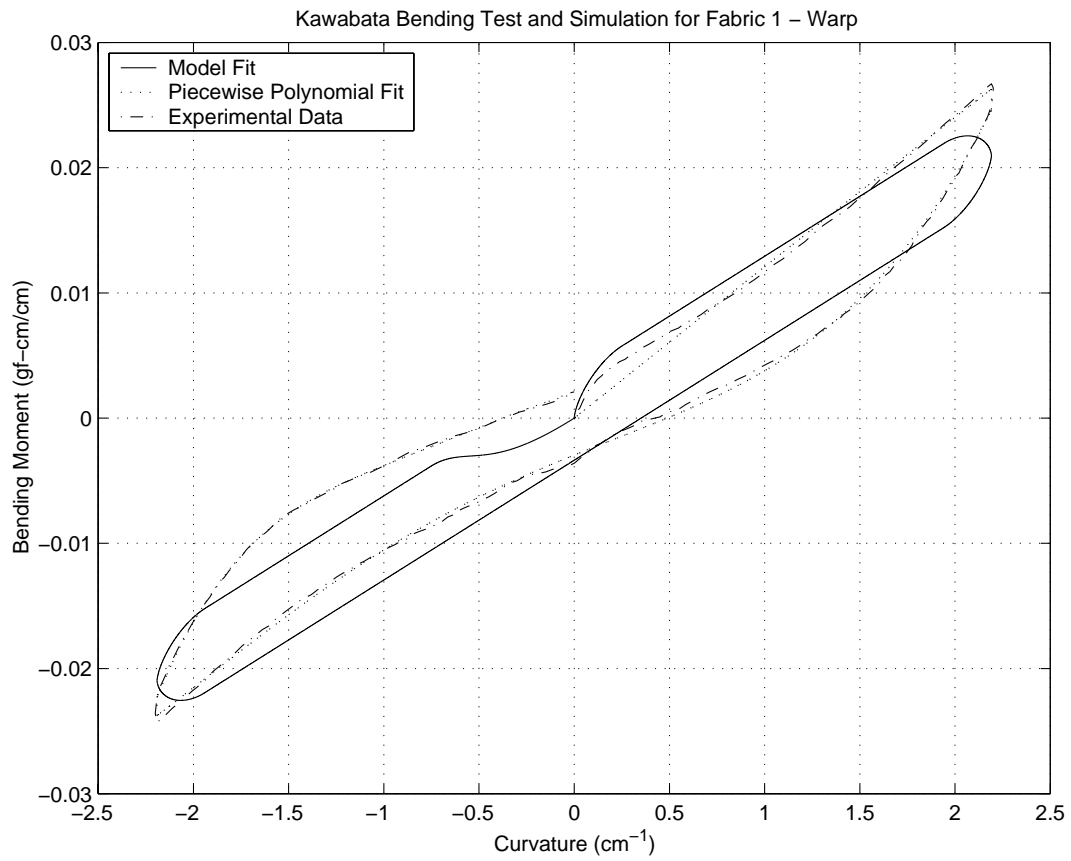
Figure 4.12: Fabric 1 - Warp Direction (No Cubic or Friction Term)

less than the external moment exhibited in Figure 4.14. Yet, the friction plays a key role in acheiving a good overall fit.

Initially, the inertial term dominates the behaviour of the model. This can be seen from the similarities in the initial portion of the loading curve (Figures 4.8-4.12), even without the cubic and friction terms. It is believed that the friction arises due to the slipping of the yarns with respect to each other. In this case, we have the warp yarn slipping over the weft yarns which act like ball bearings. This is consistent with the frictional response given in Figure 4.13. The cubic term appears to arise from the jamming of the yarns and their subsequent compression, although some of the response may be due to a non-linear yarn bending response.
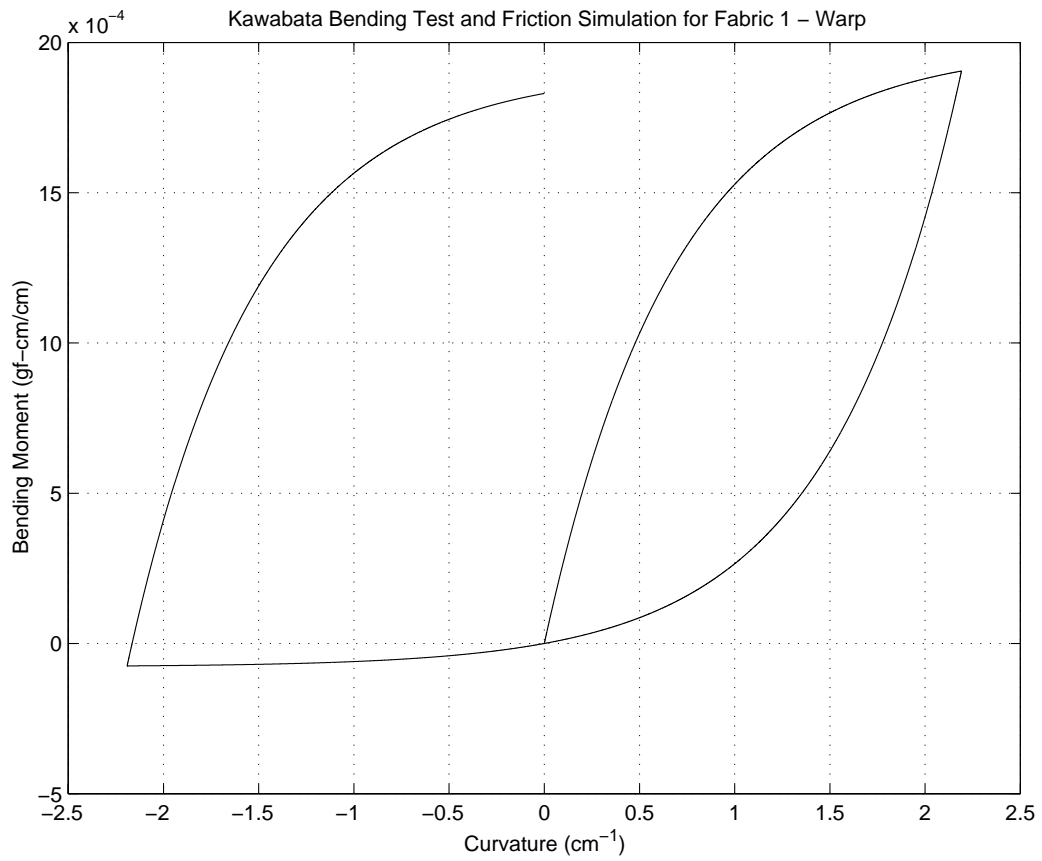
Figure 4.13: Fabric 1 Warp - Frictional Contribution
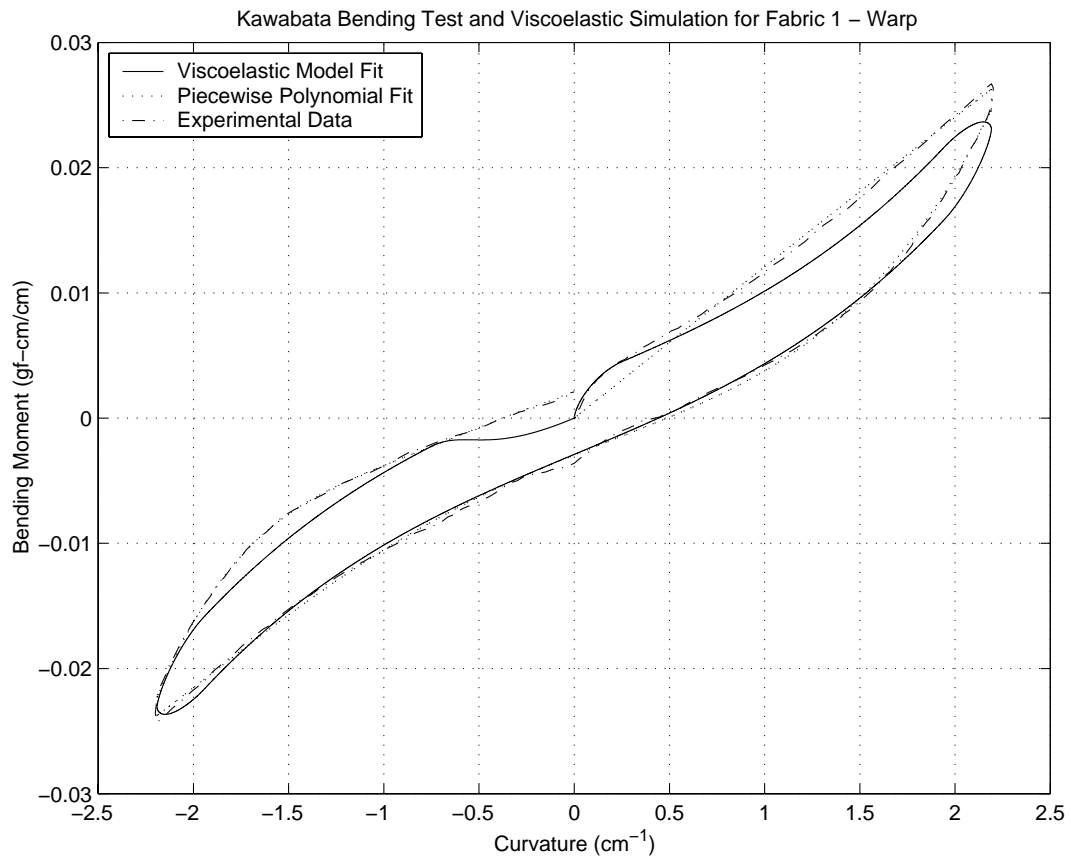
Figure 4.14: Fabric 1 Warp - Non-linear Visco-elastic Contribution

Weft Direction

In contrast to the warp direction, the weft direction for this fabric exhibits more complicated behaviour. First, the maximum bending moment measured is approximately half that of the warp direction. Second, the reverse bending portion (the negative half the of graph) has a smaller loop width and slope. This would indicate that the fabric has different parameters for forward and reverse bending. This behaviour is not implemented in the current model so it cannot accurately capture this behaviour.

Parameter	Value
f_1	$2.173 \times 10^{-1} \ gmf - cm$
f_2	$2.161 \times 10^{-1} \ gmf - cm$
η	9.876×10^{-1}
ϵ_f	$7.316 \times 10^{-1} \ gmf - cm/cm$
d	$2.141 \times 10^{-3} \ gmf - cm/s$
k_1	$4.548 \times 10^{-3} \ gmf - cm$
k_3	$1.619 \times 10^{-4} \ gmf - cm^3$

Table 4.7: Fabric 1 - Weft Direction: Model Parameters

Parameter	Value
s_e	$1.07 \ cm^{-1}$
s_p	$2.19 \ cm^{-1}$
f_k	$0.127 \times 10^{-2} \ gmf - cm$
f_s	$0.189 \times 10^{-2} \ gmf - cm$

Table 4.8: Fabric 1 - Weft Direction: Supplementary Friction Results

From Table 4.8 we can see that the maximum frictional moment f_s occurs at 1.07 cm^{-1} (s_e) which is approximately halfway through the initial loading path. We only approach the s_p value at the end of the initial loading path. In addition, the static

frictional moment f_s is about 6×10^{-4} $gmf - cm$ greater than the dynamic frictional moment f_k.

While none of the models provide an excellent fit, the full model still provides the best fit. As with the warp direction, the model fits better than the polynomial for the initial acceleration region. With respect to Figure 4.15, at a curvature of 1 cm^{-1} the model underestimates the external moment. On the reverse bending portion of the experiment, the model overestimates the external moment.

The magnitudes of the linear model parameters (d and k_1) are roughly half to three-quarters that of the warp direction (see Table 4.7). However, the magnitude of the frictional restraint (Table 4.8) is close to that in the warp direction and the non-linear stiffness k_3 is considerably smaller than that in the warp direction. If the non-linear stiffness is due to jamming of the yarns this behaviour could be due to a greater spacing between yarns in the warp direction than the weft.

Test Case	Residual
Full Model	1.974×10^{-2}
No Deceleration at End	2.250×10^{-2}
No Friction Term	3.879×10^{-2}
No Cubic Term	2.138×10^{-2}
No Friction or Cubic Term	4.474×10^{-2}

Table 4.9: Fabric 1 - Weft Direction: Model Comparision

As shown in Figure 4.16, if we remove the friction term, we get an excellent fit for the initial acceleration region, but a poorer overall fit. For the weft direction, the addition of the friction term contributes more to the overall fit than the cubic term as is shown in Table 4.9. As expected there is no external moment at the completion of the test.

If the cubic term is omitted from the model, there is little difference in the overall quality of the fit. This could be expected from examining the parameter k_3 parameter
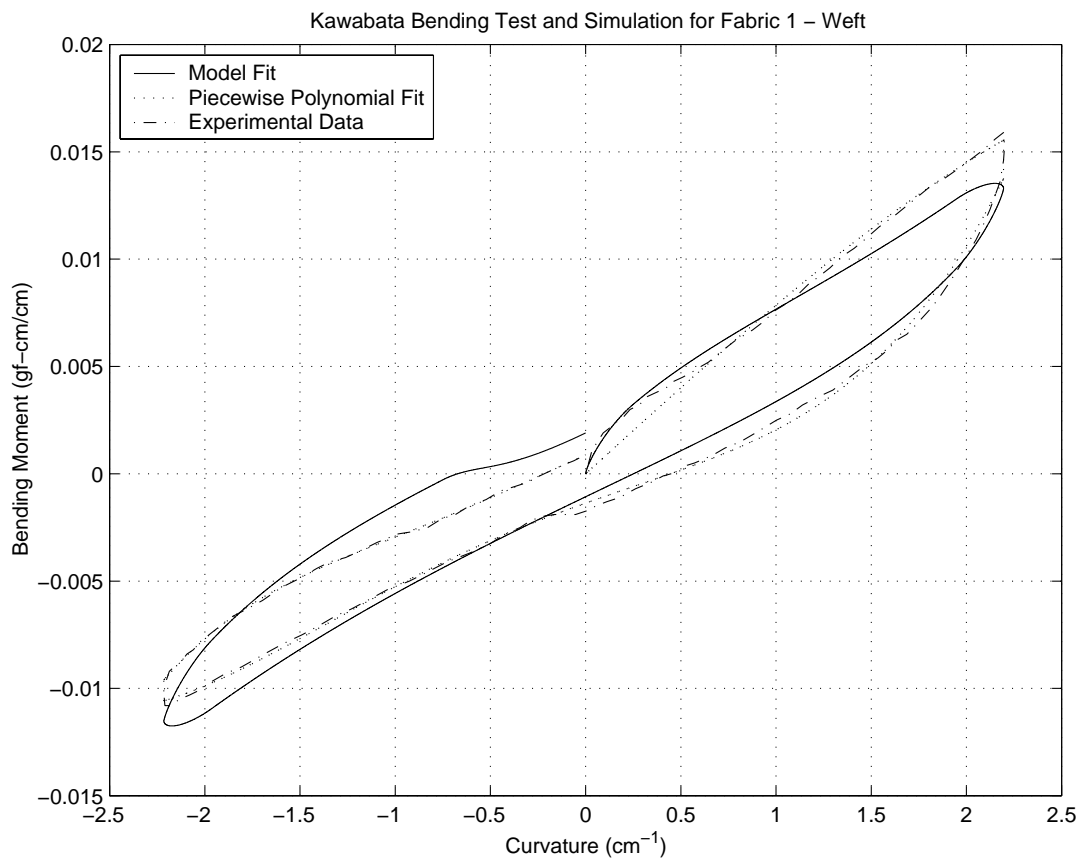
Figure 4.15: Fabric 1 - Weft Direction Full Model
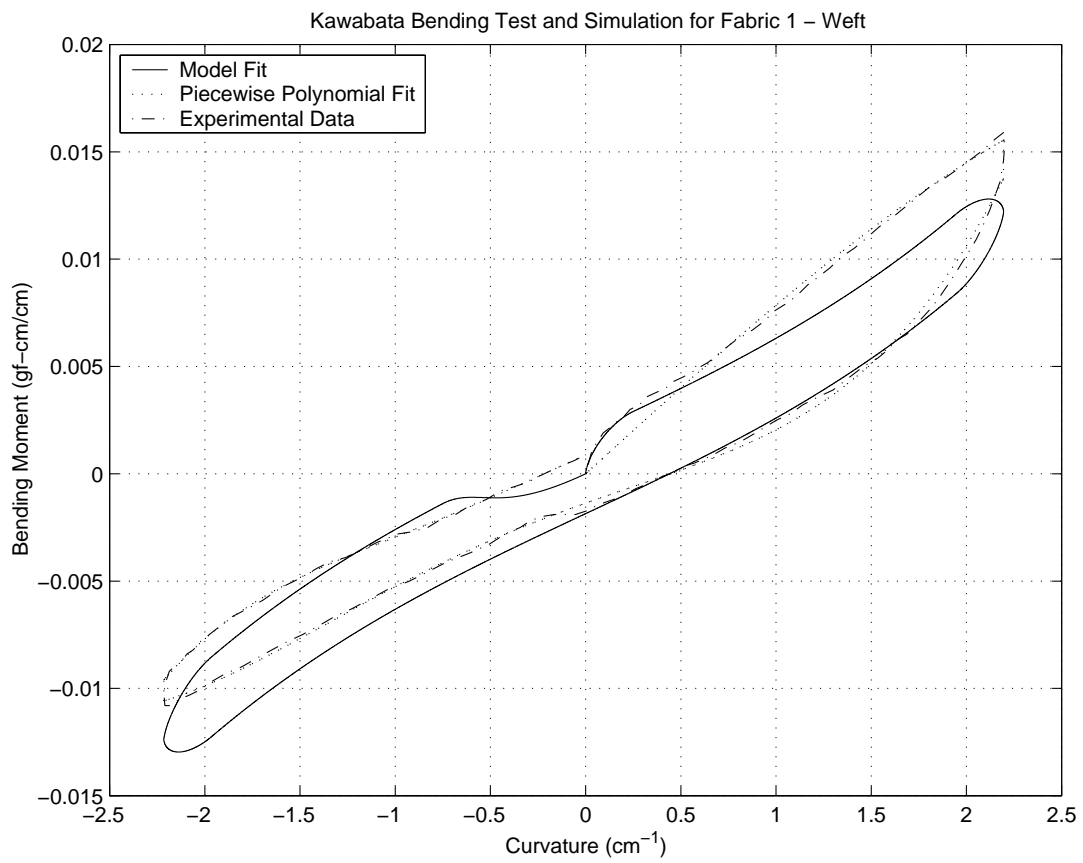
Figure 4.16: Fabric 1 - Weft Direction (No Friction Term)

value in Table 4.7 since it is an order of magnitude smaller than the other parameters.
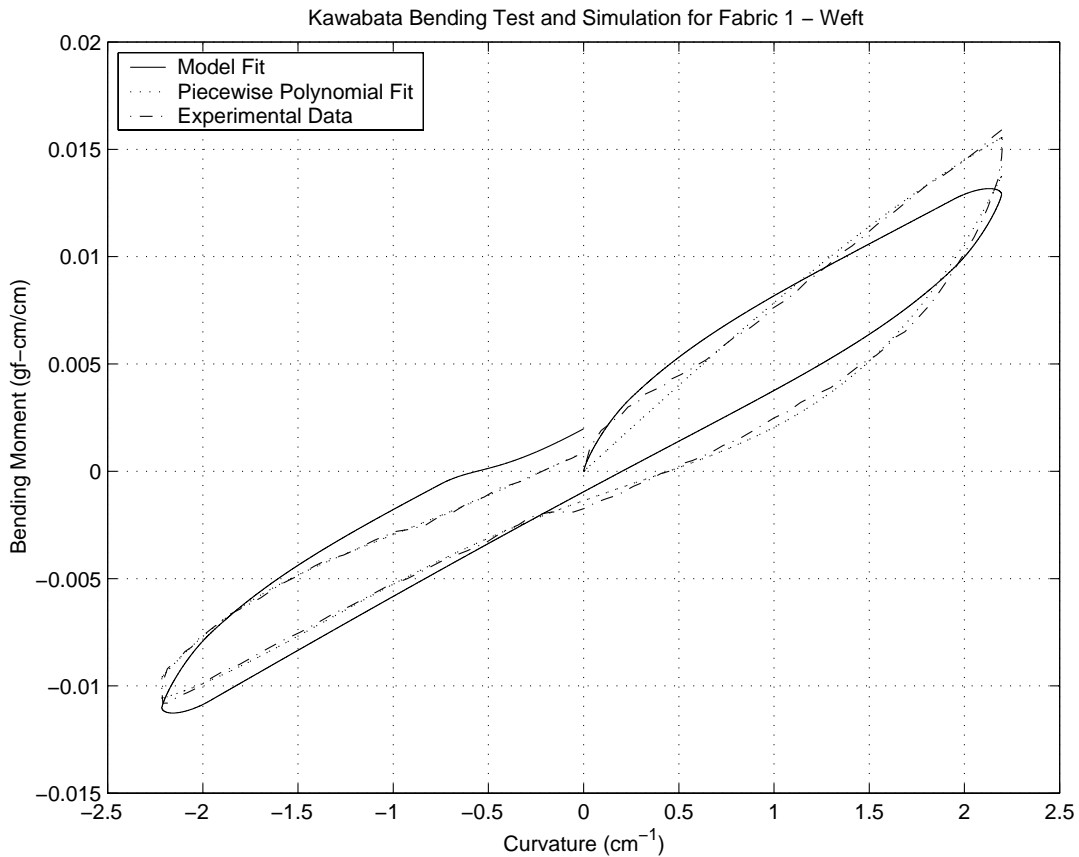
Figure 4.17: Fabric 1 - Weft Direction (No Cubic Term)

The difference without the friction and cubic terms for the weft direction is not as dramatic as in the warp direction case. However, as is shown in Figure 4.18, with these effects absent the model is unable to capture the subtle curve exhibited during the unloading portion of the experiment.

Unlike the warp direction, second order friction effects are observed. Examining Figure 4.19, we see that during initial loading static friction is overcome, but does not
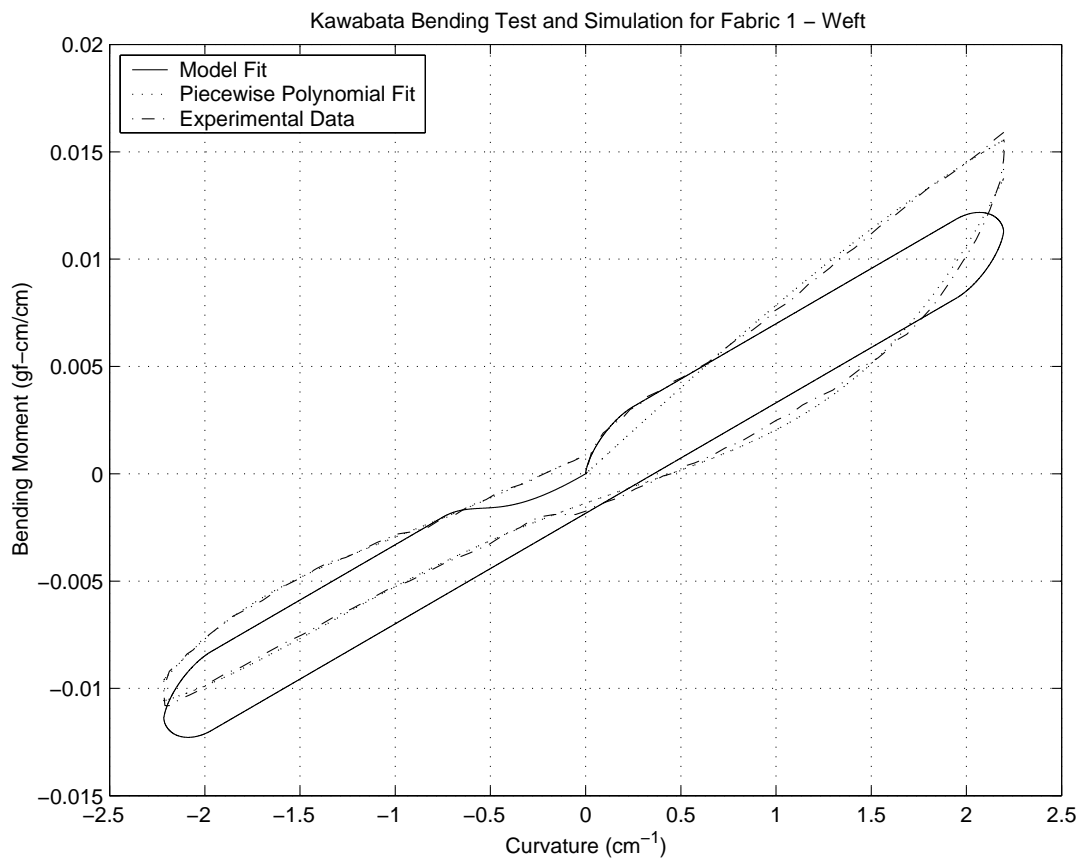
Figure 4.18: Fabric 1 - Weft Direction (No Cubic or Friction Term)

reach the dynamic friction value during the decay from the static friction peak. Using the results from Chapter 3, we see that the value of s_e is 1.071 cm^{-1} and a value of 2.195 cm^{-1} for s_p. We therefore see the decay to the dynamic friction during the reverse path.

In Figure 4.20 we can see that the loops are roughly half the width of the full model. In fact, the size of the loop for reverse bending is roughly the size of the experimental loop. This may indicate that there is little frictional restraint for reverse bending. Alternatively, this may be due to the characteristics of the test as only dynamic friction is present during the reverse loading path.
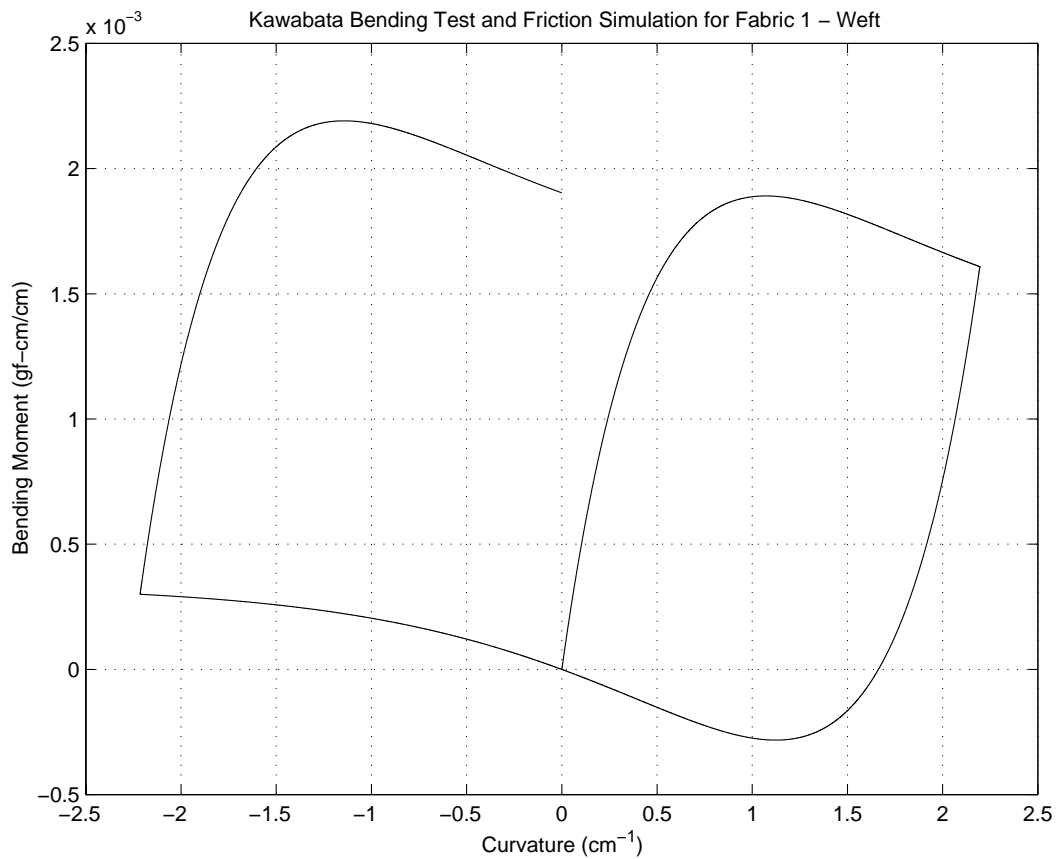
Figure 4.19: Fabric 1 Weft - Frictional Contribution
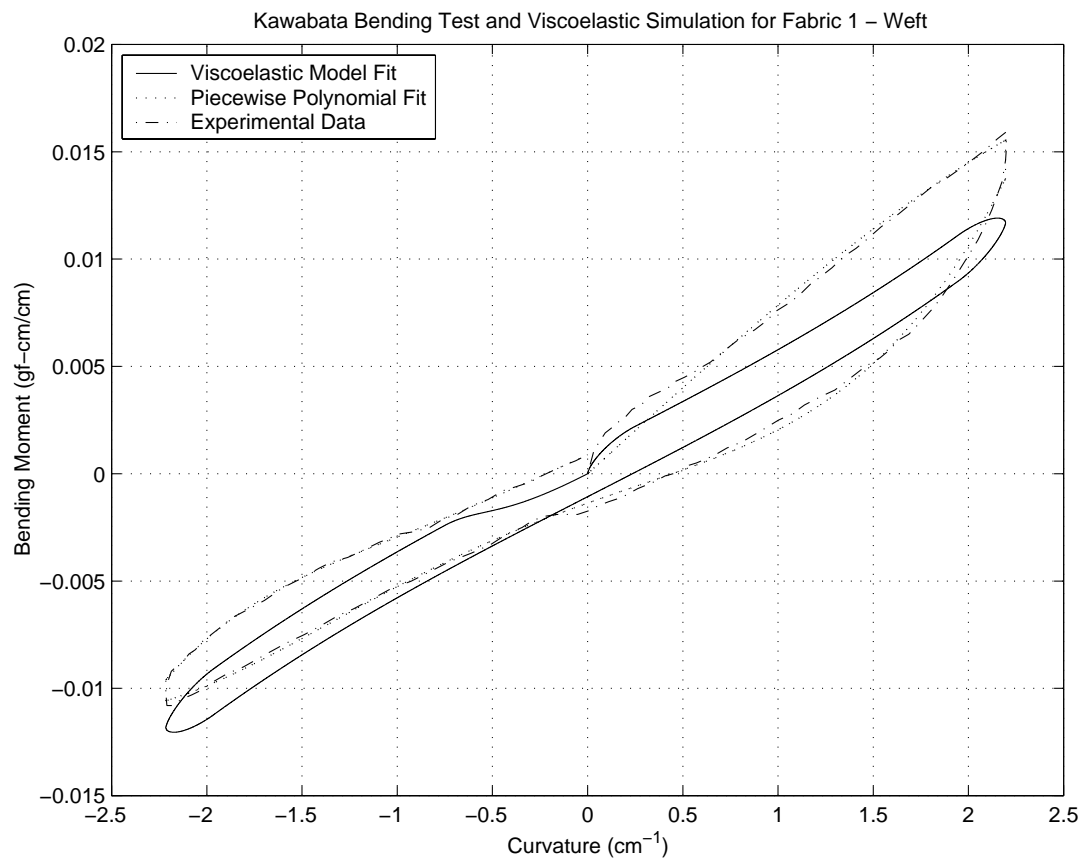
Figure 4.20: Fabric 1 Weft - Non-linear Visco-elastic Contribution

4.3.2   Fabric 2 Results
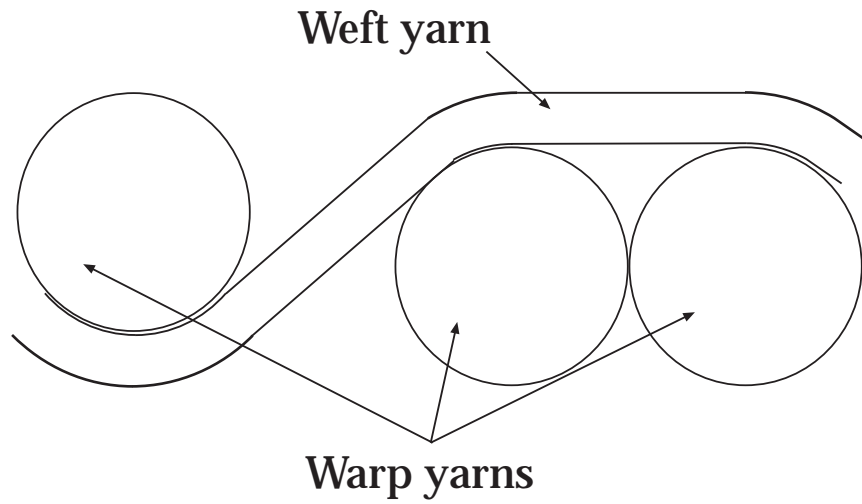
Figure 4.21: Twill (1x2) Weave Cross-section
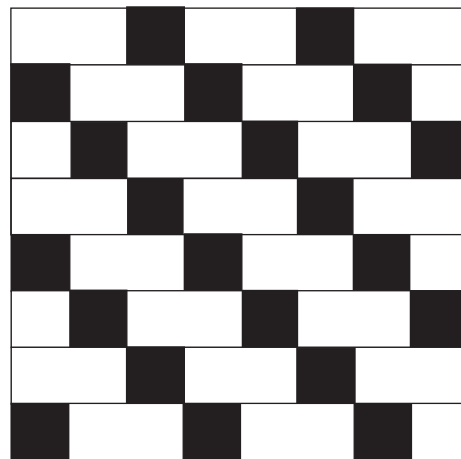
Figure 4.22: Twill (1x2) Weave Pattern

As stated in Table 4.1, this fabric is a twill fabric which means that there is a diagonal pattern of alternating weft and warp floats. Figure 4.21 shows a cross-section of a 1x2 twill weave while Figure 4.22 shows the pattern. The warp is represented in black while the weft is represented in white. In addition, this fabric is a 100 % cotton fabric. From Meredith [Mer59], we know that cotton fibres during tensile tests show hysteresis and that under cyclic loading conditions the slope of the curve (the modulus) becomes progressively steeper from one step to the next. These observations combined indicate that there are more factors than in the previous fabric, to consider in understanding the fabric's behaviour.

Warp Direction

Parameter	Value
f_1	$7.836 \times 10^{-1}\ gmf - cm$
f_2	$7.810 \times 10^{-1}\ gmf - cm$
η	9.949×10^{-1}
ϵ_f	$7.207 \times 10^{-1}\ gmf - cm/cm$
d	$1.474 \times 10^{-2}\ gmf - cm/s$
k_1	$1.154 \times 10^{-2}\ gmf - cm$
k_3	$1.092 \times 10^{-3}\ gmf - cm^3$

Table 4.10: Fabric 2 - Warp Direction: Model Parameters

Parameter	Value
s_e	$1.17\ cm^{-1}$
s_p	$2.16\ cm^{-1}$
f_k	$0.255 \times 10^{-2}\ gmf - cm$
f_s	$0.334 \times 10^{-2}\ gmf - cm$

Table 4.11: Fabric 2 - Warp Direction: Supplementary Friction Results

As with the weft direction of fabric 1, from Table 4.11 the maximum frictional moment occurs about half way through the initial loading path. In addition, the static and dynamic frictional moments are much greater than those exhibited by fabric 1.

Test Case	Residual
Full Model	1.067×10^{-1}
No Slow Down at End	1.200×10^{-1}
No Friction Term	1.663×10^{-1}
No Cubic Term	1.780×10^{-1}
No Friction or Cubic Term	2.791×10^{-1}

Table 4.12: Fabric 2 - Warp Direction: Model Comparision

Figure 4.23 shows that the model slightly underestimates the maximum loading moment. In addition, the loading slope of the model is slightly less than the loading slope of the experiment. However, the model does show a good fit for the the reverse loading portion from $0\ cm^{-1}$ through $-1.6\ cm^{-1}$. There is also a good fit for the region from $-2.25\ cm^{-1}$ to $-1.5\ cm^{-1}$ on the reverse unloading portion of the test.

As with the other direction (and fabric), when we omit the friction term, as shown in Figure 4.24, the model does not exhibit a final moment since both κ and $\dot{\kappa}$ go to zero. Therefore, only the friction term contributes to the final moment. The model has a poorer fit on the initial loading curve and the final deceleration region.

If we omit the cubic term in the model (Figure 4.25), we have an excellent fit through the reverse loading/unloading portion of the test. However, the model overestimates the moment throughout most of the initial loading and unloading. If both of the frictional and cubic terms are removed (Figure 4.26), the model is unable to provide a good fit except during the initial loading regions.

The experimental curve is linear for most of the loading path which may result from the close packing acting more like a continuous material. However, the cubic
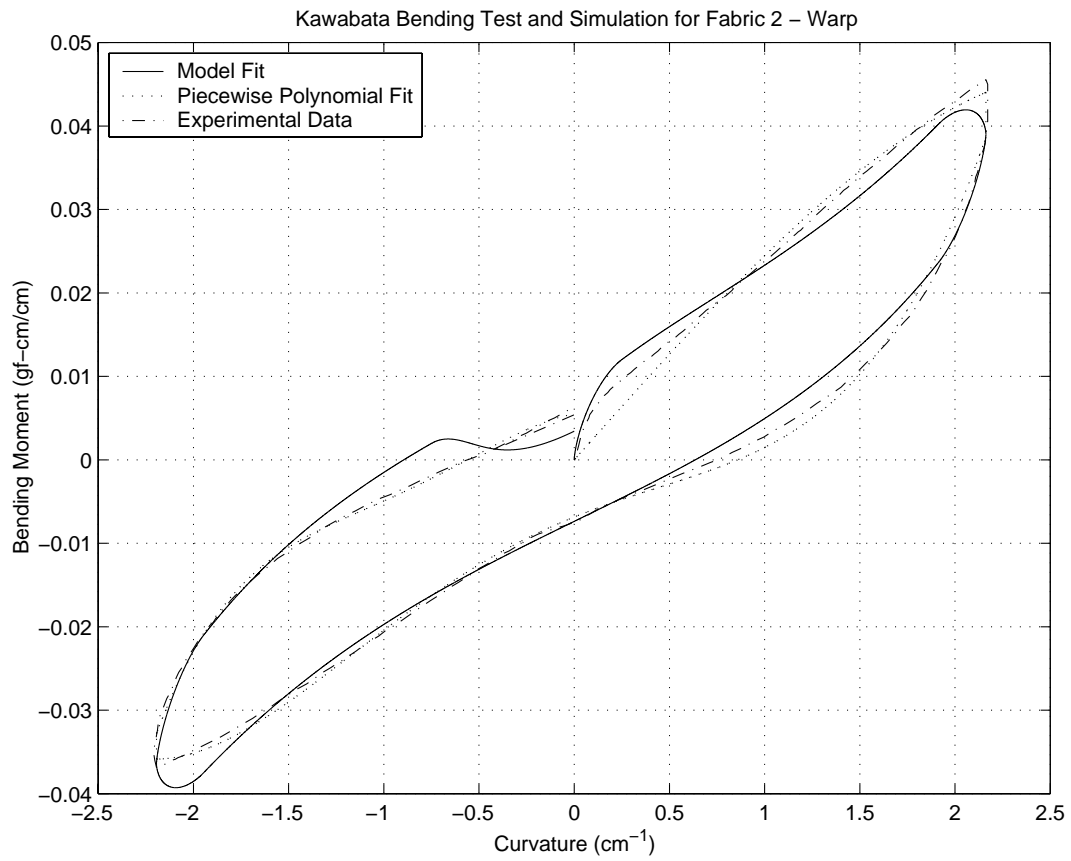
Figure 4.23: Fabric 2 - Warp Direction Full Model
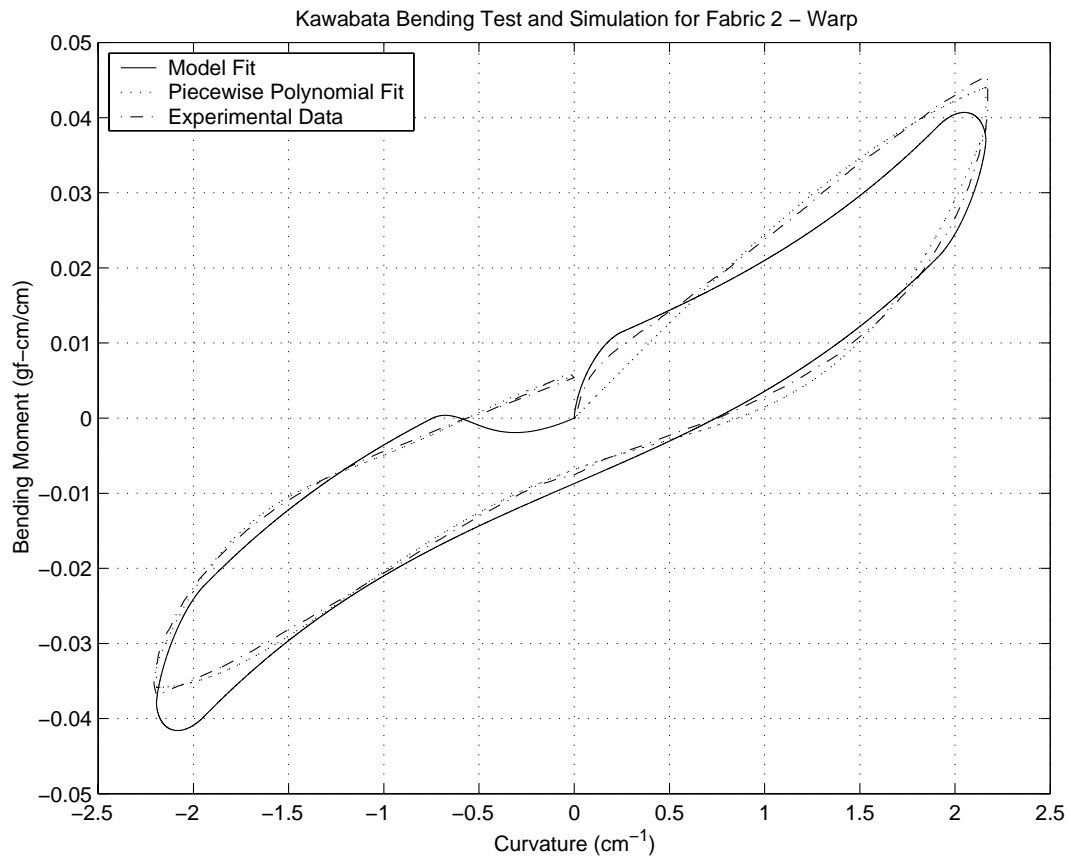
Figure 4.24: Fabric 2 - Warp Direction (No Friction Term)

term appears to play an important role during the unloading path. The reasons for this are not clear, but it is likely due to the recovery behaviour of the cotton yarns.
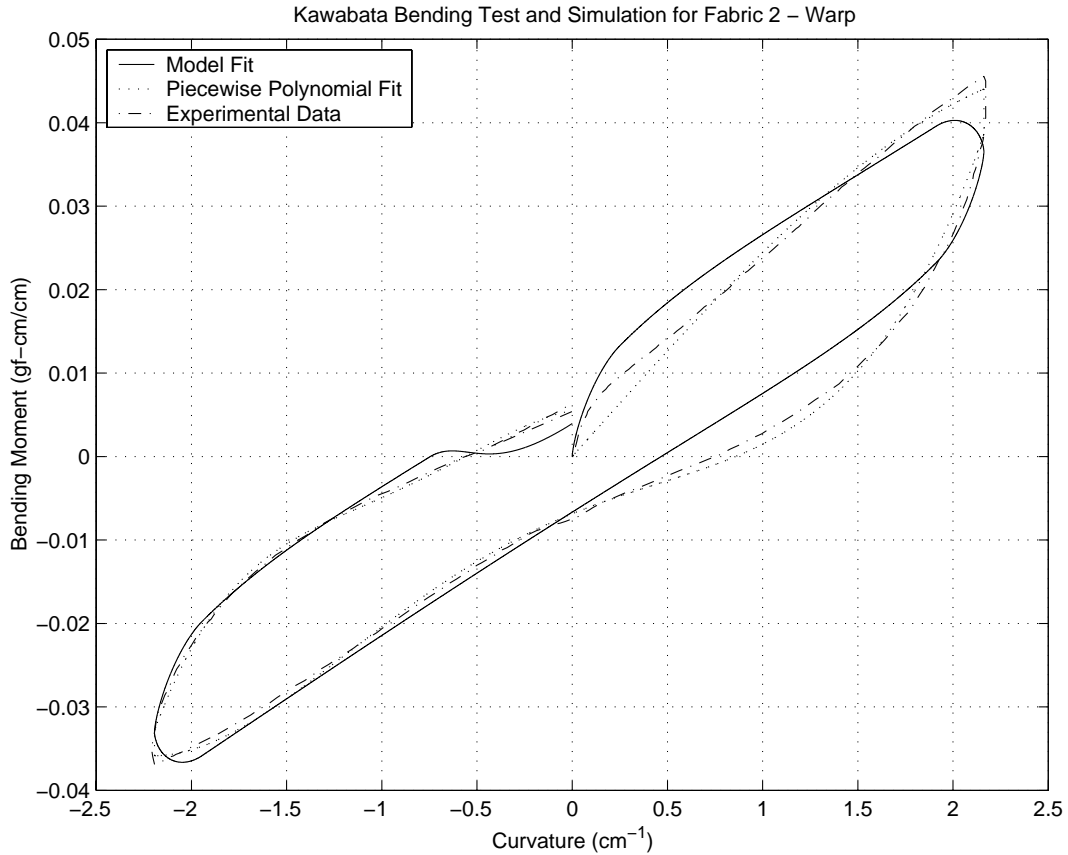
Figure 4.25: Fabric 2 - Warp Direction (No Cubic Term)

Like the weft direction of Fabric 1, we see the participation of both static and dynamic friction in the model. Figure 4.27 shows the distinct static friction peak (f_s in Table 4.11) followed by the decay to the dynamic friction value (f_k in the same table). However, as mentioned earlier, we see larger values for static and dynamic friction moments. This is not suprising as the experimental moments are greater than that of
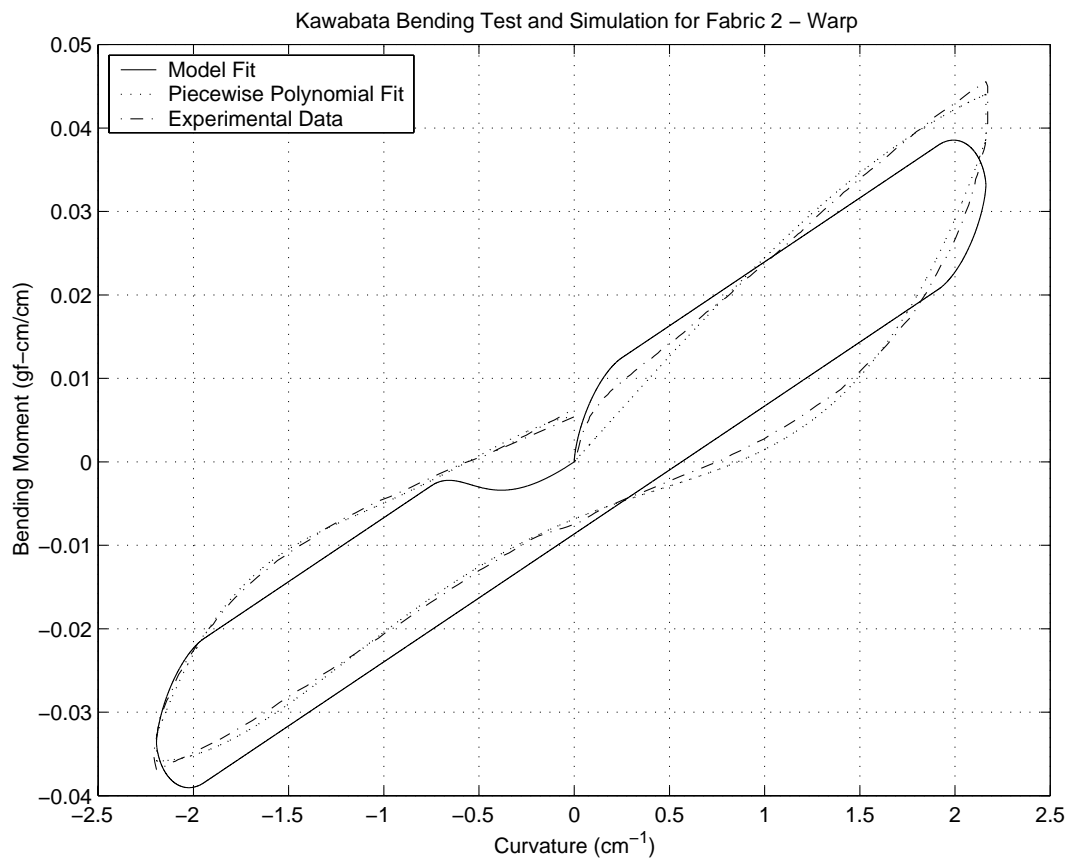
Figure 4.26: Fabric 2 - Warp Direction (No Cubic or Friction Term)

Fabric 1. In addition, there is a larger separation between the static and dynamic friction values.
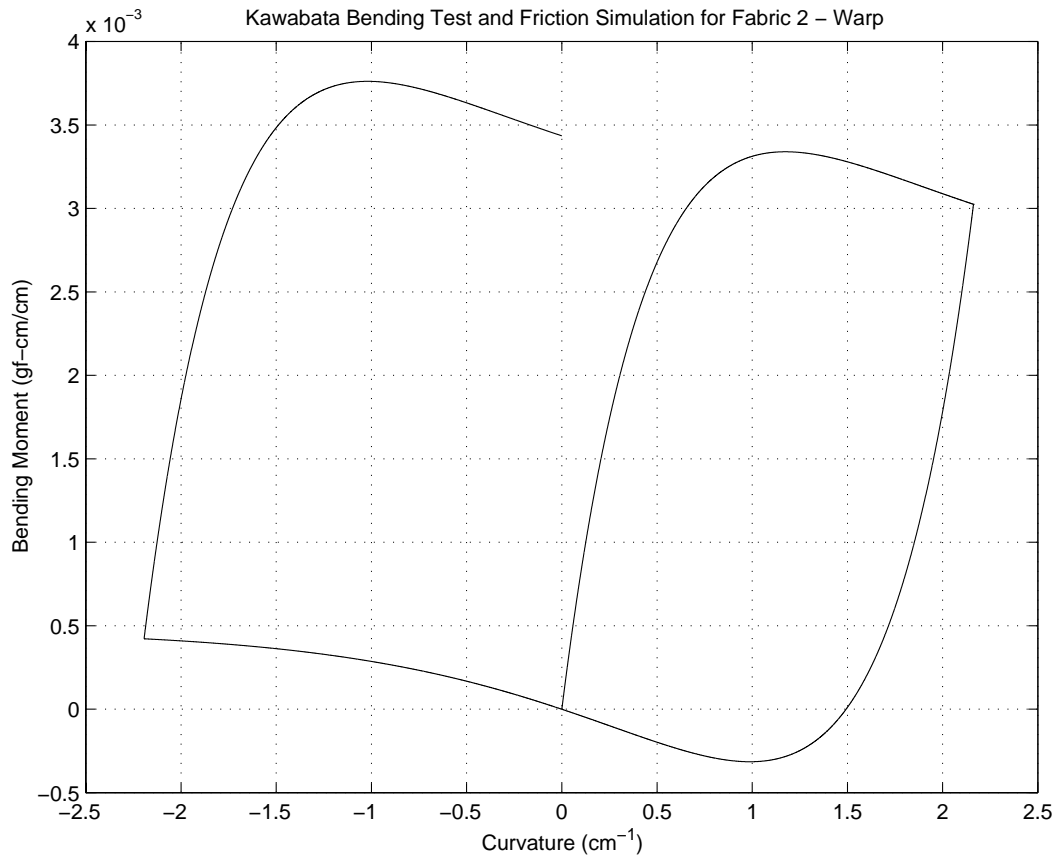
Figure 4.27: Fabric 2 Warp - Frictional Contribution
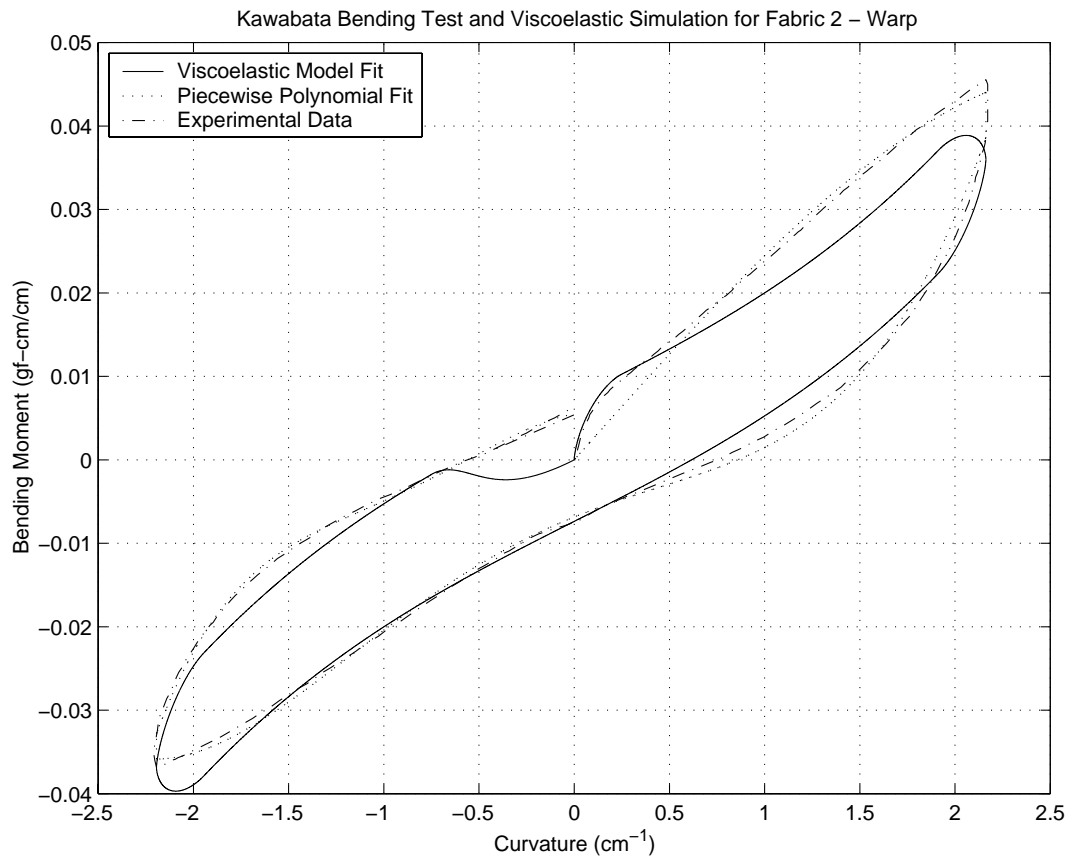
Figure 4.28: Fabric 2 Warp - Non-linear Visco-elastic Contribution

Weft Direction

Examining Table 4.14, we can see that we have very little dynamic friction, and very small curvatures to reach the maximum static friction s_e and to get within 5% of the dynamic friction value. This indicates that the model is approximating Coloumb static friction. This is verified by examing the friction contribution to the model in Figure 4.33. This would lead one to conclude that static friction does not play a large role in the overall fit of the model. From Table 4.15 it appears that alone it does not, but it does appear to couple with the cubic term in providing a better fit.

Parameter	Value
f_1	$1.600 \times 10^{-1}\ gmf - cm$
f_2	$1.600 \times 10^{-1}\ gmf - cm$
η	9.932×10^{-1}
ϵ_f	$7.646 \times 10^{-4}\ gmf - cm/cm$
d	$5.637 \times 10^{-3}\ gmf - cm/s$
k_1	$3.722 \times 10^{-3}\ gmf - cm$
k_3	$5.436 \times 10^{-4}\ gmf - cm^3$

Table 4.13: Fabric 2 - Weft Direction: Model Parameters

Parameter	Value
s_e	$7.62 \times 10^{-2}\ cm^{-1}$
s_p	$2.29 \times 10^{-1}\ cm^{-1}$
f_k	$2.120 \times 10^{-6}\ gmf - cm$
f_s	$4.045 \times 10^{-2}\ gmf - cm$

Table 4.14: Fabric 2 - Weft Direction: Supplementary Friction Results

Figure 4.29 shows the kind of compromises the model fit makes. Although the fit is poor on the initial loading path, the model provides a good fit through parts of the unloading/reverse loading path. It also predicts the correct shape of this path as well

Test Case	Residual
Full Model	4.479×10^{-2}
No Slow Down at End	4.486×10^{-2}
No Friction Term	4.482×10^{-2}
No Cubic Term	5.367×10^{-2}
No Friction or Cubic Term	6.683×10^{-2}

Table 4.15: Fabric 2 - Weft Direction: Model Comparision

as the right shape for most of the reverse unloading path. Note that from Table 4.3, this is the only direction for the two fabrics that has a increase in slope from $+\kappa$ to $-\kappa$.

Without the friction term in the model (Figure 4.30), there is very little change in the overall fit which is confirmed by the residual values in Table 4.15. Tight packing of the warp threads may be preventing the movement of the yarns with respect to each other. Without the cubic term (Figure 4.31) we can see noticeable differences in the shape of the curve. As with the other fabric and direction, removing the cubic term eliminates the inward sloping curve on the unloading/reverse loading path. Without both the cubic and frictional terms (Figure 4.32) we have a poor fit throughout most of the experiment.

Although the type of twill weave is not mentioned in Deng's thesis [Den94] the large asymmetry in the material behaviour suggests that this is a 1x2 twill weave. On loading, the 2 warp threads on the back of the fabric move apart while only 1 is compressed. On reverse loading, the 2 warp threads will be pressed together causing a jammed condition. This would account for the large non-linearity in the reverse loading direction.
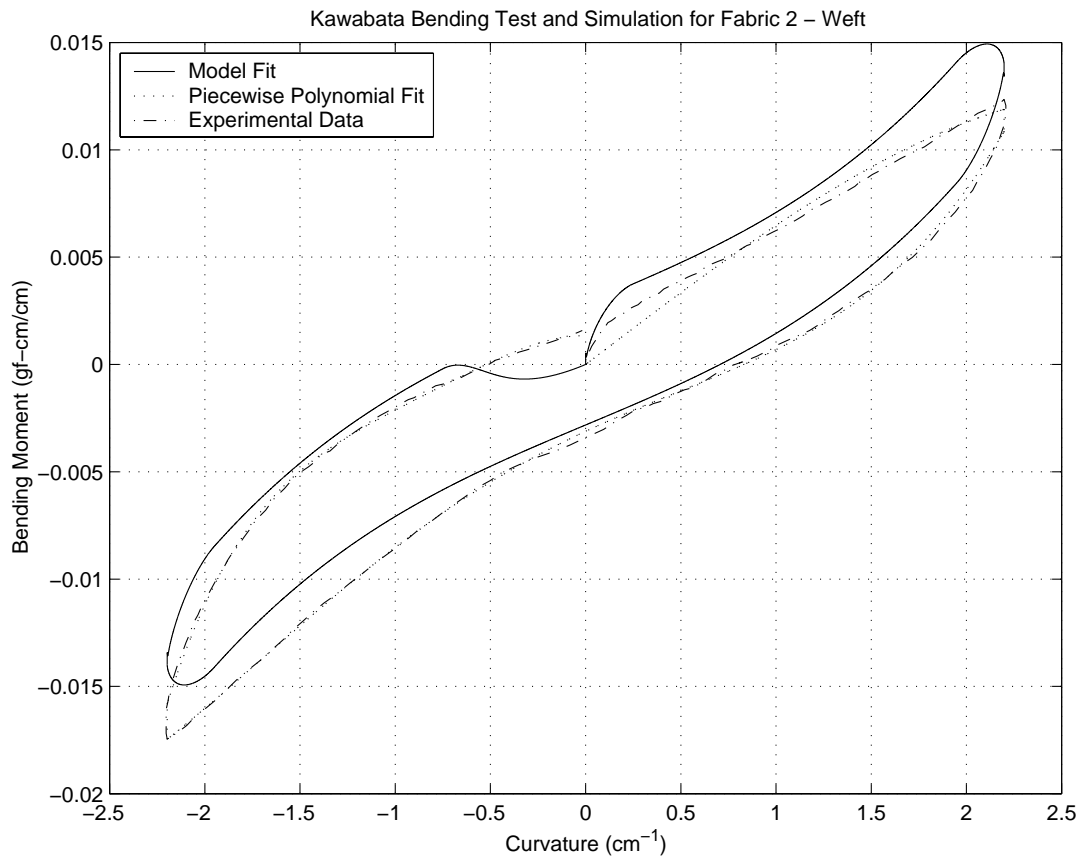
Figure 4.29: Fabric 2 - Weft Direction Full Model
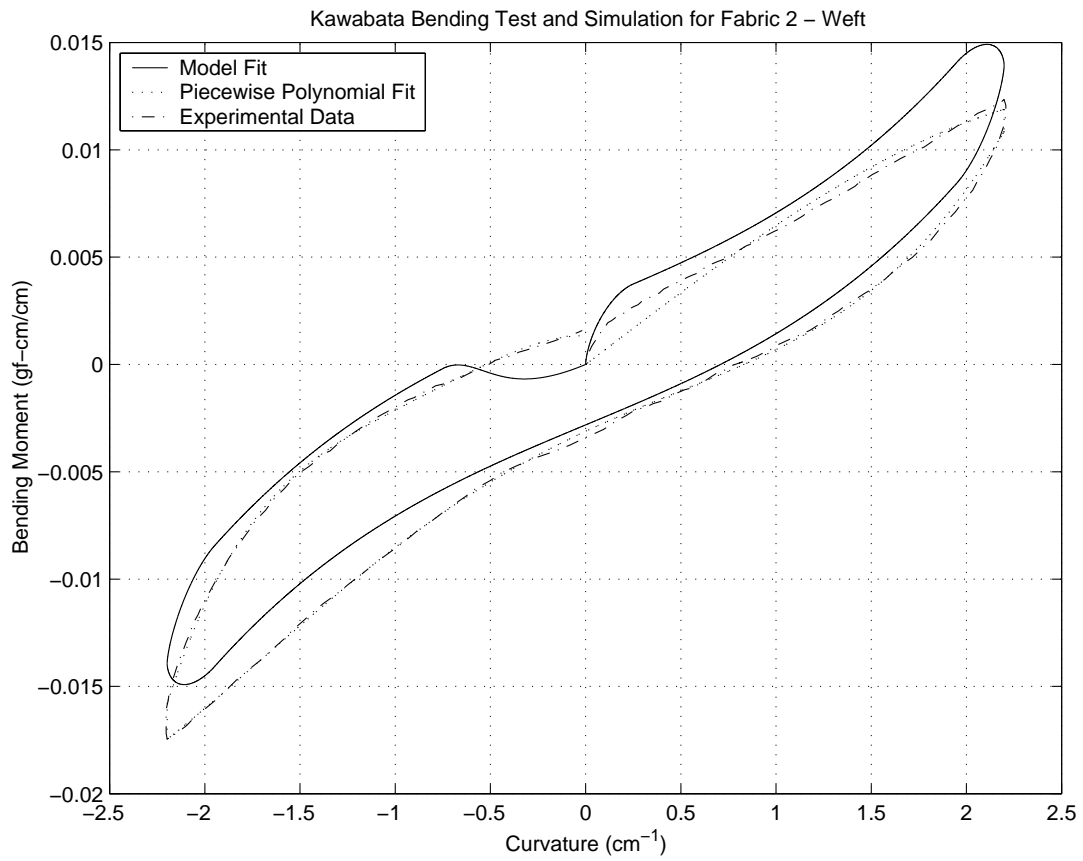
Figure 4.30: Fabric 2 - Weft Direction (No Friction Term)
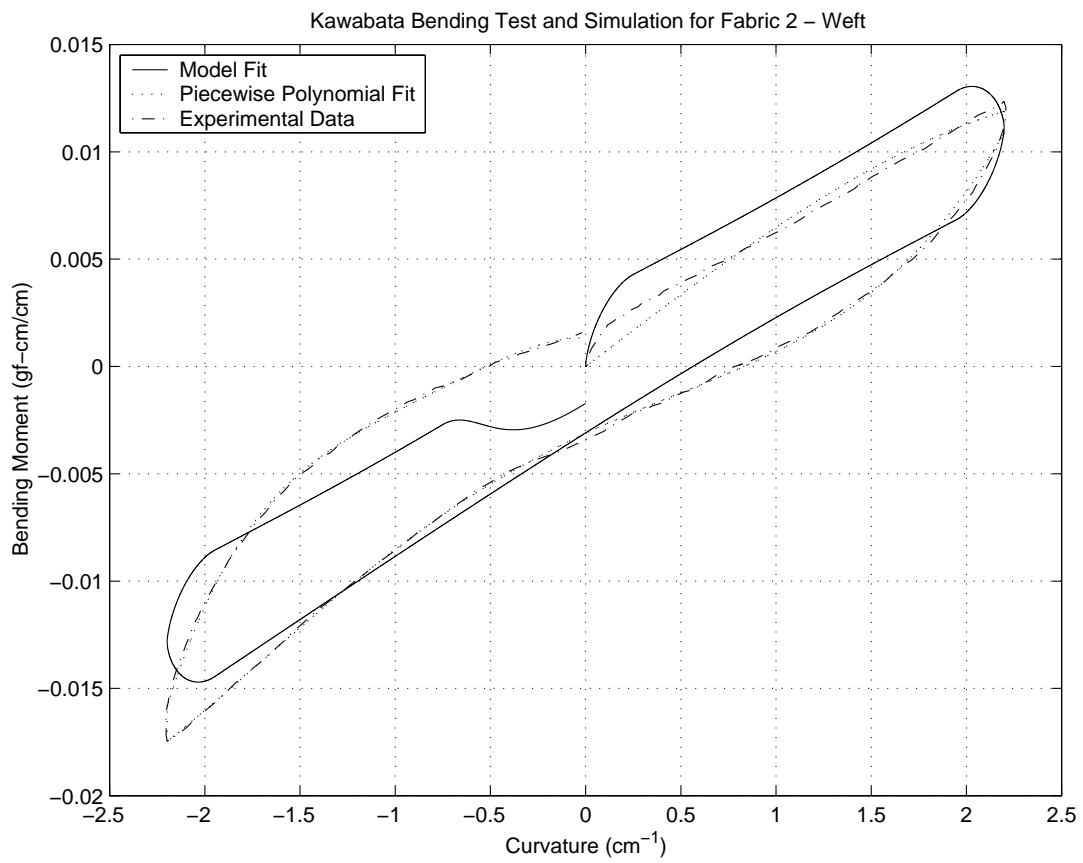
Figure 4.31: Fabric 2 - Weft Direction (No Cubic Term)
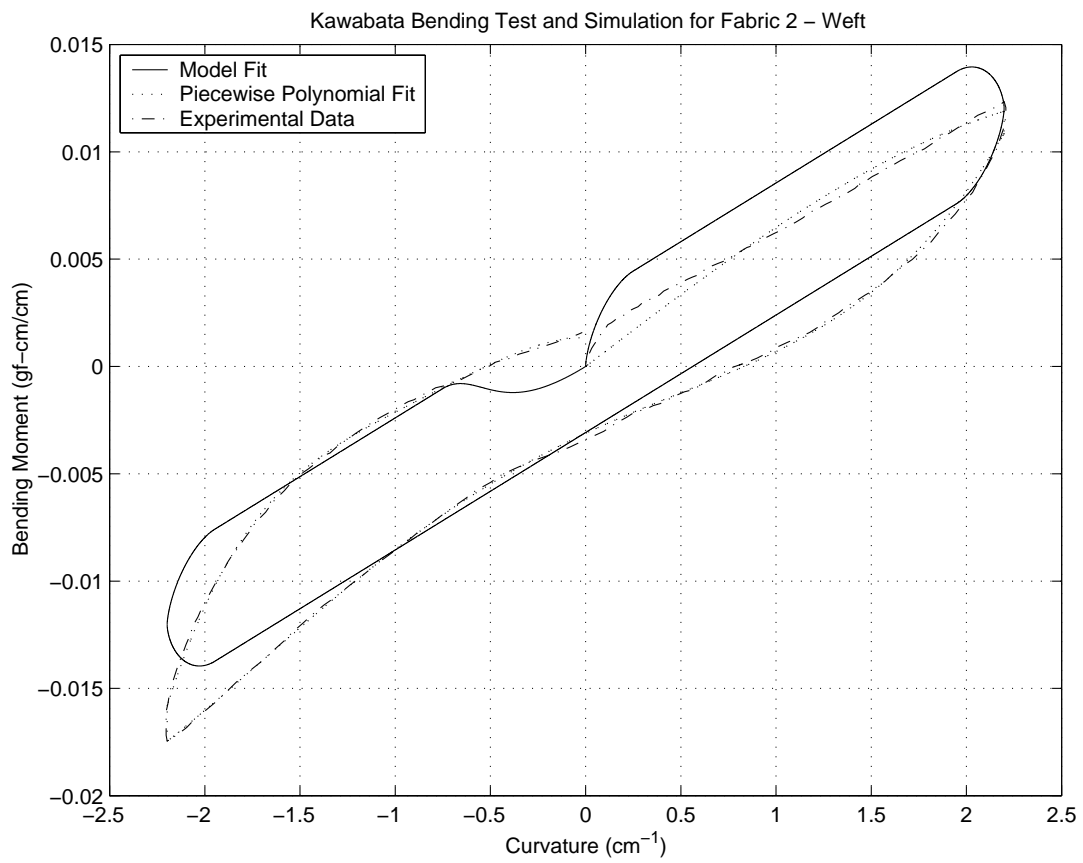
Figure 4.32: Fabric 2 - Weft Direction (No Cubic or Friction Term)
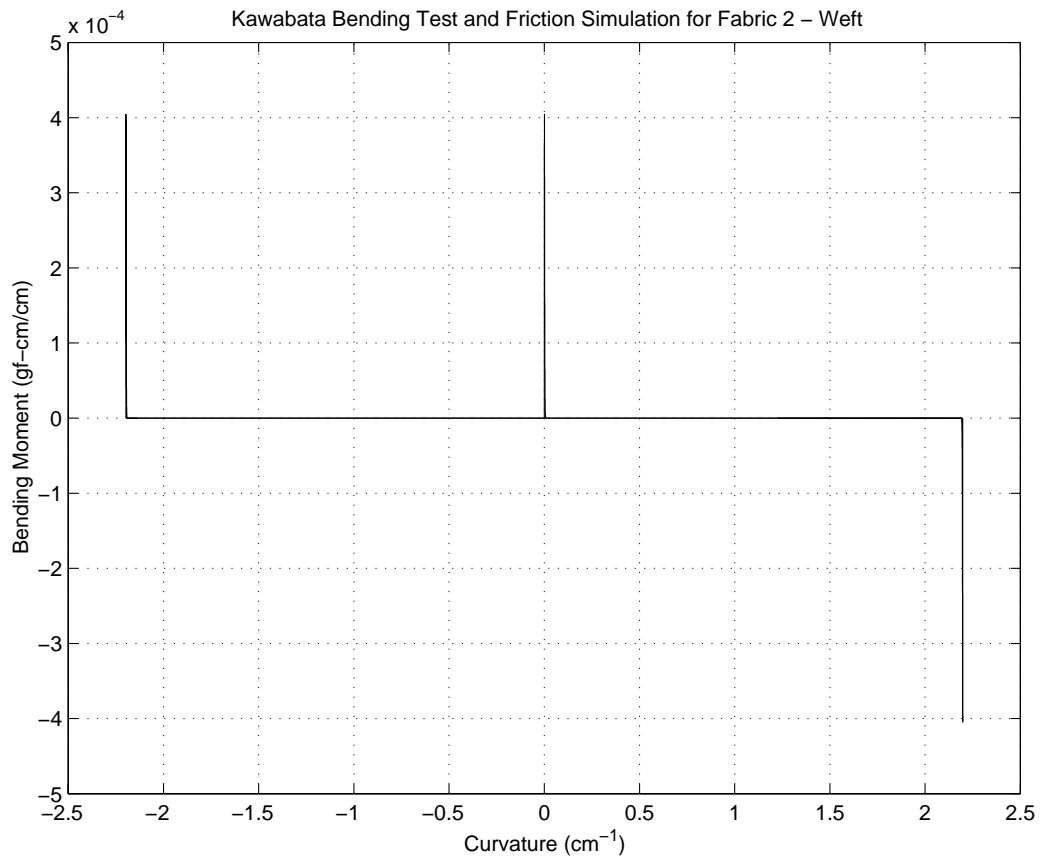
Figure 4.33: Fabric 2 Weft - Frictional Contribution
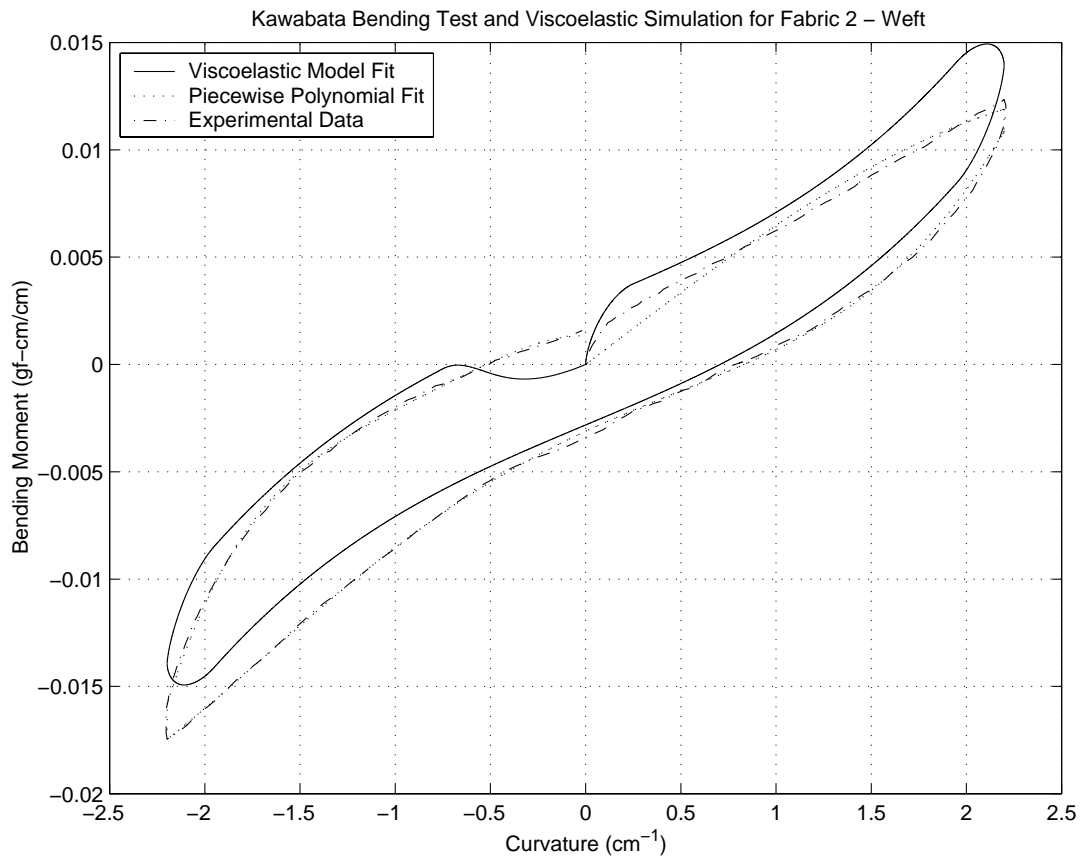
Figure 4.34: Fabric 2 Weft - Non-linear Visco-elastic Contribution

Chapter 5

The Fabric Drape Simulation Model

To demonstrate the utility of the constitutive model developed in Chapter 4, it will be used in a simulation of fabric drape. The model from the previous chapter defined the bending of a fabric using the equation:

$$m\ddot{\kappa} = k_1\kappa + d\dot{\kappa} + k_3\kappa^3 + f(\dot{\kappa}) + M_{ext} \tag{5.1}$$

where $f(\dot{\kappa})$ is the friction function and M_{ext} is the external moment exerted on the body. It is necessary to put this constitutive model into a form that can be discretised by the FEM (or some other Ritz-based method) such that the deflections can be obtained.

The layout of this chapter is as follows: Section 5.1 of this chapter presents the discretisation method; Section 5.2 presents a model with the linear term of Equation (5.1) in one dimension; Section 5.3 extends the model to a plate; Section 5.4 adds the cubic term to the simulation model; Section 5.5 includes the frictional term in the simulation model; and lastly, Section 5.6 the describes the problems in implementing the model.

5.1 The B-spline Field Approximation Method

The B-spline field approximation model (FAM) used in this thesis is a technique developed by Allan Vermeulen in his PhD thesis [Ver95]. In the B-spline FAM, the field variables u are discretised using B-splines, rather than the more traditional Lagrange polynomials.

The governing variational principle for structural dynamics is Hamilton's Principle:

$$\delta \int_{t_1}^{t_2} (T(\dot{u}) - U(u) + W(u)) dt = 0 \tag{5.2}$$

where $T(\dot{u})$ is the kinetic energy of the structure, $U(u)$ is the strain energy, and $W(u)$ is the work due to conservative forces. Non-conservative forces must be handled separately as variational methods cannot be used for non-conservative forces. If we discretise the field variables using B-splines we get:

$$\hat{u} = \sum_{i=1}^{n} N_i u_i \tag{5.3}$$

where N_i are the basis functions and u_i are the control vertices (CVs) for the discretisation. Substituting this into Equation (5.2) gives:

$$\delta \int_{t_1}^{t_2} (T(\dot{\hat{u}}) - U(\hat{u}) + W(\hat{u})) dt = 0 \tag{5.4}$$

From this equation, $T(\dot{\hat{u}})$ gives rise to the mass matrix $\mathbf{M}$, $U(\hat{u})$ leads to the stiffness matrix $\mathbf{K}$, and $W(\hat{u})$ the consistent force vector $\mathbf{F}$. During the simulation model development, in subsequent sections, each of the above will be handled separately.

5.1.1 Properties of the B-spline discretisation

The B-spline discretisation has a number of useful properties:

1. Convex Hull Property: The degree m spline function is bounded by $m + 1$ CVs at each point. Therefore, the CVs approximate the curve and provide a minimum and maximum for the curve at each point.

2. Variation Diminishing Property. The spline crosses the line $y = c$ for some constant c, no more often than the polyline formed by the CVs.

3. Local Continuity Control. It is possible to control continuity at each point. This allows one to have regions (or points) of different continuity than the rest of the domain.

4. Numerically Stable. B-splines have a evaluation scheme that only requires convex combinations of the CVs which has little computational error.

5. Completeness. B-splines are a complete basis for the space of all polynomials of degree m.

5.2 A Linear Approximation: Pure Bending of a Beam

5.2.1 Formation of the Mass Matrix

The kinetic energy of a structure is given by:

$$T = \frac{1}{2} \int_V \rho \dot{\mathbf{d}}^T \dot{\mathbf{d}} dV \tag{5.5}$$

where $\dot{\mathbf{d}}$ is given by:

$$\dot{\mathbf{d}} = \frac{\partial}{\partial t} \begin{bmatrix} u(x, y, z, t) \\ v(x, y, z, t) \\ w(x, y, z, t) \end{bmatrix} \tag{5.6}$$

where u, v, and w the displacements in the x, y, z directions respectively. In the pure bending case, we are assuming $u = 0$, $v = 0$ and $w(x, y, z, t) = w(x, t)$, so in this case $\dot{\mathbf{d}}$ is

$$\dot{\mathbf{d}} = \frac{\partial}{\partial t} w(x, t) \tag{5.7}$$

Using a separation of variables,

$$w(x, t) = \mathbf{N}^T(x)\mathbf{w}(t) \tag{5.8}$$

where $\mathbf{N}(x)$ are the basis functions for the discretisation and $\mathbf{w}(t)$ are the undetermined coefficients. Substituting into Equation (5.7) we get:

$$\dot{\mathbf{d}} = \mathbf{N}^T \frac{d}{dt} \mathbf{w} \tag{5.9}$$

Substituting this result into Equation (5.5):

$$T = \frac{1}{2} \int_V \rho (\dot{\mathbf{w}}^T \mathbf{N})(\mathbf{N}^T \dot{\mathbf{w}}) dV \tag{5.10}$$

since $\dot{\mathbf{w}}$ has no spatial dependence, those entries can be moved outside the integral to get:

$$T = \frac{1}{2} \dot{\mathbf{w}}^T \int_V \rho \mathbf{N} \mathbf{N}^T dV \dot{\mathbf{w}} \tag{5.11}$$

or,

$$T = \frac{1}{2} \dot{\mathbf{w}}^T \mathbf{M} \dot{\mathbf{w}} \tag{5.12}$$

where,

$$\mathbf{M} = \rho \int_V \mathbf{N} \mathbf{N}^T dV \tag{5.13}$$

Taking the variation of T over $\dot{\mathbf{w}}$ leads to a system of equations (with consistent force vector):

$$\mathbf{M}\ddot{\mathbf{w}} = \mathbf{F} \tag{5.14}$$

5.2.2 Formation of the Stiffness Matrix

In general, the strain in the system is of the form:

$$\epsilon = \epsilon_0 + z\kappa \tag{5.15}$$

for pure bending, we assume $\epsilon_0 = 0$ and with a small deflection assumption,

$$\kappa = -\frac{d^2 w}{dx^2}$$

Given that,

$$M = \int_{-\frac{h}{2}}^{\frac{h}{2}} z\sigma dz = k_1\kappa \tag{5.16}$$

σ is of the form:

$$
\begin{aligned}
\sigma &= E_1\epsilon \\
&= zE_1\kappa
\end{aligned}
\tag{5.17}
$$

where we need to find E_1 in terms of k_1. From M compute

$$
\begin{aligned}
M &= \int_{-h/2}^{h/2} z^2 E_1 \kappa dz \\
&= \frac{h^3}{12} E_1 \kappa
\end{aligned}
\tag{5.18}
$$

For a rectangular cross section (which is what we have) recall

$$I = \frac{bh^3}{12}$$

so

$$k_1 = \frac{E_1 I}{b} \tag{5.19}$$

or

$$E_1 = \frac{k_1 b}{I} \tag{5.20}$$

Now, the strain energy density is

$$
\begin{aligned}
\mathcal{U} = \int_0^\epsilon \sigma d\epsilon &= \frac{1}{2} E_1 \epsilon^2 \\
&= \frac{1}{2} E_1 z^2 \kappa^2
\end{aligned}
\tag{5.21}
$$

and integration of $\mathcal{U}$ over the cross section area ($dydz$) yields

$$
\begin{aligned}
\mathcal{U}_{yz} = \int_{-h/2}^{h/2} \int_{-b/2}^{b/2} \mathcal{U} dy dz &= \frac{1}{2} E_1 I \kappa^2 \\
&= \frac{1}{2} k_1 b \kappa^2
\end{aligned}
\tag{5.22}
$$

and therefore the total strain energy is

$$U = \int_0^L \mathcal{U}_{yz} dx = \frac{1}{2} \int_0^L (bk_1 \kappa^2) dx \tag{5.23}$$

For the discretisation introduce a trial function of the form (as was used in Equation (5.8)):

$$w(x) = \mathbf{N}^T(x)\mathbf{w} \tag{5.24}$$

where $\mathbf{N}$ is the matrix of basis functions and $\mathbf{w}$ is the vector of undetermined parameters. From the definition of κ we find that

$$\kappa(x) = \mathbf{N''}^{T}(x)\mathbf{w} \tag{5.25}$$

Substitution into (5.23) yields

$$U = \frac{1}{2}\int_0^L bk_1\mathbf{w}^T\mathbf{N''}\mathbf{N''}^T\mathbf{w}dx \tag{5.26}$$

Taking the variation over $\mathbf{w}$ yields

$$
\begin{aligned}
\delta U &= b\int_0^L k_1\delta\mathbf{w}^T(\mathbf{N''}\mathbf{N''}^T)\mathbf{w}dx \\
&= \delta\mathbf{w}^T b\int_0^L k_1(\mathbf{N''}\mathbf{N''}^T)\mathbf{w}dx \\
&= \delta\mathbf{w}^T b\int_0^L k_1(\mathbf{N''}\mathbf{N''}^T)dx\mathbf{w}
\end{aligned} \tag{5.27}
$$

This will lead to a system of equations of the form (includes a consistent force vector):

$$\mathbf{K}_1\mathbf{w} = \mathbf{F} \tag{5.28}$$

where

$$\mathbf{K}_1 = k_1 b\int_0^L \mathbf{N''}\mathbf{N''}^T dx \tag{5.29}$$

5.2.3 Formation of the Consistent Force Vector

In order to form the consistent force vector $\mathbf{F}$, we must first calculate the work done by the applied surface tractions and the body forces. The formula for this is:

$$\mathbf{W} = \int_V \mathbf{B}^T\mathbf{d}dV + \sum_s\int_{\mathbf{S}_s} \mathbf{S}_s^T\mathbf{d}dA \tag{5.30}$$

where **B** is the vector of body forces (e.g., gravity), $\mathbf{S}_s$ the vector of surface tractions, and **d** a vector of displacements.

Ignoring in-plane displacements and assuming only gravity is acting on the body (and substituting Equation (5.24)) we get:

$$\mathbf{W} = \rho g \int_V \mathbf{N}^T \mathbf{w} \, dV \tag{5.31}$$

Taking the variation of **W** with respect to **w** gives us the consistent force vector,

$$\mathbf{F} = \rho g \int_V \mathbf{N} \, dV \tag{5.32}$$

5.2.4   Application of Boundary Conditions

To apply a forced boundary condition, there are two main techniques:

1. Removal of the degrees of freedom from the system;

2. Modify the system of equations to enforce the constraint.

While the first is more computationally efficient, the second is easier to implement so the second approach is used. Since the system of equations represents a deflection from the original configuration, we will only consider the zero deflection boundary conditions. The process for setting a zero deflection constraint is:

1. Ensure that a CV is set for the location of the boundary condition on the mesh;

2. Set the knot multiplicity for the point equal to the degree of the curve;

3. Zero the row and column corresponding to the CV;

4. Set the diagonal entry equal to -1.0;

5. Set the consistent force vector row equal to zero.

5.2.5 Solution of the System of Equations

From subsections 5.2.1 through 5.2.3 we have developed the system of equations:

$$\mathbf{M\ddot{w}} + \mathbf{K}_1\mathbf{w} = \mathbf{F} \tag{5.33}$$

we incorporate damping as proportional to the stiffness matrix $\mathbf{K}_1$ (Rayleigh damping) so that the damping matrix $\mathbf{D}$ is:

$$\mathbf{D} = db \int_0^L \mathbf{N}''\mathbf{N}''^T dx \tag{5.34}$$

where d is the damping coefficient from Equation (5.1). We add this to the system of equations to get:

$$\mathbf{M\ddot{w}} + \mathbf{D\dot{w}} + \mathbf{K}_1\mathbf{w} = \mathbf{F} \tag{5.35}$$

To facilitate solution of this system of equations, we reduce the system to first order form using the technique described by Foss [Fos58]. Equation (5.35) can be written in reduced form as:

$$\mathbf{R}\dot{Z} + \mathbf{K}_r Z = \mathbf{F}_r \tag{5.36}$$

where

$$\mathbf{R} = \begin{bmatrix} [0] & \mathbf{M} \\ \mathbf{M} & \mathbf{D} \end{bmatrix}, \quad \mathbf{K}_r = \begin{bmatrix} -\mathbf{M} & [0] \\ [0] & \mathbf{K}_1 \end{bmatrix}$$

$$Z = \begin{bmatrix} \mathbf{\dot{w}} \\ \mathbf{w} \end{bmatrix}, \quad \mathbf{F}_r = \begin{bmatrix} [0] \\ \mathbf{F} \end{bmatrix}$$

This is now a system of linear first-order differential equations that can be solved using standard ODE methods.

5.3 A Linear Approximation: Pure Bending of a Plate

The main difference between the beam and plate models is that we define the discretisation as

$$w(x, y) = \mathbf{N}^T(x, y)\mathbf{w} \tag{5.37}$$

where,

$$\mathbf{N}(x, y) = \begin{bmatrix} N_{1x}(x)N_{1y}(y) & N_{2x}(x)N_{1y}(y) & \dots & N_{nx}(x)N_{1y}(y) & \dots & N_{nx}(x)N_{ny}(y) \end{bmatrix}$$

that is, $w(x, y)$ is discretised using a tensor product of the B-spline basis functions in the x and y directions. The development of the mass matrix $\mathbf{M}$ proceeds in the same manner as Section 5.2.1 with the only difference being the definition of $\mathbf{N}$. For curvature κ we are now concerned with curvature in the principal directions κ_x and κ_y. They can be obtained by taking the second partial derivative with respect to x and y respectively.

$$\mathbf{N}_{xx} = \begin{bmatrix} N_{1x}''(x)N_{1y}(y) & N_{2x}''(x)N_{1y}(y) & \dots & N_{nx}''(x)N_{1y}(y) & \dots & N_{nx}''(x)N_{ny}(y) \end{bmatrix}$$

$$\mathbf{N}_{yy} = \begin{bmatrix} N_{1x}(x)N_{1y}''(y) & N_{2x}(x)N_{1y}''(y) & \dots & N_{nx}(x)N_{1y}''(y) & \dots & N_{nx}(x)N_{ny}''(y) \end{bmatrix}$$

$$\kappa_x = \mathbf{N}_{xx}\mathbf{w} \tag{5.38}$$

$$\kappa_y = \mathbf{N}_{yy}\mathbf{w} \tag{5.39}$$

If there is no coupling between bending in the prinicipal directions, the stiffness matrix calculations decouple resulting in,

$$\mathbf{K}_1 = \mathbf{K}_{1x} + \mathbf{K}_{1y} \tag{5.40}$$

where,

$$\mathbf{K}_{1x} = k_{1x} \int_A \mathbf{N}''_{xx} \mathbf{N}''_{xx}{}^T dA \tag{5.41}$$

$$\mathbf{K}_{1y} = k_{1y} \int_A \mathbf{N}''_{yy} \mathbf{N}''_{yy}{}^T dA \tag{5.42}$$

with the damping matrix $\mathbf{D}$ calculated in the same manner. We therefore have the following equations:

$$\mathbf{M} = \rho t \int_A \mathbf{N} \mathbf{N}^T dA \tag{5.43}$$

$$\mathbf{K}_1 = k_{1x} \int_A \mathbf{N}''_{xx} \mathbf{N}''_{xx}{}^T dA + k_{1y} \int_A \mathbf{N}''_{yy} \mathbf{N}''_{yy}{}^T dA \tag{5.44}$$

$$\mathbf{D} = d_x \int_A \mathbf{N}''_{xx} \mathbf{N}''_{xx}{}^T dA + d_y \int_A \mathbf{N}''_{yy} \mathbf{N}''_{yy}{}^T dA \tag{5.45}$$

$$\mathbf{F} = \rho g t \int_A \mathbf{N} dA \tag{5.46}$$

The reduction of the system of equations into first order form as done in Section 5.2.5 proceeds in the same manner.

5.4   Modelling the Non-linear Elastic Component

Since we assume separation of the bending behaviour in the principal directions, this section will develop the behaviour for one direction only, with the recognition that the same procedure will also apply for the other direction. Now, we have developed a moment-curvature relation of the form:

$$M = k_1 \kappa + k_3 \kappa^3 \tag{5.47}$$

Now, the moment can be determined from

$$M = \int_{-\frac{h}{2}}^{\frac{h}{2}} z\sigma dz = k_1\kappa + k_3\kappa^3 \tag{5.48}$$

We can define σ as an odd polynomial of the form:

$$\begin{aligned} \sigma &= E_1\epsilon + E_3\epsilon^3 \\ &= zE_1\kappa + z^3 E_3\kappa^3 \end{aligned} \tag{5.49}$$

Now, since we have handled the κ term in earlier analyses, we shall consider only the κ^3 term for the moment. From M compute:

$$\begin{aligned} M_3 &= \int_{-\frac{h}{2}}^{\frac{h}{2}} z^4 E_3\kappa^3 dz \\ &= \frac{h^5}{80} E_3\kappa^3 \end{aligned} \tag{5.50}$$

Using the moment of inertia relationship, we get

$$E_3 = \frac{20k_3 b}{3Ih^3} \tag{5.51}$$

Now, the strain energy density is:

$$\begin{aligned} \mathcal{U} = \int_0^\epsilon \sigma d\epsilon &= \frac{1}{4} E_3\epsilon^4 \\ &= \frac{1}{4} E_3 z^4 \kappa^4 \end{aligned} \tag{5.52}$$

and integration of $\mathcal{U}$ over the thickness yields:

$$
\begin{aligned}
\mathcal{U}_z = \int_{-h/2}^{h/2} \mathcal{U} dz &= \frac{1}{4} \frac{3 E_3 I h^2}{20 b} \kappa^4 \\
&= \frac{1}{4} k_3 \kappa^4
\end{aligned}
\tag{5.53}
$$

and therefore, the total strain energy for the cubic term is,

$$
U_3 = \int_A \mathcal{U}_z dA = \frac{1}{4} \int_A k_3 \kappa^4 dA
\tag{5.54}
$$

Substituting the definition of κ from equation 5.25 we have:

$$
U_3 = \int_A \mathcal{U}_z dA = \frac{1}{4} \int_A k_3 (\mathbf{w}^T \mathbf{N}'' \mathbf{N}''^T \mathbf{w})^2 dA
\tag{5.55}
$$

Variation over $\mathbf{w}$ yields:

$$
\begin{aligned}
\delta U_3 &= \int_A k_3 \delta \mathbf{w}^T \mathbf{N}'' \mathbf{N}''^T \mathbf{w} (\mathbf{w}^T \mathbf{N}'' \mathbf{N}''^T \mathbf{w}) dx \\
&= \delta \mathbf{w}^T \int_A k_3 (\mathbf{N}'' \mathbf{N}''^T)(\mathbf{w}\mathbf{w}^T)(\mathbf{N}'' \mathbf{N}''^T) \mathbf{w} dx \\
&= \delta \mathbf{w}^T \int_A k_3 (\mathbf{N}'' \mathbf{N}''^T)(\mathbf{w}\mathbf{w}^T)(\mathbf{N}'' \mathbf{N}''^T) dx \mathbf{w}
\end{aligned}
\tag{5.56}
$$

which leads to a system of equations of the form:

$$
\mathbf{K}_1 \mathbf{w} + \mathbf{K}_3(\mathbf{w}) \mathbf{w} = \mathbf{F}
\tag{5.57}
$$

where $\mathbf{K}_1$ is the linear stiffness matrix computed earlier and $\mathbf{K}_3(\mathbf{w})$ is the non-linear stiffness matrix.

5.5 Modelling the Frictional Component

It is necessary to use the integral form of the frictional model from Chapter 4 and not the differential equation form since it is necessary to be able to integrate over the area.

The virtual work done by the moment $M_f(\dot{\kappa})$ can be defined as

$$dW = \int_{S_s} S_s^T d\kappa dA \qquad (5.58)$$

with S_s a vector of $M_f(\dot{\kappa})$ at each of the CVs. The frictional term is defined as (from equation 4.2):

$$S_s = (f_1 - f_2)\text{sign}[\dot{\kappa}(t)] + \text{sign}[\dot{\kappa}(0)]\left(e^{-\frac{s(t)}{\epsilon_f}}f_2 - e^{-\frac{s(t)}{\epsilon_f\eta}}f_1\right) \qquad (5.59)$$

where $s(t)$ is the time integral of κ. Substitution of equation 5.25 yields:

$$dW = \int_{S_s}\left[(f_1 - f_2)\text{sign}(N''^T\dot{w}(t)) + \text{sign}(N''^T\dot{w}(0))\left(e^{-\frac{s(t)}{\epsilon_f}}f_2 - e^{-\frac{s(t)}{\epsilon_f\eta}}f_1\right)\right]N''^T w dA dw \qquad (5.60)$$

In an implementation integral $s(t)$ can be accumulated at each of the CVs, then the integral over the area can be performed.

5.6 Implementation Details and Problems

The above model was implemented in Fortran 95 using the B-spline software from the SLATEC library [Law01]. NAG F77 stiff ODE routines [Num01] were used to solve the system of ODEs.

The following results were found: without in-plane strains, the fabric deformation was unrealistic; and, the inclusion of the frictional term sigificantly slowed the calculation time. On a Pentium III 600 Mhz machine running Linux, one millisecond of simu-

lation time takes approximately five minutes of wall clock time. Without the frictional term, a full second of simulation time can be completed in five minutes of wall clock time.

There was considerable difficulty in finding a method of coupling in-plane and out-of-plane deformation using this bending model. No satisfactory method was found during the course of this research. As a result, we were unable to accurately model the drape of fabric and therefore, no results of the simulations are reported.

Chapter 6

Summary

Most of the previous work on fabric mechanics has either used linear models or relied upon micromechanical models. In Chapter 4 the problems of using linear models for modelling bending have been explored. Micromechanical models use a unit cell to represent the behaviour of the fabric which causes difficulty due to the idealisation of the structure of the fabric. These idealisations do not account for the finish applied to the fabric which is important in the overall properties [WKL+00], or variations in the weave, either due to imperfections or by design.

6.1 Discussion of the Current Model

From Chapter 4 it is clear that the additional cubic term and frictional term have a significant impact on the quality of the model (as measured by the fit to experiment). The frictional term models the slip of the yarns with respect to each other while the cubic term models the jamming behaviour and the non-linear yarn bending properties. However, to accurately determine the model parameters, it is important to have a detailed understanding of the curvature rate profile throughout the experiment. This will assist

in improving the model. From experimental results (Table 4.3) it appears that including differing behaviour for forward and reverse bending would assist in improving the model as well.

6.2   Discussion of Modelling for Simulation Purposes

The model presented herein relates moments and curvature. However, in order to include it as part of a simulation model, it is necessary to have a displacement relation. If the experimental results were in terms of displacement, it would faciliate the modelling for simulation purposes. In addition, there is currently no knowledge on how tension, shear, and bending are coupled. Further research is needed to characterise this coupling in order to include the model as part of a FE model.

Appendix A

Glossary

Fabric Hand The concept of fabric "hand" is ill-defined. Fabric "hand" is examined mainly by the sense of touch. Fabrics with a different "hand" are used for different purposes and may be judged to have a different quality. Kawabata [Kaw80] tried to convert this subjective measurement to an objective measurement. The qualities he considered are: smoothness, crispness, stiffness, spread (or anti-drape), fullness, softness, and the appearance of the surface.

Grey Fabric A term used to refer to fabrics that have just left the loom or knitting machine (from Collier [Col70]). These fabrics usually undergo a finishing process before being used.

Jammed Condition A geometrical state of the fabric where there is no space between the yarns.

Micromechanical Model A model where the overall properties of the material are determined by models of the micro-scale interactions.

Relaxed Fabric	A fabric which has released the stresses and strains occurred during manufacture.
Satin	Satin is a type of weave characterised by long floats (or runs) on the face of the fabric. These floats are caught under cross yarns as far apart as possible. Also of note is that at no time do parallel yarns come in contact with each other. In satin weaves, the warp yarns float. If the weft yarns float, the weave is known as *sateen*. [Jos77]
Thread	From Joseph (pp. 218) [Jos77], the term thread indicates "a product used to join pieces of fabric together to create textile products."
Twill	Twill is a type of weave characterised by a diagonal line on the face and possibly the back of the fabric. The warp yarn floats (goes over) two weft yarns and under one in a 2/1 twill. In a regular twill, each succeeding float begins one weft yarn higher or lower than the adjacent float. This creates the diagonal pattern on the surface of the fabric. Of note is that the twill weave permits close packing and produces strong, durable fabrics. Examples of common fabrics wth a twill weave are denim and flannel.
Warp	Yarns that run parallel to the selvage or to the longer dimension of a bolt of fabric are called *warp* yarns or *ends*.
Weft	Yarns that run perpendicular to the long direction of the bolt of fabric. Also yarns in this direction may be referred to as the *woof yarns*, *filling yarns* or *picks*.

Yarn From Joseph (pp. 203) [Jos77], "a generic term for a continuous strand of textile fibres, filaments or material in a form suitable for knitting, weaving, or otherwise intertwining to form a textile fabric. Yarn occurs in the following forms:

- a number of fibres twisted together

- a number of filaments laid together without twist

- a number of filaments laid together with more or less twist

- a single filament ... monofilament

- One or more strips made by the lengthwise divisions of a sheet of material such as a natural or synthetic polymer, a paper, a metal foil, used with or without twist in a textile construction."

Appendix B

Further Information

B.1 Equations of an Elastica

Rewriting Equations (2.6) and (2.5) respectively we get:

$$\rho = \frac{ds}{d\psi} \tag{B.1}$$

$$\frac{m}{\rho} = -Vx \tag{B.2}$$

Also, we have an equation for x (Equation (2.12)) repeated here for clarity:

$$x = \sqrt{\frac{2m}{V}} \sqrt{\sin\theta - \sin\psi} \tag{B.3}$$

Substituting Equation (B.3) into Equation (B.2) we get:

$$\rho = -\frac{m}{Vx} = -\frac{m}{V}\sqrt{\frac{V}{2m}}[\sin\theta - \sin\psi]^{-\frac{1}{2}}$$

$$= -\frac{1}{\sqrt{2}}\sqrt{\frac{m}{V}}[\sin\theta - \sin\psi]^{-\frac{1}{2}} \tag{B.4}$$

From Equation (B.1) we have:

$$ds = \rho d\psi \tag{B.5}$$

Using Equation (B.4) in Equation (B.5):

$$ds = -\frac{1}{\sqrt{2}}\sqrt{\frac{m}{V}}[\sin\theta - \sin\psi]^{-\frac{1}{2}}d\psi \tag{B.6}$$

$$ds = -\frac{1}{\sqrt{2}}\sqrt{\frac{m}{V}}[(1+\sin\theta)-(1+\sin\psi)]^{-\frac{1}{2}}d\psi \tag{B.7}$$

From trigonometry:

$$\sin(\frac{\theta}{2}+\frac{\pi}{2}) = \sin\frac{\theta}{2}\cos\frac{\pi}{4} + \cos\frac{\theta}{2}\sin\frac{\pi}{4}$$
$$= \frac{1}{\sqrt{2}}(\sin\frac{\theta}{2}+\cos\frac{\theta}{2}) \tag{B.8}$$

Also, from Esbach's Handbook (pp. 2-69) [Tap89]:

$$\sin\frac{\theta}{2} = \frac{1}{2}\sqrt{1+\sin\theta} - \frac{1}{2}\sqrt{1-\sin\theta} \tag{B.9}$$

$$\cos\frac{\theta}{2} = \frac{1}{2}\sqrt{1+\sin\theta} + \frac{1}{2}\sqrt{1-\sin\theta} \tag{B.10}$$

Combining Equations (B.8), (B.9), and (B.10):

$$\sin(\frac{\theta}{2}+\frac{\pi}{2}) = \frac{1}{2}\sqrt{1+\sin\theta} \tag{B.11}$$

Defining $k = \sin(\frac{\theta}{2}+\frac{\pi}{2})$ we have:

$$2k^2 = 1+\sin\theta \tag{B.12}$$

Similarly,

$$1+\sin\psi = 2\sin^2(\frac{\psi}{2}+\frac{\pi}{4}) \tag{B.13}$$

Using Equations (B.12) and (B.13) in B.7:

$$ds = -\frac{1}{\sqrt{2}}\sqrt{\frac{m}{V}}[2k^2 - 2\sin^2(\frac{\psi}{2} + \frac{\pi}{4})]^{-\frac{1}{2}}d\psi$$
$$= -\frac{1}{\sqrt{2}}\sqrt{\frac{m}{V}}\frac{1}{\sqrt{2}k}(1 - \frac{1}{k^2}\sin^2(\frac{\psi}{2} + \frac{\pi}{4})]^{-\frac{1}{2}}d\psi \qquad \text{(B.14)}$$

Also, define:

$$\sin\phi = \frac{1}{k}\sin(\frac{\psi}{2} + \frac{\pi}{4}) \qquad \text{(B.15)}$$

Use Equation (B.15) in (B.14):

$$ds = -\frac{1}{\sqrt{2}}\sqrt{\frac{m}{V}}\frac{1}{k}[1 - \sin^2\phi]^{-\frac{1}{2}}d\psi$$
$$= -\frac{1}{\sqrt{2}}\sqrt{\frac{m}{V}}\frac{1}{k\cos\phi}d\psi \qquad \text{(B.16)}$$

Implicitly differentiating Equation (B.15):

$$\cos\phi d\phi = \frac{1}{2k}\cos(\frac{\psi}{2} + \frac{\pi}{4})d\psi$$
$$\frac{d\psi}{\cos\phi} = \frac{2k}{\cos(\frac{\psi}{2} + \frac{\pi}{4})}d\phi \qquad \text{(B.17)}$$

Similar to the simplifications that were done in Equations (B.8)-(B.10) we can simplify $\cos(\frac{\psi}{2} + \frac{\pi}{4})$:

$$\cos(\frac{\psi}{2} + \frac{\pi}{4}) = \cos\frac{\psi}{2}\cos\pi4 - \sin\frac{\psi}{2}\sin\pi4$$
$$= \frac{1}{\sqrt{2}}(\cos\frac{\psi}{2} - \sin\frac{\psi}{2})$$
$$= \frac{1}{\sqrt{2}}\sqrt{1 - \sin\psi} \qquad \text{(B.18)}$$

From Equation (B.13):

$$\sin\psi = \sin^2(\frac{\psi}{2} + \frac{\pi}{4}) - 1 \tag{B.19}$$

and from Equation (B.15), Equation (B.19) can be written as:

$$\sin\psi = 2k^2\sin^2\phi - 1 \tag{B.20}$$

Using Equation (B.20) in Equation (B.18) to get

$$
\begin{aligned}
\cos(\frac{\psi}{2} + \frac{\pi}{4}) &= \frac{1}{\sqrt{2}}\sqrt{1 + 1 - 2k^2\sin^2\phi} \\
&= \frac{\sqrt{2}}{\sqrt{2}}\sqrt{1 - k^2\sin^2\phi} \\
&= \sqrt{1 - k^2\sin^2\phi}
\end{aligned}
\tag{B.21}
$$

Using Equation (B.21) in Equation (B.17) such that

$$\frac{d\psi}{\cos\phi} = \frac{2k}{\sqrt{1 - k^2\sin^2\phi}} \tag{B.22}$$

Using Equation (B.22) in Equation (B.16) produces

$$
\begin{aligned}
ds &= -\frac{1}{2}\sqrt{\frac{m}{V}}\frac{1}{k}\frac{2k\,d\phi}{\sqrt{1 - k^2\sin^2\phi}} \\
&= -\sqrt{\frac{m}{V}}\frac{d\phi}{\sqrt{1 - k^2\sin^2\phi}}
\end{aligned}
\tag{B.23}
$$

Integrating Equation (B.23) such that

$$\int_0^s ds = -\sqrt{\frac{m}{V}}\int_{\frac{\pi}{2}}^{\phi_0}\frac{d\phi}{\sqrt{1 - k^2\sin^2\phi}} \tag{B.24}$$

at $\psi = \theta$, from Equation (B.15)

$$\sin \phi = \frac{1}{k} \sin(\frac{\theta}{2} + \frac{\pi}{4})$$
$$= \frac{1}{k} k = 1$$
$$\therefore \phi = \frac{\pi}{2}$$

From Equation (B.24)

$$\boxed{s = \sqrt{\frac{m}{V}}[F(\frac{\pi}{2}) - F(\phi_0)]} \tag{B.25}$$

Now deriving the elliptic integral for y, from Equation (2.11) we have:

$$dy = tan\psi dx \tag{B.26}$$

From Using Equations (2.7) and (B.5) in Equation (B.26):

$$dy = \sin \psi ds = \rho \sin \psi d\psi \tag{B.27}$$

Using ρ from Equation (B.4) in Equation (B.27):

$$dy = -\frac{1}{\sqrt{2}}\sqrt{\frac{m}{V}}[\sin \theta - \sin \psi]^{-\frac{1}{2}} \sin \psi d\psi$$
$$= -\frac{1}{\sqrt{2}}\sqrt{\frac{m}{V}}[(1 + \sin \theta) - (1 + \sin \psi)]^{-\frac{1}{2}} \sin \psi d\psi \tag{B.28}$$

Recall that,

$$\text{from Equation (B.12)} \qquad 1 + \sin\theta = 2k^2 \qquad \text{(B.29)}$$

$$\text{from Equation (B.13)} \qquad 1 + \sin\psi = 2\sin^2(\frac{\psi}{2} + \frac{\pi}{2}) \qquad \text{(B.30)}$$

$$\text{from Equation (B.22)} \qquad d\psi = \frac{2k\cos\phi}{\sqrt{1 - k^2\sin^2\phi}}d\phi \qquad \text{(B.31)}$$

$$\text{from Equation (B.20)} \qquad \sin\phi = 2k^2\sin^2\phi - 1 \qquad \text{(B.32)}$$

Using Equations (B.29) through (B.32) in Equation (B.28):

$$dy = -\frac{1}{\sqrt{2}}\sqrt{\frac{m}{V}}[2k^2 - 2\sin^2(\frac{\psi}{2} + \frac{\pi}{4})]^{-\frac{1}{2}}(2k^2\sin^2\phi - 1)\frac{2k\cos\phi d\phi}{\sqrt{1 - k^2\sin^2\phi}}$$

$$= -\sqrt{\frac{m}{V}}(\frac{1}{k})[1 - \sin^2\phi]^{-\frac{1}{2}}(2k^2\sin^2\phi - 1)\frac{k\cos\phi}{\sqrt{1 - k^2\sin^2\phi}}d\phi$$

$$= \sqrt{\frac{m}{V}}\frac{1}{\cos\phi}\frac{(1 - 2k^2\sin^2\phi)\cos\phi}{\sqrt{1 - k^2\sin^2\phi}}d\phi$$

$$= \sqrt{\frac{m}{V}}\frac{1 - 2k^2\sin^2\phi}{(1 - k^2\sin^2\phi)^{\frac{1}{2}}}d\phi$$

$$= \sqrt{\frac{m}{V}}\frac{2(1 - k^2\sin^2\phi) - 1}{\sqrt{1 - k^2\sin^2\phi}}d\phi$$

$$dy = \sqrt{\frac{m}{V}}2\sqrt{1 - k^2\sin^2\phi}d\phi - \sqrt{\frac{m}{V}}\frac{1}{\sqrt{1 - k^2\sin^2\phi}}d\phi \qquad \text{(B.33)}$$

Integrate Equation (B.33) to get

$$\int_0^y = \int_{\frac{\pi}{2}}^{\phi_0} 2\sqrt{\frac{m}{V}}\sqrt{1 - k^2\sin^2\phi}d\phi - \int_{\frac{\pi}{2}}^{\phi_0}\sqrt{\frac{m}{V}}\frac{1}{\sqrt{1 - k^2\sin^2\phi}}d\phi$$

$$y = \sqrt{\frac{m}{V}}[(2E(\phi_0) - 2E(\frac{\pi}{2})) + (F(\frac{\pi}{2}) - F(\phi_0))] \qquad \text{(B.34)}$$

B.2 Derivation of Bliman and Sorine results

This section provides derivations for the Equations (3.10) through (3.12) and Equation (3.14). We start with the integral form of the system:

$$F(u)(t) = f_1\left(1 - e^{\left(-\frac{s(0)+s(t)}{\epsilon\eta}\right)}\right) - f_2\left(1 - e^{\left(-\frac{s(0)+s(t)}{\epsilon}\right)}\right) \qquad \text{(B.35)}$$

Our definition of f_k from Equation (3.7) is restated below:

$$f_k = \lim_{\dot{u}>0,u(t)} F(u)(t) \qquad \text{(B.36)}$$

which when applied to Equation (B.35) gives:

$$\boxed{f_k = f_1 - f_2} \qquad \text{(B.37)}$$

The definition of f_s is given in Equation (3.8) is:

$$f_s = \sup_{u,t>0} F(u)(t) \qquad \text{(B.38)}$$

Differentiate $F(u)(t)$ with respect to time as the first step to finding the maximum:

$$\frac{\partial F(u)(t)}{\partial t} = \left(\frac{\partial}{\partial t}s(t)\right)\left(\frac{f_1 e^{\left(-\frac{s(0)+s(t)}{\epsilon_f\eta}\right)}}{\epsilon_f\eta} - \frac{f_2 e^{\left(-\frac{s(0)+s(t)}{\epsilon_f}\right)}}{\epsilon_f}\right) \qquad \text{(B.39)}$$

Since $s(t)$ will always be positive, the second term must go to zero at the maximum. Solving for the value of $s(t)$ that results in that term going to zero (and assuming $s(0) =$

0), results in s_e:

$$s_e = \frac{\epsilon_f \eta}{1 - \eta} \log \frac{f_1}{\eta f_2}$$

(B.40)

subtituting this into $F(u)(t)$ and simplifying gives:

$$f_s = f_k + f_2 \left(\frac{\eta f_2}{f_1} \right)^{\frac{\eta}{1-\eta}} (1 - \eta)$$

(B.41)

Determining $k_F^{\pm}$ is slightly more complicated. Starting with k_F^{-} we have the following definition:

$$k_F^{-} = \sup_{u, t > 0} -\frac{F(u)(t)}{\dot{u}(t)}$$

(B.42)

First, we form the ratio:

$$-\frac{F(u)(t)}{\dot{u}(t)} = -\frac{f_1 e^{\left(\frac{s(0) - s(t)}{\epsilon_f \eta} \right)} - f_2 e^{\left(\frac{s(0) - s(t)}{\epsilon_f} \right)} \eta}{\epsilon_f \eta}$$

(B.43)

Differentiating with respect to time and factoring the result:

$$-\frac{\partial}{\partial t} \frac{F(u)(t)}{\dot{u}(t)} = \left(\frac{\partial}{\partial t} s(t) \right) \frac{\left(f_1 e^{\left(-\frac{s(t)}{\epsilon_f \eta} \right)} - f_2 e^{\left(-\frac{s(t)}{\epsilon_f} \right)} \eta^2 \right)}{\eta^2 \epsilon_f{}^2}$$

(B.44)

Which results in the following equation for the maximum:

$$\frac{\left(f_1 e^{\left(-\frac{s(t)}{\epsilon_f \eta} \right)} - f_2 e^{\left(-\frac{s(t)}{\epsilon_f} \right)} \eta^2 \right)}{\eta^2 \epsilon_f{}^2} = 0$$

(B.45)

Solving for the value of $s(t)$:

$$s_- = \frac{\log \left(\frac{f_1}{f_2 \eta^2} \right) \epsilon_f \eta}{1 - \eta}$$

(B.46)

Substituting this result into Equation (B.43) and simplifying:

$$k_{F}^{-} = \frac{f_2}{\epsilon_f} \left(\frac{\eta^2 f_2}{f_1} \right)^{\frac{\eta}{1-\eta}} (1 - \eta) \qquad \text{(B.47)}$$

B.3 KES Bending Test Profile Equations

This section continues the derivation of the equations given Section 4.2.1 for the remaining six regions of the curve in Figure 4.2.

B.3.1 Unloading/Reverse Bending Path (Regions 4-6)

This path consists of reversing the direction of bending after first unbending the fabric. It is assumed that the test continues at a constant velocity through zero curvature.

Negative Acceleration (Region 4)

Initially, we have a total displacement d_{3f}, zero velocity, and zero acceleration. The acceleration profile is given in Equation (B.48) and can be determined by taking the negative of the acceleration profile given in Equation (4.9) and shifting the time through the substitution of $t = t - T_{fl}$ where T_{fl} is the time at which the initial loading is complete.

$$a_4(t) = 3\frac{(t - T_{fl})(t - T_{fl} - T)}{T^3} \qquad \text{(B.48)}$$

As with region 3, the change in velocity is given by the negative of the velocity profile in region 1 $v_0(t)$, but in this case timeshifted as above to T_{fl}, resulting in a velocity as given in Equation (B.49).

$$v_4(t) = 3\frac{(t - T_{fl})^2(2t - 2T_{fl} - 3T)}{2T^3} \qquad \text{(B.49)}$$

The displacement profile over this region is:

$$d_4(t) = d_{3f} + \frac{(t - T_{fl})^3(t - T_{fl} - 2T)}{4T^3} \tag{B.50}$$

Constant Negative Velocity (Region 5)

Since the acceleration and velocity are constant, the displacement profile is easily determined to be:

$$d_5(t) = d_{4f} + \frac{T_{fl} + T - t}{2} \tag{B.51}$$

where d_{4f} is the displacement at the end of region 4.

Deceleration (Region 6)

Given that we are decelerating from a negative velocity, the acceleration and velocity profiles from region 1 are correct if we timeshift the profile with $t = t - (T_{fu} - T)$ where T_{fu} is the time where we end this path. Performing this, we get the following equations:

$$a_6(t) = -3\frac{(t - T_{fu} + T)(t - T_{fu})}{T^3} \tag{B.52}$$

$$v_6(t) = -\frac{1}{2} - 3\frac{(t - T_{fu} + T)^2(2t - 2T_{fu} - T)}{2T^3} \tag{B.53}$$

The displacement over this region is given by:

$$d_6(t) = T_{fl} - \frac{T}{4} - \frac{t}{2} - \frac{(t - T_{fu} + T)^3(t - T_{fu} - T)}{4T^3} \tag{B.54}$$

B.3.2   Re-Loading Bending Path (Regions 7-9)

The procedure for this region is the same as regions 1-3 except the profiles are timeshifted with $t = t - T_{fu}$.

B.4   Polynomial Fit to Experimental Data

Power	Value
x^4	-1.034 $\times 10^{-18}$
x^3	-2.744 $\times 10^{-5}$
x^2	3.898 $\times 10^{-5}$
x^1	1.212 $\times 10^{-2}$
x^0	1.716 $\times 10^{-18}$

Table B.1: Fabric 1 - Warp Direction: Loading Polynomial Coefficients

Power	Value
x^4	2.956 $\times 10^{-4}$
x^3	1.022 $\times 10^{-3}$
x^2	-7.164 $\times 10^{-4}$
x^1	6.131 $\times 10^{-3}$
x^0	2.950 $\times 10^{-3}$

Table B.2: Fabric 1 - Warp Direction: Unloading/Reverse Loading Polynomial Coefficients

Power	Value
x^4	-2.287 $\times 10^{-3}$
x^3	-6.208 $\times 10^{-3}$
x^2	-6.022 $\times 10^{-3}$
x^1	3.605 $\times 10^{-3}$
x^0	1.923 $\times 10^{-3}$

Table B.3: Fabric 1 - Warp Direction: Reverse Unloading Polynomial Coefficients

Power	Value
x^4	-9.201 $\times 10^{-19}$
x^3	-2.028 $\times 10^{-4}$
x^2	3.779 $\times 10^{-18}$
x^1	8.059 $\times 10^{-3}$
x^0	-3.219 $\times 10^{-18}$

Table B.4: Fabric 1 - Weft Direction: Loading Polynomial Coefficients

Power	Value
x^4	2.240 $\times 10^{-4}$
x^3	4.910 $\times 10^{-4}$
x^2	-4.607 $\times 10^{-4}$
x^1	3.165 $\times 10^{-3}$
x^0	-1.368 $\times 10^{-3}$

Table B.5: Fabric 1 - Weft Direction: Unloading/Reverse Loading Polynomial Coefficients

Power	Value
x^4	-4.661 $\times 10^{-4}$
x^3	-1.096 $\times 10^{-3}$
x^2	-4.812 $\times 10^{-4}$
x^1	3.982 $\times 10^{-3}$
x^0	8.17 $\times 10^{-4}$

Table B.6: Fabric 1 - Weft Direction: Reverse Unloading Polynomial Coefficients

Power	Value
x^4	4.697×10^{-18}
x^3	-1.114×10^{-3}
x^2	-9.870×10^{-18}
x^1	2.558×10^{-2}
x^0	9.126×10^{-21}

Table B.7: Fabric 2 - Warp Direction: Loading Polynomial Coefficients

Power	Value
x^4	1.193×10^{-3}
x^3	1.706×10^{-3}
x^2	-3.808×10^{-3}
x^1	9.244×10^{-3}
x^0	-6.849×10^{-3}

Table B.8: Fabric 2 - Warp Direction: Unloading/Reverse Loading Polynomial Coefficients

Power	Value
x^4	-5.485×10^{-3}
x^3	-1.789×10^{-2}
x^2	-1.911×10^{-2}
x^1	3.703×10^{-3}
x^0	5.482×10^{-3}

Table B.9: Fabric 2 - Warp Direction: Reverse Unloading Polynomial Coefficients

Power	Value
x^4	-7.839×10^{-19}
x^3	-2.793×10^{-4}
x^2	2.155×10^{-18}
x^1	6.759×10^{-3}
x^0	-9.275×10^{-19}

Table B.10: Fabric 2 - Weft Direction: Loading Polynomial Coefficients

Power	Value
x^4	1.996×10^{-4}
x^3	4.785×10^{-4}
x^2	-1.003×10^{-3}
x^1	4.132×10^{-3}
x^0	-3.115×10^{-3}

Table B.11: Fabric 2 - Weft Direction: Unloading/Reverse Loading Polynomial Coefficients

Power	Value
x^4	-2.112×10^{-3}
x^3	-6.842×10^{-3}
x^2	-8.550×10^{-3}
x^1	-3.615×10^{-4}
x^0	1.329×10^{-3}

Table B.12: Fabric 2 - Weft Direction: Reverse Unloading Polynomial Coefficients

Bibliography

[Abb51]   N.J. Abbott. The Measurement of Stiffness in Textile Fabrics. *Textile Research Journal*, 21:435–444, June 1951.

[ABW93]   M. Aono, D. Breen, and M. Wozny. *A Computer Aided Broadcloth Composite Layout Design System*, pages 223–250. North-Holland, 1993.

[ABW94]   M. Aono, D. Breen, and M. Wozny. Fitting a Woven Cloth Model to a Curved Surface: Mapping Algorithms. *Computer Aided Design*, 26(4):278–292, April 1994.

[ADBW96]   M. Aono, P. Denti, D. Breen, and M. Wozny. Fitting a Woven Cloth to a Curved Surface: Dart Insertion. *IEEE Computer Graphics and Applications*, 16(4):60–70, September 1996.

[BHG92]   D. Breen, D. House, and P. Getto. A Physically-Based Particle Model of Woven Cloth. *The Visual Computer*, 8(5-6):264–277, 1992.

[BHW94]   D. Breen, D. House, and M. Wozny. A Particle-based Model for Simulating the Draping Behaviour of Woven Cloth. *Textile Research Journal*, 64:663–685, November 1994.

[BS93a]   P.A. Bliman and M. Sorine. Friction modeling by hysteresis operators. Application to Dahl, stickton, and Stribeck effects. In *Models of Hysteresis*. Longman Scientific and Technical, 1993.

[BS93b]   P.A. Bliman and M. Sorine. A system-theoretic approach of systems with hysteresis. application to friction modelling and compensation. In *Proceedings of the 2nd European Control Conference*, pages 1844–1849, Gronigen, Netherlands, 1993.

[BS95]   P.A. Bliman and M. Sorine. Easy-to-use realistic dry friction models for automatic control. In *Proceedings of the 3rd European Control Conference*, pages 3788–3794, Rome, Italy, September 1995.

[BSBG98]   Smita Bais-Singh, Sherrill B. Biggers, Jr., and Bhuvenesh C. Goswami. Finite Element Modeling of the Nonuniform Deformation of Spun-Bonded Nonwovens. *Textile Research Journal*, 68(5):327–342, May 1998.

[BW98a]   David Baraff and Andrew Witkin. Faster cloth dynamics. In *Cloth and Clothing in Computer Graphics*, number 31 in SIGGRAPH 98 Course Notes, pages G–1, Orlando, Florida, July 19-24 1998. ACM SIGGRAPH.

[BW98b]   David Baraff and Andrew Witkin. Large steps in cloth simulation. In *Proceedings of SIGGRAPH 98*, Annual Conference Series, pages 43–54, Orlando, Florida, July 19-24 1998. ACM SIGGRAPH.

[CG95]   B. Chen and M. Govindaraj. A Physically Based Model of Fabric Drape Using Flexible Shell Theory. *Textile Research Journal*, 65:324–330, June 1995.

[Col70]   Ann M. Collier. *A Handbook of Textiles*. Pergamon Press, Oxford, 1970.

[CSWY99]   M.X. Chen, Q.P. Sun, Z. Wu, and M.M.F. Yuen. A Discretized Linear Elastic Model for Cloth Buckling and Drape. *Journal of Manufacturing Science and Engineering*, 121:695–700, November 1999.

[CYMTT92]   M. Carignan, Y. Yang, N. Magnenat-Thalmann, and D. Thalmann. Dressing Animated Synthetic Actors with Complex Deformable Clothes. *Computer Graphics*, 26(2):99–104, July 1992.

[Dah76]   Phillip R. Dahl. Solid friction damping of mechanical vibrations. *AIAA Journal*, 14(12):1675–1682, December 1976.

[Den94]   Shigan Deng. *Nonlinear Fabric Mechanics Including Material Nonlinearity, Contact, and an Adaptive Global Solution Algorithm*. PhD thesis, North Carolina State University, 1994.

[DGR00]   José Miguel S. Dias, Manuel N. Gamito, and José M. Rebordão. A Discretized Linear Elastic Model for Cloth Buckling and Drape. *Textile Research Journal*, 70(4):285–297, April 2000.

[DJP78]   S. De Jong and R. Postle. A General Energy Analysis of Fabric Mechanics Using Optimal Control Theory. *Textile Research Journal*, 48:127–135, March 1978.

[EDC96]   J. Eischen, S. Deng, and T. Clapp. Finite-Element Modeling and Control of Flexible Fabric Parts. *IEEE Computer Graphics and Applications*, 16(4):71–80, September 1996.

[Eis98a]   Jeffrey W. Eischen. Drape Modeling of Cloth. In *Cloth and Clothing in Computer Graphics*, number 31 in SIGGRAPH 98 Course Notes, pages E–1 through E–23, Orlando, Florida, July 19-24 1998. ACM SIGGRAPH.

[Eis98b]   Jeffrey W. Eischen. Finite Element Modeling of Cloth - Implementation. In *Cloth and Clothing in Computer Graphics*, number 31 in SIGGRAPH 98 Course Notes, pages E–24 through E–50, Orlando, Florida, July 19-24 1998. ACM SIGGRAPH.

[EW97]   B. Eberhardt and A. Weber. Modeling the Draping Behaviour of Woven Cloth. *MapleTech*, 4(2):25–31, 1997.

[EW99]   B. Eberhardt and A. Weber. A particle system approach to knitted textiles. *Computers and Graphics*, 23:599–606, 1999.

[EWS96]   B. Eberhardt, A. Weber, and W. Strasser. A Fast, Flexible Particle System Model for Cloth Draping. *IEEE Computer Graphics and Applications*, 16(4):52–59, September 1996.

[Fos58]   K.A. Foss. Co-ordinates which uncouple the equations of motion of damped linear dynamic systems. *ASME Journal of Applied Mechanics*, pages 361–364, September 1958.

[GA66a]   P. Grosberg and G.M. Abbott. Measurement of Fabric Stiffness and Hysteresis in Bending. *Textile Research Journal*, 36:928–930, October 1966.

[GA66b]   P. Grosberg and G.M. Abbott. The Fabric Cantilever. *Textile Research Journal*, 36:930–932, October 1966.

[GLS95]   L. Gan, N.G. Ly, and G.P. Steven. A Study of Fabric Deformation Using Nonlinear Finite Elements. *Textile Research Journal*, 65:660–668, November 1995.

[GP66]   P. Grosberg and B.J. Park. The Mechanical Properties of Woven Fabric - Part V: The Initial Modulus and the Frictional Restraint in Shearing of Plain Weave Fabrics. *Textile Research Journal*, 36:420–431, May 1966.

[Gro66a]   P. Grosberg. The Mechanical Properties of Woven Fabric - Part I: The Initial Load Extension Modulus of Woven Fabrics. *Textile Research Journal*, 36:71–79, January 1966.

[Gro66b]   P. Grosberg. The Mechanical Properties of Woven Fabric - Part II: The Bending of Woven Fabrics. *Textile Research Journal*, 36:205–211, March 1966.

[GS66]   P. Grosberg and N.M. Swani. The Mechanical Properties of Woven Fabric - Part IV: The Determination of the Bending Rigidity and Frictional Restraint in Woven Fabrics. *Textile Research Journal*, 36:338–345, May 1966.

[HB98]   Donald H. House and David E. Breen. Representation of Woven Fabrics. In *Cloth and Clothing in Computer Graphics*, number 31 in SIGGRAPH 98

Course Notes, pages B–1 through B–17, Orlando, Florida, July 19-24 1998. ACM SIGGRAPH.

[HC98]   Jinlian Hu and Yuk-Fung Chan. Effect of Fabric Mechanical Properties on Drape. *Textile Research Journal*, 68(1):57–64, January 1998.

[HC00a]   Jinlian Hu and Shui-Fu Chen. Numerical Drape Behaviour of Circular Fabric Sheets Over Circular Pedestals. *Textile Research Journal*, 70(7):593–603, July 2000.

[HC00b]   Jinlian Hu and Siuping Chung. Bending Behaviour of Woven Fabrics with Vertical Seams. *Textile Research Journal*, 70(2):148–153, February 2000.

[HGB69]   J.W.S. Hearle, P. Grosberg, and S. Backer. *Structural Mechanics of Fibres, Yarns, and Fabrics (Volume 1)*. Wiley-Interscience, New York, 1969.

[HLL00]   J.L. Hu, W.M. Lo, and M.T. Lo. Bending Hysteresis of Plain Woven Fabrics in Various Directions. *Textile Research Journal*, 70(3):237–242, March 2000.

[HM90]   B.K Hinds and J. McCartney. Interactive Garment Design. *The Visual Computer*, 6:53–61, 1990.

[HM91]   B.K Hinds and J. McCartney. Pattern Development for 3D Surfaces. *Computer Aided Design*, 23(8):583–592, August 1991.

[HZ97]   Jin-Lian Hu and Yi-Tong Zhang. The KES Shear Test for Fabrics. *Textile Research Journal*, 67:654–664, September 1997.

[Ing89]   Lester Ingber. Very fast simulated re-annealing. *Mathematical Computer Modelling*, 12(8):967–973, 1989.

[Ing92]   Lester Ingber. Genetic algorithms and very fast simulated reannealing: A comparison. *Mathematical Computer Modelling*, 16(11):87–100, 1992.

[Ing93]   Lester Ingber. Simulated annealing: Practice versus theory. *Mathematical Computer Modelling*, 18(11):29–57, 1993.

[Ing96]   Lester Ingber. Adaptive Simulated Annealing (ASA): Lessons learned. *Control and Cybernetics*, 25(1):33–54, 1996.

[Ing00]   Lester Ingber. Adaptive Simulated Annealing (ASA). http://www.ingber.com/ASA.tar.gz, August 2000. Version 21.3.

[Jos77]   Marjory L. Joseph. *Introductory Textile Science, 3rd Edition*. Holt, Rinehart, and Winston, New York, 1977.

[JP98]   Y.J. Jeong and D.G. Phillips. A Study of Fabric-drape Behaviour with Image Analysis Part II: The Effects of Fabric Structure and Mechanical Properties on Fabric Drape. *Journal of the Textile Institute*, 89(1):70–79, 1998.

[Kaw80]   Sueo Kawabata. *The Standardization and Analysis of Hand Evaluation*. The Textile Machinery Society of Japan, Osaka, 2nd edition, 1980.

[KP89]   Mark A. Krasnosel'skii and Aleksei V. Pokrovskii. *Systems with Hysteresis*. Springer-Verlag, New York, 1989.

[LA85]   G.A.V. Leaf and R.D. Anandjiwala. A Generalized Model of Plain Woven Fabric. *Textile Research Journal*, 52:92–99, February 1985.

[Law01]   Lawrence Livermore and Sandia National Labs. SLATEC Common Mathematical Library. http://www.netlib.org/slatec/, May 2001. Version 4.1.

[LBD61]   J. Lindberg, B. Behre, and B. Dahlberg. Mechanical Properties of Textile Fabrics - Part III: Shearing and Buckling of Various Commerical Fabrics. *Textile Research Journal*, 31:99–122, February 1961.

[LDG96]   L. Ling, M. Damodaran, and R.K.L. Gay. Aerodynamic force models for animating cloth motion in air flow. *The Visual Computer*, 12:84–104, 1996.

[LKC96]   J.-D. Liu, M.-T. Ko, and R.-C. Chang. Collision Avoidance in Cloth Animation. *The Visual Computer*, 12:234–243, 1996.

[LPC95]   J. Louchet, X. Provot, and D. Crochemore. Evolutionary Identification of Cloth Animation Models. *Proceedings of the 6th Eurographics Workshop on Animation and Simulation*, pages 30–43, 1995.

[MDS66]   D. Moskowitz, Gordon, J. H. Dillon, and Edward W. Suppiger. Large Lateral Deflection of Textile Fabric Structures. *Textile Research Journal*, 36:770–786, September 1966.

[Mer59]   Reginald Meredith, editor. *The Mechanical Properties of Textile Fibres*. North-Holland Publishing Company, Amsterdam, 1959.

[MT98]   Nadia Magnenat Thalmann. Clothing Virtual Actors. In *Cloth and Clothing in Computer Graphics*, number 31 in SIGGRAPH 98 Course Notes, pages D–1 through D–26, Orlando, Florida, July 19-24 1998. ACM SIGGRAPH.

[MTS71]   J.F. Martin, T. Topper, and G.M. Sinclair. Computer Based Simulation of Cyclic Stress-Strain Behaviour with Applications to Fatigue. *Materials Research and Standards*, 11:23, 1971.

[NGA95]   H.N Ng, R.L. Grimsdale, and W.G. Allen. A System for Modelling and Visualization of Cloth Material. *Computers and Graphics*, 19(3):423–430, 1995.

[Nis86]   J. Nisselson. Computer Graphics and the Fashion Industry. *Proceedings Graphics Interface '86*, 1986.

[Num01]   Numerical   Algorithms   Group.   NAG   F77   Library.
           http://www.nag.com/asliR5/, May 2001. ASLI Mark 5.

[NWGC87]   J. Nisselson, J. Weil, R. Gordon, and J. Charles. Computer Graphics and
           Fashion. *Computer Graphics*, 21(4):333–334, July 1987.

[OITN92]   H. Okabe, H. Imoaka, T. Tomiha, and H. Niwaya. Three Dimensional
           Apparel CAD System. *Computer Graphics*, 26(2):105–110, July 1992.

[PP99]   Jacqueline R. Postle and Ron Postle. The Dynamics of Fabric Drape. *Textile
           Research Journal*, 69(9):623–629, September 1999.

[Pro95]   X. Provot. Deformation Constraints in a Mass-Spring Model to Describe
           Rigid Cloth Behaviour. *Proceedings of Graphics Interface '95*, April 1995.

[Pro96]   X. Provot. Collision and Self-Collision Handling in a Cloth Model Dedi-
           cated to Design Garments. *Proceedings of Graphics Interface '96*, 1996.

[RBB97]   M.L. Realff, M.C. Boyce, and S. Backer. A Micromechanical Model of the
           Tensile Behaviour of Woven Fabric. *Textile Research Journal*, 67(6):445–459,
           June 1997.

[RO43]   W. Ramberg and W.R. Osgood. Technical Note No. 902 - Description of
           Stress-Strain Curves by Three Parameters. Technical report, National Ad-
           visory Committee For Aeronautics, 1943.

[Rob01]   Barbara Robertson. Monster Mash. *Computer Graphics World*, October
           2001.

[Sak00]   Shinichi Sakata. ASAMIN.
           http://www.econ.lsa.umich.edu/~ssakata/software/, August 2000. Ver-
           sion 1.7.

[SD97]   A. Sinoimeri and J.Y. Dréan. Mechanical Behaviour of the Plain Weave
           Structure Using Energy Methods. *Textile Research Journal*, 67(5):370–378,
           May 1997.

[SE98]   W. Strasser and B. Eberhardt. Representation of Knit Fabrics or the art of
           knitted fabrics. In *Cloth and Clothing in Computer Graphics*, number 31 in
           SIGGRAPH 98 Course Notes, pages F–1 through F–20, Orlando, Florida,
           July 19-24 1998. ACM SIGGRAPH.

[Set00]   Ajay Seth. A Predictive Control Method For Human Upper-Limb Motion:
           Graph-Theoretic Modelling, Dynamic, Optimization, and Experimental
           Investigations. Master's thesis, University of Waterloo, 2000.

[SHY00]   Fengjun Shi, Jinlian Hu, and Tongxi Yu. Modeling the Creasing Properties
           of Woven Fabrics. *Textile Research Journal*, 70(3):247–255, March 2000.

[Ske76] J. Skelton. The Fundamentals of Fabric Shear. *Textile Research Journal*, 46:862–869, September 1976.

[SLH78] W. Shanahan, D.W. Lloyd, and J.W.S. Hearle. Characterizing the Elastic Behaviour of Textile Fabrics in Complex Deformations. *Textile Research Journal*, 48:495–505, September 1978.

[SSG97] Fangning Sun, Abedelfattah M. Seyam, and B. S. Gupta. A Generalized Model for Predicting Load-Extension Properties of Woven Fabrics. *Textile Research Journal*, 67(12):866–874, December 1997.

[Tap89] Byron D. Tapley, editor. *Esbach's Handbook of Engineering Fundamentals*. John Wiley and Sons, New York, 4th edition, 1989.

[Tav93] L. Tavernini. Differential automata models of hysteresis models. In *Models of Hysteresis*. Longman Scientific and Technical, 1993.

[VCMT95] P. Volino, M. Courchesne, and N. Magnenat-Thalmann. Versatile and Efficient Techniques for Simulating Cloth and Other Deformable Surfaces. *Proceedings of SIGGRAPH '95*, 1995.

[Ver95] Allan H. Vermeulen. *The B-Spline Field Approximation Method in Solid Mechanics*. PhD thesis, University of Waterloo, 1995.

[VMT94] P. Volino and N. Magnenat-Thalmann. Efficient self-collision detection on smoothly discretized surface animations using geometrical shape regularity. *Proceedings of Eurographics '94*, 1994.

[VMT95] P. Volino and N. Magnenat-Thalmann. Collision and Self-Collision Detection: Efficient and Robust Solutions for Highly Deformable Surfaces. *Proceedings of Eurographics '95*, 1995.

[VMTJT96] P. Volino, N. Magnenat-Thalmann, S. Jianhua, and D. Thalmann. An Evolving System for Simulating Clothes on Virtual Actors. *IEEE Computer Graphics and Applications*, 16(4):42–51, September 1996.

[VOVL92] C.W.A.M. Van Overveld and E. Van Loon. Hanging Cloths and Dangling Rods: a Unified Approach to Constraints in Computer Animation. *The Journal of Visualization and Computer Animation*, 3:45–59, 1992.

[VT98] Pascal Volino and Nadia Magnenat Thalmann. Developing Simulation Techniques for an Interactive Clothing System. In *Cloth and Clothing in Computer Graphics*, number 31 in SIGGRAPH 98 Course Notes, pages D–51 through D–63, Orlando, Florida, July 19-24 1998. ACM SIGGRAPH.

[Wei86] J. Weil. The Synthesis of Cloth Objects. *Computer Graphics*, 20(4):49–54, August 1986.

[WKL⁺00] Tomiji Wakida, Kyoko Kida, Muncheul Lee, Soyeung Bae, Hiromu Yoshioka, and Yuichi Yanai. Dyeing and Mechanical Properties of Cotton Fabrics Treated with Sodium Hydroxide/Liquid Ammonia and Liquid Ammonia/Sodium Hydroxide. *Textile Research Journal*, 70(4):328–332, April 2000.

[ZG99] Naiyue Zhou and Tushar K. Ghosh. On-Line Measurement of Fabric Bending Behaviour - Part III: Dynamic Considerations and Experimental Implementation. *Textile Research Journal*, 69(3):176–184, March 1999.